Texas Medical Center Library
DigitalCommons@The Texas Medical Center

UT GSBS Dissertations and Theses (Open Access)

Graduate School of Biomedical Sciences

5-2010

Smooth Muscle Hyperplasia due to ACTA2/MYH11 Mutations: Identification of Novel Pathology and Pathways Leading to Aneurysms and Diverse Vascular Occlusive Diseases

Christina L. Papke

Follow this and additional works at: http://digitalcommons.library.tmc.edu/utgsbs_dissertations

Part of the Cardiovascular Diseases Commons, and the Cell Biology Commons

Recommended Citation

Papke, Christina L., "Smooth Muscle Hyperplasia due to ACTA2/MYH11 Mutations: Identification of Novel Pathology and Pathways Leading to Aneurysms and Diverse Vascular Occlusive Diseases" (2010). *UT GSBS Dissertations and Theses (Open Access)*. Paper 16.

This Dissertation (PhD) is brought to you for free and open access by the Graduate School of Biomedical Sciences at DigitalCommons@The Texas Medical Center. It has been accepted for inclusion in UT GSBS Dissertations and Theses (Open Access) by an authorized administrator of DigitalCommons@The Texas Medical Center. For more information, please contact laurel.sanders@library.tmc.edu.

CHAPTER I

INTRODUCTION AND LITERATURE REVIEW

Thoracic Aortic Aneurysms and Dissections

An aneurysm is an enlargement or dilatation of an artery, and a dissection is a tear partway through the aortic wall, creating a false lumen for blood flow. Aortic aneurysms and dissections are the most common type of aortic disease and are a leading cause of death in the U.S., affecting approximately 6 out of every 100,000 people and claiming approximately 16,000 lives each year (1;2). Aneurysms of the ascending aorta are defined as greater than or equal to 1.5 times the size of the normal aorta (3). Aneurysms can occur anywhere along the length of the aorta and are classified according to anatomical location. Thoracic aortic aneurysms account for approximately 48% of all aneurysms (2). The natural progression of aneurysms is to progressively enlarge over time until the vessel wall weakens and eventually dissects. An aortic dissection can either be acute (diagnosed less than 2 weeks after the dissection occurred) or chronic, and can occur as part of a spectrum of aortic disease even without aneurysm formation (4). Dissections are most commonly classified using either the Stanford system or the DeBakey system. According to the Stanford classification, Type A dissections involve the ascending aorta, and may also involve the arch or descending aorta, while Type B dissections involve only the descending aorta. According to the DeBakey system, dissections are classified as Type I, Type II, or Type III. A Type I dissection involves the entire length of the aorta, a Type II dissection includes only the ascending aorta, and a Type III dissection includes only the descending aorta (5).

Aneurysms are generally asymptomatic until a catastrophic event i.e. a dissection occurs. Some patients develop chronic heart failure as the aneurysm expands due to distortion of the aortic valve and subsequent aortic valve insufficiency, but aneurysms remain largely undetected until they either dissect or rupture (5). Symptoms of an aortic dissection, including sudden and severe chest pain, are similar to those of a myocardial infarction and are initially misdiagnosed in up to 30% of cases, and this misdiagnosis can prove to be deadly (5-7). Beta-adrenergic receptor blocking agents are currently used to lower blood pressure in patients (8;9). However, while these drugs can slow the rate of aneurysm growth, they do not prevent aortic disease from eventually progressing to dissection (10). No drug treatment to prevent the underlying disease process exists. The only available treatment option when the aorta continues to enlarge despite beta-blocker therapy is surgical repair of the aorta once an aneurysm reaches a certain size or growth rate (5). A dissection must be emergently repaired in order to prevent death, since the mortality rate increases by 1% to 2% every hour after an acute dissection (9). Recommendations for treatment are based on the size of the aneurysm, its location, and its rate of growth. Individuals are generally referred for surgery when the aneurysm reaches a diameter of 5.5-6.0 cm for patients, or if the aneurysm grows more than 0.5 cm in 6 months as assessed by serial MRI scans. For patients with a family history, surgery is recommended once the aneurysm reaches a diameter between 4.5-5.0 cm. Surgical repair involves replacing the aneurysmal portion of the aorta with a Dacron graft (5).

The aortic wall is composed of three major layers: the intima, media, and adventitia. The intima is composed of one layer of endothelial cells. Although the endothelial layer in small arteries is responsive to shear stress and is involved in regulation of vascular tone, it is not clear whether the endothelium of large arteries, including the aorta, is involved in this type of regulation. The medial layer is composed of smooth muscle cells and elastic fibers. Elastic fibers are composed of elastin as well as fibulin and fibrillin-containing microfibrils, and enable the aorta to return to a normal size and shape after stretching due to pulsatile blood flow (**Figure I-1**) (11).

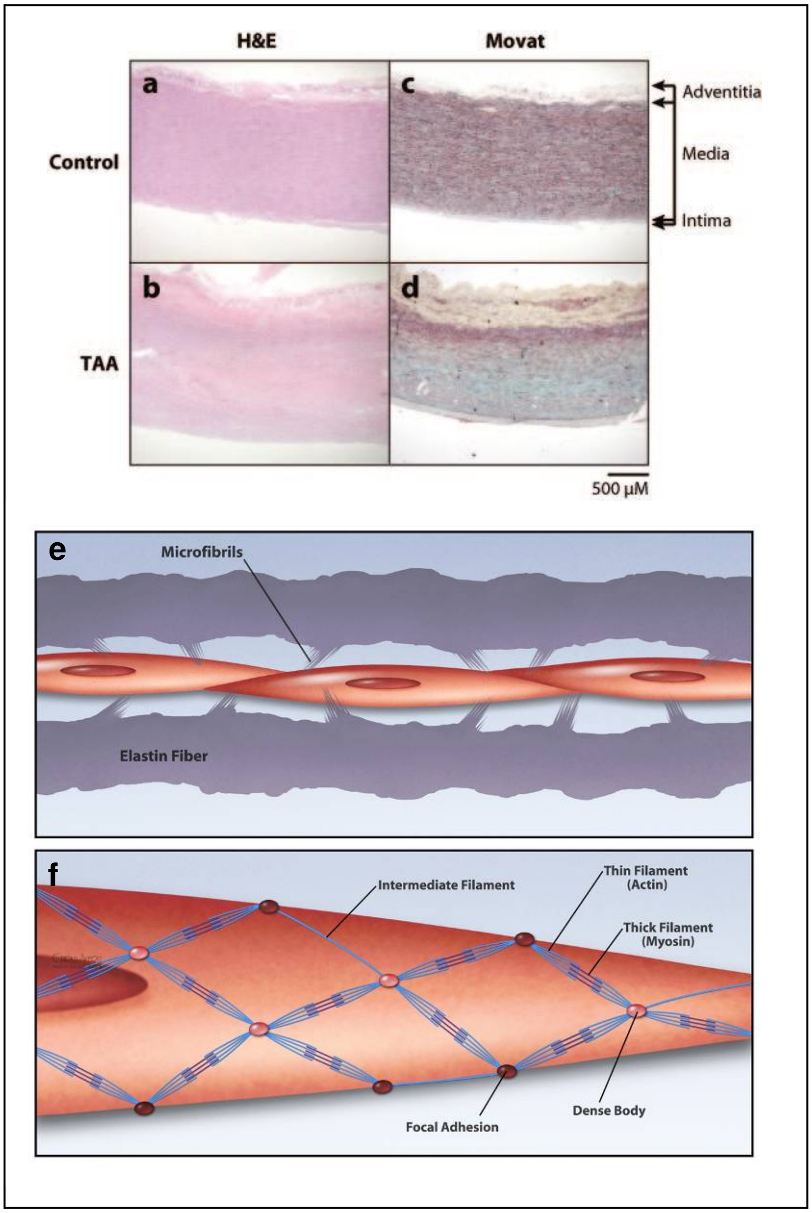
H&E
Movat
a
c
Adventitia
Media
Intima
Control
b
d
TAA
500 μM
e
Microfibrils
Elastin Fiber
f
Intermediate Filament
Thin Filament (Actin)
Thick Filament (Myosin)
Dense Body
Focal Adhesion

Figure I-1. Aortic wall structure. H&E and Movat staining of control (A,C) and aneurysmal (B,D) aortic tissue, showing the three major layers of the aortic wall. Tissues are oriented with the adventitial layer at the top of the image. In the Movat stains, elastic fibers are black, cells are red, proteoglycans are blue, and collagens are yellow. In normal aortas (A,C), the outer adventitial layer contains small blood vessels that supply nutrients to the aortic wall, a

medial layer composed of elastic fibers (black) and SMCs (red), and an intimal layer composed of endothelial cells. SMCs and elastic fibers are arranged in concentric layers (E) and are interconnected with contractile filaments in SMCs through focal adhesions (E,F). In contrast, aneurysmal aortas (B,D) are characterized by areas of proteoglycan accumulation (blue) and focal areas of SMCs loss. Adapted from (12).

****

Fibrillin-1 has both a structural role and a regulatory role within the vessel wall. Fibrillin-1 binds to αvβ3, α5β1, and αvβ6 integrins on the surface of SMCs, contributing to aortic wall structure (13). Additionally, fibrillin contains multiple latent TGF-β binding protein (LTBP) domains and a specific fragment of fibrillin-1 is capable of releasing TGF-β1 from large latent complexes in the ECM, leading to TGF-β1 activation (**Figure I-2**) (14).

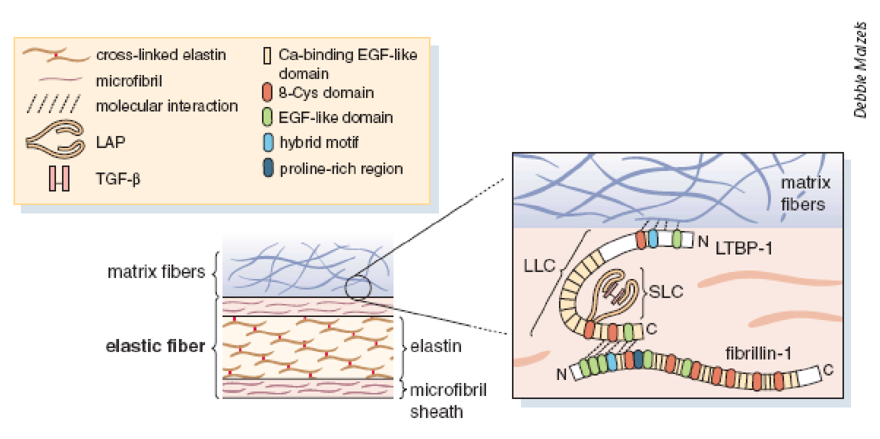
cross-linked elastin
microfibril
molecular interaction
LAP
TGF-β
Ca-binding EGF-like domain
8-Cys domain
EGF-like domain
hybrid motif
proline-rich region
Debbie Maizels
matrix fibers
elastic fiber
elastin
microfibril sheath
matrix fibers
LLC
N
LTBP-1
SLC
C
N
fibrillin-1
C

Figure I-2. Fibrillin-1 controls TGF-β1 activation. Fibrillin-1 has structural similarities to and associates with large latent complexes containing LTBP-1, latency-associated peptide (LAP), and TGF-β1. The small latent complex (SLC) is composed of TGF- β1 and LAP. Breakdown in the structure of fibrillin-1 can lead to TGF- β1 activation through cleavage of the latent complex and release of TGF-β1 peptide into the extracellular matrix. Adapted by permission from Macmillan Publishers Ltd: [Nature Genetics] (15), copyright (2003).

****

Fibulin-4 and fibulin-5 play an essential role in assembly of elastic fibers within the vessel wall, and loss of either of these proteins results in severe vascular defects (16;17). Elastin deficiency in mice and humans results in excessive SMC proliferation and the development of supravalvular aortic stenosis (SVAS), highlighting the importance of elastin in both maintaining the structural integrity of the aorta and in maintaining SMCs in a quiescent, contractile state (18). Elastic fibers and SMCs are arranged in concentric layers within the aortic wall, with each layer of SMCs and its associated elastic fibers representing one lamellar unit (**Figure I-1E**) (11).

The third major layer of the aorta is an outer adventitial layer containing myofibroblasts, adipose tissue, small nerve endings, and vasa vasorum, small blood vessels located close to the medial surface that supply nutrients to the vessel wall. Aneurysms are characterized by medial degeneration, including loss and fragmentation of elastic fibers, SMC loss, proteoglycan accumulation, and in some cases are accompanied by inflammation (**Figure I-1B,D**) (19-21). Proteoglycan accumulation is one of the earliest pathologic findings and has been found prior to aneurysm formation (22). Fragmentation of elastic fibers is the most common feature and is found in >90% of aneurysms, while cystic medial changes, SMC loss, atherosclerotic changes, and thickening of the vasa vasorum were found in 70%, 45%, 41%, and 20% of ascending aneurysms (19). Numerous studies have shown increased expression of multiple matrix metalloproteases (MMPs), which cause ECM degradation and account for some of the pathologic changes observed in TAAD, particularly elastic fiber degradation (23-25). These processes lead to weakening of the aortic wall, leaving it more prone to dissect.

In 1991, missense mutations in *FBN1*, encoding fibrillin-1, were found to cause Marfan syndrome (MFS, OMIM no. 154700) (26). MFS is inherited in an autosomal dominant manner, occurs in approximately 1 out of every 5,000 individuals, and leads to TAAD as well as a number of pleiotropic effects including mitral valve prolapse, long bone overgrowth, joint hypermobility, and ectopia lentis (27). *FBN1* mutations result in altered secretion and deposition of fibrillin-1 in the ECM (28). These studies provided the first evidence that aortic aneurysms could be caused due to a single gene defect.

Approximately 20% of individuals with TAAD have one or more affected family members, providing evidence of a genetic basis for nonsyndromic TAAD (29;30). Aneurysms are inherited in these families in an autosomal dominant manner, and exhibit variable ages of onset and decreased penetrance (4). In addition, these families show variability in the associated cardiovascular complications associated with the thoracic aortic disease, including bicuspid aortic valve, intracranial aneurysms and popliteal aneurysms (3). So far, seven published loci have been linked to TAAD, and the putative genes at four of these loci have been identified (20;31-34). Several additional mutations and/or loci have been identified and are currently being further confirmed and characterized.

Mutations in *TGFBR1* and *TGFBR2*, encoding for the transforming growth factor-β type I and II receptors, respectively, have been identified as causes of familial TAAD (32;35). These findings, along with studies of TGF-β1 signaling in other aneurysm syndromes associated with *TGFBR1* or *TGFBR2* mutations, led to the hypothesis that familial TAAD may be driven, at least in part, by dysregulation of TGF-β signaling (3). However, mutations in *TGFBR1* or *TGFBR2* account for less than 5% of familial TAAD. Furthermore, dysregulation of TGF-β signaling as a common mechanism driving TAAD is controversial. More recently, mutations in *ACTA2* and *MYH11* encoding for the smooth muscle cell (SMC)-specific contractile proteins SM α-actin and myosin heavy chain (SM-MHC), were found to cause TAAD (34;36). While *MYH11* mutations account for <2% of familial TAAD cases, *ACTA2* mutations account for approximately 15% of familial TAAD cases, making contractile gene mutations the most common cause of familial TAAD (34;36). Subsequently, mutations in MLCK, encoding myosin light chain kinase, were identified as a cause of familial TAAD (Wang et al, manuscript submitted).

Approximately 80% of TAAD cases occur in individuals with no known family history of aortic disease. Sporadic aneurysms generally have a later age of onset than familial aneurysms (30). The major causes remain unknown; however, the pathology associated with the TAAD cases is highly similar. Regardless of the major causes of sporadic TAAD, much insight can be gained from study of the pathogenesis of familial TAAD and potentially applied to aid in management of sporadic patients also.

In addition to MFS and nonsyndromic familial TAAD, multiple genetically inherited syndromes are associated with this spectrum of disease. Part of this spectrum of diseases includes defined syndromes as well as nonsyndromic familial TAAD due to mutations in the TGF-β receptors. Furlong et al. described a Marfan-like syndrome in 1987 characterized by craniosynostosis and TAAD; however, the genetic mutation was not identified (37). Loeys-Dietz syndrome was characterized in 2005, was found to share similar characteristics with Furlong syndrome, and was found to be caused by mutations in either the TGF-β type I or II receptors (38). Subsequently, patients with the originally diagnosed Furlong syndrome were also found to harbor *TGFBR2* mutations (39). Mutations in these receptors also lead to familial TAAD. In this subgroup of patients, major features of Loeys-Dietz syndrome are missing but aneurysms also present in arteries other than the aorta, particularly in patients with *TGFBR1* mutations (35).

Some degree of overlap exists in the aneurysm disease phenotypes caused by these mutations. For example, *TGFBR2* mutations have been shown to lead to multiple distinct aneurysm disorders, including LDS, familial TAAD, and MFS (32;38;40). Unique features found in LDS but not MFS or one other closely related syndrome include arterial tortuosity, cleft palate, atrial septal defects, and patent ductus arteriosus; however, a patient with Furlong/LDS was found to harbor an *FBN1* mutation (38;39). Additionally, *TGFBR2* mutations were found in a subset of patients with clinical features of Marfan syndrome (40). An ongoing controversy exists over whether *TGFBR2* in addition to *FBN1* mutations result in true cases of MFS (41). A more recent study of 547 probands showed that *TGFBR1* and *TGFBR2* mutations cause LDS in 87.5% of cases, but also cause MFS or familial TAAD in the remainder of the cases (42). The majority of the data indicate that these disorders represent a spectrum of disease caused by multiple different mutations, rather than single, isolated clinical entities. The presence of these overlaps in phenotype could have implications for the clinical management of disease.

Vascular Ehlers-Danlos syndrome (EDS) represents another inherited genetic syndrome associated with aneurysms, and is caused by mutations in the *COL3A1* gene, encoding type III procollagen (43). Individuals with vascular EDS have aneurysms, dissections, and rupture of various arteries throughout the body but can also develop TAAD. In addition, these individuals have thin, translucent skin, atrophic scars, and are predisposed to bowel rupture, along with rupture of the gravid uterus. Repair of ascending aneurysms in these individuals is difficult due to the fragility of the vessel tissue (43). Other disorders that also lead to TAAD in more rare cases include EDS associated with filamin A mutations, tuberous sclerosis caused by *TSC2* mutations, Turner syndrome, osteogenesis imperfecta, Alagille syndrome, and adult polycystic kidney disease (44-48).

Additional factors contributing to the development of TAAD include genetic polymorphisms and environmental risk factors. A polymorphism in the MMP9 gene is associated with TAAD (49). Hypertension and environmental factors, including weightlifting, can also both induce aneurysm formation and aggravate aneurysm phenotypes in individuals who are already genetically predisposed to TAAD (12).

In summary, TAAD represents a spectrum of disease exhibiting both genetic and phenotypic heterogeneity, as well as overlap among some of the specific defined syndromes. Although much has been done to advance the field in terms of improving surgical techniques and outcomes and identifying novel mutations leading to disease, the precise mechanisms leading to medial degeneration and expansion of the vessel wall are still not completely understood, and viable non-surgical treatment options for this spectrum of disease are lacking.

SMC Biology and Blood Vessel Biology

An understanding of the structure and function of SMCs and arteries is essential for gaining insight into the pathogenesis of TAAD. Vascular SMCs arise from multiple different origins during development, and a summary of these origins is shown in **Figure I-3**.

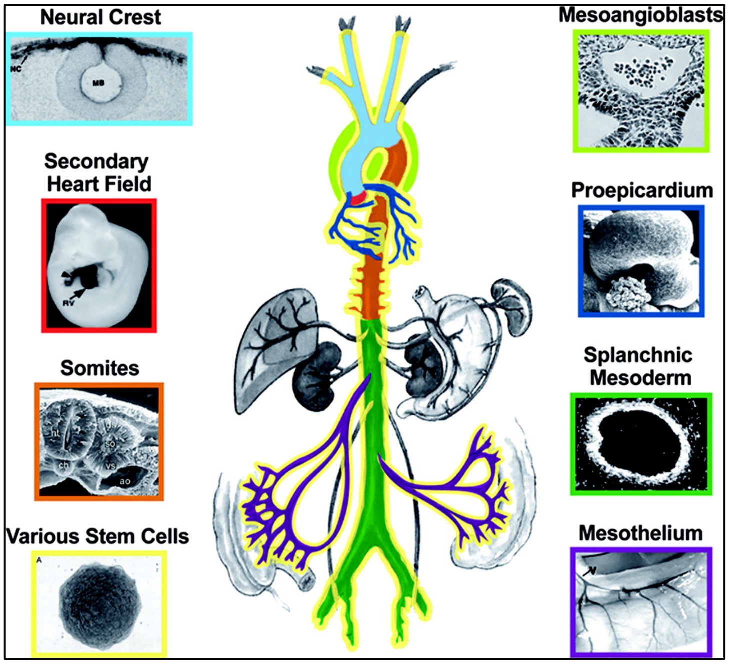
Neural Crest
NC
MB
Secondary Heart Field
RV
Somites
ch
ao
Various Stem Cells
A
Mesoangioblasts
Proepicardium
Splanchnic Mesoderm
Mesothelium

Figure I-3. Diverse developmental origins of vascular SMCs. Vascular SMCs arise from multiple embryonic origins, and are color coded accordingly. Reprinted by permission from Wolters Kluwer Health (50), copyright (2007).

****

For example, SMCs in the ascending aorta as well as the carotid arteries arise from neural crest cells, while SMCs in the descending aorta are mesenchymal derived (50). Treatment of neural crest derived vs. mesenchymal derived cells with TGF-β1 results in different cellular responses, suggesting that these cells are functionally similar but not completely identical (51).

In contrast to skeletal and cardiac myocytes, which are terminally differentiated, SMCs are able to switch between a quiescent, contractile phenotype and a proliferative, synthetic phenotype (52;53). SMC phenotypic plasticity is closely tied with contractile function and response to external stimuli including stretch (54). Differentiated SMCs are generally quiescent and non-proliferative, and are characterized by prominent stress fibers and high expression of contractile proteins including SM α-actin, smooth muscle β-myosin, calponin, smoothelin, SM22, and tropomyosins (54;55). Dedifferentiated SMCs have a more synthetic phenotype characterized by increased amounts of rough endoplasmic reticulum and large Golgi complexes, decreased contractile protein expression, more production of ECM proteins, and increased proliferation and migration (55). These two phenotypes are not necessarily mutually exclusive of one another, however (56).

Phenotypic switching to a more de-differentiated state allows SMCs to repair the vessel wall after injury. However, in disease states an overabundance of this response proves to be detrimental (54). SMC phenotypic modulation plays an important role in vascular proliferative diseases including atherosclerosis and restenosis of vascular stent grafts (57). Dedifferentiated SMCs are also found in aneurysms (22). Regulation of SMC phenotype is highly complex, is mediated by a variety of extracellular signals, and is transcriptionally regulated through multiple different pathways. Serum response factor (SRF) acts as a molecular switch, regulating either a contractile phenotype or a proliferative phenotype, dependent on its binding to either the myocardin family of transcription factors to promote SMC gene expression, or ternary complex factors (TCFs), to promote expression of proliferative genes (58). Multiple cytokines and growth factors also contribute to SMC phenotypic modulation. PDGF-β is known to potent stimulator of SMC proliferation and migration, while TGF-β1 has been known to promote either differentiation or proliferation depending on the concentration used (51;54).

The proper contractile function of differentiated SMCs is essential for maintaining structural integrity within the vascular wall. SMCs differ from cardiac and skeletal muscle in that they lack sarcomeres, but the sliding filament mechanism of contraction in SMCs is similar to the mechanism in striated muscle cells, and provides a means of generating contractile force (59;60). Multiple proteins are involved in the regulation of SMC actin-myosin crossbridge cycling, including tropomyosin, calponin, and caldesmon: actin and myosin are the major focus of this study. Myosin consists of two heavy chains, two essential light chains, and two regulatory light chains. Each myosin heavy chain is composed of a globular head domain that has ATPase activity, and an α-helical coiled-coil region (61). ATP exchange causes release of myosin from actin filaments, along with a conformational change in the myosin head domain (**Figure I-4A,B**).

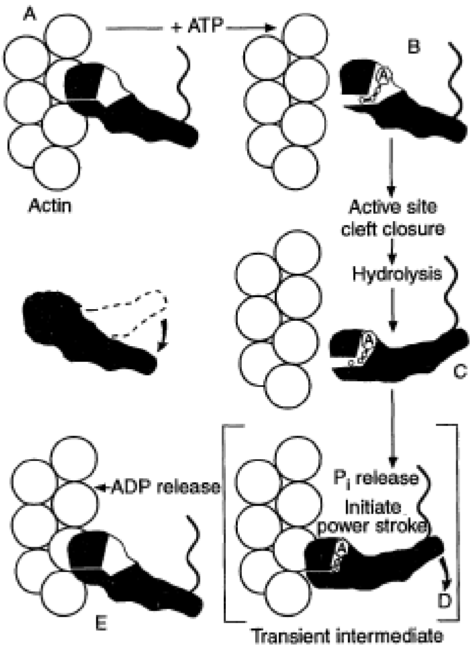
A
+ ATP
B
Actin
Active site
cleft closure
Hydrolysis
C
ADP release
P_i release
Initiate
power stroke
D
E
Transient intermediate

Figure I-4. Myosin crossbridge cycling. ATP exchange and hydrolysis results in a “power stroke” that results in shortening of actin and myosin filaments and subsequent muscle contraction. From (62). Reprinted by permission from AAAS.

****

Binding of actin to myosin accelerates the rate of ATP hydrolysis. Subsequent release of the phosphate causes in another conformational change in myosin, pulling on the filaments and resulting in muscle shortening (**Figure I-4C-E**) (61).

In contrast to the structure of skeletal and cardiac myocytes, where filaments are bundled together in a distinct pattern into myofibrils, contractile filaments in SMCs are distributed in a nonuniform manner, and can adapt their length and organization in response to stimuli (60;63). Additionally, SMCs are thought to bundle and act together in a mechanical syncytium rather than as single cells contracting individually, allowing for force to be distributed uniformly among the cells (60). In this model, contractile filaments are attached to the cell membrane at dense plaques, which are structures homologous to the focal adhesions (FA) observed in other cell types (60;64). FAs form a critical link between the ECM and contractile elements in the cell, creating a continuum along which mechanical force signals can be transduced, and also regulate intracellular signaling (65;66). Focal adhesion kinase (FAK) is a critical part of the FA complex, acting as a mechanosensor, a scaffold for recruitment of other proteins to these complexes, and a regulator of FA turnover (67;68). In FAK-deficient SMCs, Ca2+ signaling and cellular contractility in response to acetylcholine and KCl are disrupted, demonstrating the importance of intact FAK activation for proper SMC contractile function (69). Overall, FAs play an essential role in both regulating tension development and SMC contractility and mediating cell signaling events; however, specific roles of FAs in TAAD pathogenesis have not yet been described.

As stated previously, SMCs are arranged in concentric layers between elastic lamellae in the aortic wall (70). Large arteries have a high elastin content and are able to withstand higher pressures from blood flow than smaller arteries. The high elastin content promotes a differentiated SMC phenotype, and has an inhibitory effect on SMC proliferation

(57). In contrast, smaller arteries are subjected to less pressure from blood flow and are more muscular in structure, containing an internal and external elastic lamina, but no elastic lamellae. Small arteries are also prone to excessive SMC dedifferentiation, proliferation, and migration in response to injury. Numerous studies have shown that carotid artery injury causes SMC proliferation and migration, leading to formation of a neointimal layer of SMCs and ultimately to vessel occlusion (71-73).

Current Understanding of TAAD Pathogenesis

Multiple diverse pathways contribute to TAAD pathogenesis, and some insight has been gained both from the study of TAAD as well as abdominal aortic aneurysms. Some of the major pathways and processes identified include TGF-β1 signaling, SMC phenotypic switching, increased MMP expression, and more recently, SMC contractile dysfunction.

Most of the current TAAD research is focused on the role of TGF-β signaling in the disease process. This is partly owing to the fact that the *Fbn1* underexpressing and *Fbn1* mutant mice were the first mouse models developed to understand the pathogenesis of MFS, and more broadly, TAAD. These models have suggested a role for TGF-β signaling in aneurysm formation in Marfan syndrome (10). Increased phospho-Smad2, an indicator of TGF-β1 signaling, was found in aortas of patients with LDS (38). This increase is paradoxical because the mutations in *TGFBR1* and *TGFBR2* are all located in the intracellular kinase domain and are predicted to result in decreased kinase function, thereby disrupting TGF-β signaling (38). Losartan, an angiotensin II receptor antagonist, prevents Smad2 phosphorylation, medial degeneration, and aneurysm formation in the MFS mouse model (10). Clinical trials are underway to determine whether Losartan delays disease progression in individuals with MFS (74). However, no established treatment currently exists for directly delaying and/or preventing aneurysm formation either in individuals with MFS, or with other syndromic or nonsyndromic conditions that predispose to aneurysm formation.

Some controversy exists as to whether TGF-β1 signaling represents a common pathway leading to familial TAAD. SMCs from familial TAAD patients without identified mutations show a common dysregulation of stretch-induced signaling pathways (Lafont et al, manuscript submitted). Mutations leading to TAAD have been identified in genes that regulate contractility, ECM genes, and specific contractile genes, which are all part of the SMC-integrin-ECM continuum. Additionally, all existing mutations leading to TAAD can be linked, directly or indirectly, to some component of this axis (12).

SMC phenotypic switching is also likely to play an important role in the disease process. In an elastase perfusion model of abdominal aneurysms, phenotypic switching occurred, characterized by decreased levels of SM α-actin and SM22α and increased expression of MMP2 and MMP9, and preceded aneurysm formation (75). Other studies have shown that expression of proteoglycans and matrix metalloproteases (MMPs) are upregulated in the vessel wall, consistent with a more synthetic SMC phenotype. A mouse model of MFS harboring a heterozygous mutation for *Fbn1* displayed increased expression of MMP2 and MMP9 along with decreased overall aortic contractility and increased degradation of elastic fibers (24). Treatment of MFS mice with doxycycline, a nonspecific MMP inhibitor, prevented medial degeneration, aneurysm formation, and aortic rupture (76;77). One of the earliest histologic findings in medial degeneration is proteoglycan accumulation within the aortic wall (22). Data from our lab indicate that this accumulation occurs at least in part through the induction of stretch-induced signaling pathways (Lafont et al., manuscript submitted). Inflammation, angiotensin II signaling, and oxidative stress represent other factors involved in the development of TAAD (21;78;79). Additionally, SMC loss and/or SMC proliferation play a role in TAAD pathogenesis. Some debate exists, however, over whether SMC loss, SMC proliferation, or a combination of both occurs in aneurysms (80-82). Upon pathologic examination of aneurysmal aortic tissues, focal areas of SMC loss within the tissue are a clear and common finding. However, some studies have reported increased overall medial area combined with no change in SMC density in TAA, suggesting an increase rather than a decrease in SMCs (82). It is possible that an early proliferation is present, followed by later apoptosis and loss of SMCs. However, the specific contribution of cell proliferation to TAA formation is currently not known.

A growing body of evidence strongly suggests that SMC contractile dysfunction is one of the primary underlying defects leading to aneurysm formation, but the specific mechanisms by which SMC-specific contractile gene mutations cause contractile dysfunction and aneurysm formation are not yet known. Also, vascular disease in individuals heterozygous for contractile mutations is not confined just to the aorta. *ACTA2* and *MYH11* mutations lead to development of early onset coronary artery disease and stroke, in addition to TAAD. The segregation of additional vascular diseases in individuals heterozygous for these mutations represents a novel disease phenotype (83). A conclusive explanation of how aneurysms and occlusive diseases are caused by a single missense mutation is lacking. Investigation into the mechanisms leading to disease in these individuals should provide vital information about aneurysm formation, and may also provide insight into pathogenesis of these additional major cardiovascular diseases. Our overall hypothesis for this study is that that SMC-specific contractile gene mutations lead to both aneurysms and occlusive diseases through disruption of contractile filaments and loss of SMC contractility, coupled with a gain of function effect of the mutation, leading to increased SMC proliferation.

CHAPTER II

CHARACTERIZATION OF THE VASCULAR AND CELLULAR PHENOTYPE IN TAAD PATIENTS HETEROZYGOUS FOR *MYH11* MUTATIONS

Background

A study reported inheritance of thoracic aortic aneurysms/dissections associated with PDA in a single small family (84). Patent ductus arteriosus (PDA) results from a failure of the ductus arteriosus, the fetal blood vessel connecting the pulmonary artery to the aortic arch, to close properly at birth. Subsequently, Van Kien et al described familial TAAD accompanied by PDA in a large French family (85). The disease in this family was not associated with any other known locus for TAAD, or any other known locus for PDA. The disorder was hypothesized to occur due to a single gene defect (85). This hypothesis was confirmed when the disease in the French family was mapped to a single locus on chromosome 16p12.2-p13.13 using a genome-wide scan followed by fine mapping of the locus using microsatellite markers (86). In 2006, *MYH11* was identified as the disease-causing gene at this locus through sequencing in the critical interval on chromosome 16p (33). A heterozygous missense mutation and a splice-site mutation leading to deletion of exon 32 were identified in the French family, and a 72-base pair deletion in exon 28 was identified in the American family, whose TAAD/PDA had been previously reported in 2001. The mutations in both kindred were predicted to affect the coiled-coil structure of myosin, disrupting assembly of myosin filaments within the cell (33). Subsequently, our lab identified unique *MYH11* missense mutations in two unrelated families with the combined phenotype of TAAD and PDA (36). In the first family, an R712Q mutation was found in the ATPase head domain of myosin and was predicted to disrupt the ATPase activity. Two closely linked missense mutations, at R1275L and L1264P, were identified in the second family. Both residues are located on the coiled-coil domain of myosin, but only L1264P was predicted to disrupt coiled-coil formation (36).

MYH11 is the second gene to be associated directly with non-syndromic familial TAAD. Although *MYH11* mutations are relatively rare, they represent the first TAAD mutations found in a SMC-specific contractile gene, and study of the cellular effects of these mutations should yield important information about TAAD pathogenesis. All of the families assessed both by Zhu et al. and Pannu et al. displayed an inheritance pattern similar to TAAD caused by other mutations, including variable age of onset and decreased penetrance (33;36). Individuals with *MYH11* mutations were found to have increased aortic stiffness due to decreased compliance and distensibility prior to demonstrating aortic enlargement (86). Aortas of patients heterozygous for *MYH11* mutations showed typical features of medial degeneration, including fragmentation and loss of elastic fibers, areas of SMC loss, and accumulation of proteoglycans (33). Both the wildtype and mutant protein were expressed in equal amounts in the aortic wall; however, MYH11 in the mutant aortic tissue was found to be less stable. Normal immunostaining of MYH11 was observed in frozen aortic tissue from patients compared with controls, but MYH11 staining was absent in formalin-fixed tissues from patients, suggesting that the *MYH11* mutations render the protein more susceptible to denaturing by formalin fixation. Additionally, labeled mutant and wildtype constructs containing the rod domain failed to co-localized when both were expressed in Rb-1 cells (rabbit SMCs). Based on these data, the authors suggested that the mutant protein behaved in a dominant-negative manner (33).

Eight myosin heavy chain isoforms are expressed in muscle tissue, and multiple other isoforms exist as well (87). SM-MHC is an essential component of the SMC contractile apparatus, as shown by studies of knockout mice. SM-MHC knockout mice do not survive more than 72 hours after birth. These mice appear to be starved, and display a failure of proper bladder emptying, along with delayed closure of the ductus arteriosus, demonstrating the importance of this protein for proper SMC contractile function (88). Mutations in other myosin heavy chain isoforms also emphasize the indispensability of this protein in muscle contraction, and provide supporting evidence that *MYH11* mutations have deleterious effects on SMCs. Mutations in *MYH7* cause hypertrophic cardiomyopathy (89). Structural analysis of the *MYH11* mutations showed that the R712Q mutation present in one family is heterologous to the R705 mutations in *MYH9* that lead to hereditary deafness (36). The mutation in this nonmuscle myosin (myosin IIA) results in decreased stability of the protein structure, and reduced ability of the mutant myosin to couple ATPase activity with cell movement, resulting in decreased cell motility (90;91). Therefore, the mutation at R712 in *MYH11* is likely to also disrupt function of myosin within the cell.

Little is currently known about the specific pathogenic mechanisms associated with *MYH11* mutations. Some initial insight can be gained, however, through studies on mutations in other myosin heavy chain isoforms. Mutations in cardiac-specific α-actin and β-myosin cause familial hypertrophic cardiomyopathy (92). The disease is characterized by myocyte disarray and hypertrophy, and accumulation of extracellular matrix (92). Additionally, increased levels of mitotic and trophic factors, including insulin-like growth factor 1 (IGF-1), transforming growth factor β1 (TGF-β1), and platelet-derived growth factor β (PDGF-B) have been found in the myocardium of a subset of HCM patients (93-95). It has been hypothesized that altered cardiac contractility leads to increased production of growth factors, which may in turn play a role in HCM pathogenesis (96;97). Long-term overexpression of IGF-1 in mouse hearts leads to a phenotype of cardiac hypertrophy, extracellular matrix accumulation, and myocyte disarray compared with wild-type hearts, consistent with this hypothesis (98). Angiotensin II (Ang II) signaling may also contribute to HCM pathogenesis. AngII contributes to cardiac hypertrophy, and involvement of a renin-angiotensin system in pathogenesis of HCM has been reported (99;100). Specifically, ACE polymorphisms leading to increased ACE expression and concomitant increases in hypertrophy in individuals with HCM have also been reported (101). However, others have failed to find any association (102).

The same growth factors that are increased in HCM patients (TGF-β, PDGF, and IGF-1) also induce proliferation in SMCs (103). This suggests that the contractile defect may lead to the production and release of growth factors which, along with other stimuli, may be driving increased cellular proliferation in focal areas of the diseased tissue. Therefore, *we hypothesized that MYH11 patients' pathology is similar to the pathology observed in HCM.*

Materials and Methods

SMC isolation and culture

All studies involving human subjects were approved by the institutional review board at the University of Texas Health Science Center at Houston (UTHSCH), and informed consent was obtained from all study participants. SMCs, frozen aortic tissue, and paraffin-embedded tissue were obtained from one patient heterozygous for two closely linked *MYH11* mutations (L1264P and R1275L) and from controls who died of causes unrelated to vascular disease, and were processed according to an established protocol (21). An available H&E slide from a second patient heterozygous for a *MYH11* R712Q mutation was also obtained. Adventitial and intimal layers were removed from the aortic tissue. The remaining medial tissue was minced and digested in Waymouth's media (supplemented with 2.5 mM L-glutamine, 1 mM MEM non-essential amino acids, 100 mM Hepes buffer, sodium bicarbonate, and 1x antibiotic/antimycotic) and an enzyme mixture containing elastase type I (0.01875mg/mL), collagenase type I (0.1mg/mL), and soybean trypsin inhibitor (0.025 mg/mL). After 16 hours of incubation, enzymes were inactivated using FBS followed by SmBm containing insulin, rhEGF, rhFGF, antibiotic/antimycotic, and 15% FBS (Lonza). After centrifugation to remove remaining adventitial fat and any remaining Waymouth's media, tissue pieces were seeded into T25 flasks, and allowed to adhere for 4-6 weeks until SMCs migrated out of the tissue. SMCs were cultured in complete SmBm and passaged upon confluence.

RNA isolation

Cells were seeded at confluence into 60 mm dishes and allowed to adhere overnight. Cells were harvested following 18 hours of serum starvation (in media containing antibiotics only and not supplemented with serum or growth factors), and RNA was isolated using phenol-chloroform extraction (Trizol or Tri Reagent), according to the manufacturer's instructions. RNA samples were randomly tested for quality and purity using an Agilent Bioanalyzer. If necessary, RNA was purified using the RNeasy mini kit according to the manufacturer's instructions (Qiagen).

RNA was isolated from whole tissue using a similar phenol-chloroform extraction protocol. Briefly, small pieces of frozen tissue were minced in Trizol solution (Invitrogen) and then homogenized using a Polytron tissue homogenizer. Samples were centrifuged at high speed for 30 minutes at 4ºC to remove tissue pieces. Supernatants were transferred to new tubes, and RNA isolation was continued according to the manufacturer's instructions.

Gene expression analysis

50ng of total RNA from each sample was reverse transcribed in triplicate using a kit from Applied Biosystems. Quantitative PCR was carried out using pre-designed Taqman gene expression assays (Applied Biosystems, Foster City, CA) on either an ABI 7000 or ABI 7700 according to the manufacturer's instructions, with the exception that the final reaction volume was 20µL instead of 50µL. Thermal cycling parameters were as follows: 95.0ºC for 10 minutes, followed by 40 cycles of 95.0ºC for 15 seconds and 60.0ºC for 1 minute. Relative gene expression levels were calculated using the ΔΔCT method, using GAPDH as an endogenous control. Student's T-tests were used to determine statistical significance.

Histology

H&E and Movat's pentachrome stains were provided by the University of Texas-Medical School pathology core and Texas Heart Institute pathology core, respectively. Toluidine blue staining of cells was also performed by the UT pathology core.

Immunostaining of paraffin-embedded sections was performed as follows. Tissues were deparaffinized and rehydrated using a series of xylene, ethanol, and PBS washes for 2x5 minutes for each wash: xylene, 100% EtOH, 95% EtOH, 70% EtOH, and 1x PBS. Antigen retrieval was accomplished using 10mM citrate buffer, pH=6.0. Sections were submerged in citrate buffer and microwaved at 50% power for 9 minutes, followed by 1 minute at full power. Sections were monitored carefully to ensure that they did not dry out. Following antigen retrieval, sections were allowed to cool in citrate buffer for 40-60 minutes. Sections were blocked for 1 hour at room temperature in normal serum from the same species used to generate the secondary antibody (Vector Labs), and were incubated with primary antibody overnight at 4ºC (**Table 1**).

Table 1. Antibodies and dilutions.

Primary antibodies

antibody	company	species	IB	IHC	IF
β-actin	Sigma	mouse			1:100
CD3	Santa Cruz	rabbit		1:50	
CD68	Santa Cruz	rabbit		1:50	
CTGF	Santa Cruz	rabbit		1:50	
p-ERK1/2	Cell Signal	rabbit	1:1000		
ERK1/2	Cell Signal	rabbit	1:1000		
pY397 FAK	Millipore	mouse	1:750		1:50
FAK	Santa Cruz	rabbit	1:500		
Gapdh	Abcam	rabbit	1:2000		
Gapdh	Fitzgerald	mouse	1:20,000		
IGF-1	Santa Cruz	rabbit		1:25	
SM α-actin	Sigma	mouse	1:5000	1:200	1:100
PAI-1	Santa Cruz	rabbit		1:50	
PCNA	Zymed	mouse		pre-diluted	
phalloidin-Texas Red	Invitrogen	n/a			1:40
pSmad2/3	Santa Cruz	rabbit		1:50	
tensin	Santa Cruz	rabbit		1:25	
vinculin	Sigma	mouse-FITC			1:500
von Willebrand factor	Dako	rabbit		1:200	
zyxin	Santa Cruz	goat			1:25

Secondary antibodies and fluorophores

antibody or fluorophore	company	application	dilution
rabbit-HRP	Jackson Immunoresearch	IB	1:2000-1:5000
mouse-HRP	Jackson Immunoresearch	IB	1:2000-1:20,000
goat-AP	Santa Cruz	IF	1:100
mouse-AP	Vector Labs	IHC	1:200
rabbit-AP	Vector Labs	IF, IHC	1:100-1:200
mouse-FITC	Jackson Immunoresearch	IF	1:100-1:200
Fluorescein-streptavidin	Vector Labs	IF	1:100
Texas Red-streptavidin	Vector Labs	IF	1:100

****

The following day, tissue sections were washed 2x in PBS and incubated with the appropriate secondary antibody (Vector Labs) for 1 hour at room temperature, at a 1:200 dilution. Sections were washed 2x in PBS, incubated for 1 hour with a working dilution of avidin-biotin conjugating reagent (Vector Labs), and washed 2x in PBS. A Vector Red substrate kit was used to visualize immunostaining, and sections were counterstained with hematoxylin, dehydrated, and mounted with coverslips using Permount (Fisher). Specimens were viewed and photographed using an Olympus BX60 microscope (Olympus). Images were processed and prepared for publication using Adobe Photoshop 6.0.

For toluidine blue staining, SMCs were seeded at a density of 5000 cells per 22 mm glass coverslip, allowed to attach overnight, serum starved for 24 hours, and fixed with 4% paraformaldehyde for 10 minutes. Toluidine blue staining was performed by the Histology/IHC Laboratory at The University of Texas Medical School.

TGF-β1 treatment of SMCs and immunofluorescence

SMCs were seeded onto 22 mm glass coverslips at a density of 5,000 cells per coverslip and allowed to attach overnight before serum starving. Following 24 hours of serum deprivation, media was replaced with fresh serum-free media containing TGF-β1 (5ng/mL). Cells were fixed in 4% paraformaldehyde 72 hours post-TGF-β1 treatment. Coverslips were blocked for 30 minutes in PBS containing 1% BSA and 0.1% Tween20, and incubated overnight with primary antibody at 4ºC. The following day, coverslips were incubated with a FITC-conjugated mouse secondary antibody (1:200, Jackson Immunoresearch, West Grove, PA) for one hour followed by Texas Red-conjugated phalloidin for 30 minutes, and were mounted onto slides with Vectashield mounting medium with DAPI (Vector Labs, Inc., Burlingame, CA). **Table 1** lists antibody and fluorophore concentrations used. Immunofluorescently labeled SMCs were viewed and photographed using an Axioskop40 microscope, Axiocam MRm camera, and Axiovision software (Zeiss, Thornwood, NY).

Cell counting

Ten high-powered fields (400x) were photographed of each SM α-actin stained aortic tissue sample from two controls, and from the sinuses of Valsalva and ascending aorta of the *MYH11* patient. SM α-actin positive cells from the high-powered fields were counted and averaged. To assess the number of actively proliferating cells, similar photographs were taken of ten high-powered fields from each PCNA stained aortic tissue from patient and controls. Both the total number of cells and the number of PCNA positive cells from each section were counted, and the percent of actively proliferating cells was calculated. Data are represented ± S.D., and statistical significance was determined using a Student's T-test.

Organ culture and ELISA

A previously established protocol was used in order to assess the secretion of cytokines from whole aortic tissue of patients and controls (104;105). Stock solution of ITS was prepared, containing 0.5mg/mL insulin, 0.5 mg/mL transferrin, and 0.5 µg/mL sodium selenite (Sigma-Aldrich, Inc.). 10µl of ITS stock solution was added to 990ul DMEM containing 0.1% BSA. Whole aortic tissue segments from the *MYH11* patient and two unaffected controls were isolated, excess fat tissue was removed, and tissue was weighed to ensure that equal amounts of tissues were used for the organ culture. Aortas were completely submerged and incubated in the DMEM-ITS solution for 3 hours at 37ºC. The tissue culture supernatant fraction was collected and immediately frozen in 200µL aliquots and stored at -80ºC until analysis. Secretion of a panel of cytokines was analyzed using a Bio-Plex Suspension Array System (Bio-Rad Laboratories, Inc.), and was performed as previously described (104). An ELISA was performed to quantify Ang II production. Organ culturing was performed by Dr. Yaozhong Liu, and the Bio-Plex cytokine assay and Ang II ELISA were performed in collaboration with the Brasier lab at University of Texas Medical Branch in Galveston.

Results

Unique vascular pathology in two patients heterozygous for MYH11 mutations

Staining of aortic tissue with Movat's pentachrome stain provided the advantage of being able to visualize multiple components of the vascular wall simultaneously. This stain labels cells red, proteoglycans blue, collagens yellow, elastic fibers black, and nuclei violet, allowing for rapid identification of various features of medial degeneration. Aortic tissue from one patient heterozygous for two closely linked *MYH11* missense mutations (L1264P and R1275L) showed typical features of medial degeneration, including fragmentation of elastic fibers, accumulation of proteoglycans, and some areas of SMC loss, consistent with findings by Zhu et al (33). SM α-actin immunoreactivity also appeared to be normal in these tissues (data not shown). H&E staining of aortic tissue was available from one additional patient heterozygous for a different *MYH11* mutation (R712Q). In contrast to both the control aorta and the aorta of a patient with Marfan syndrome, both aortas from patients with

MYH11 mutations displayed areas of SMC accumulation within the medial layer (**Figure II-1**).

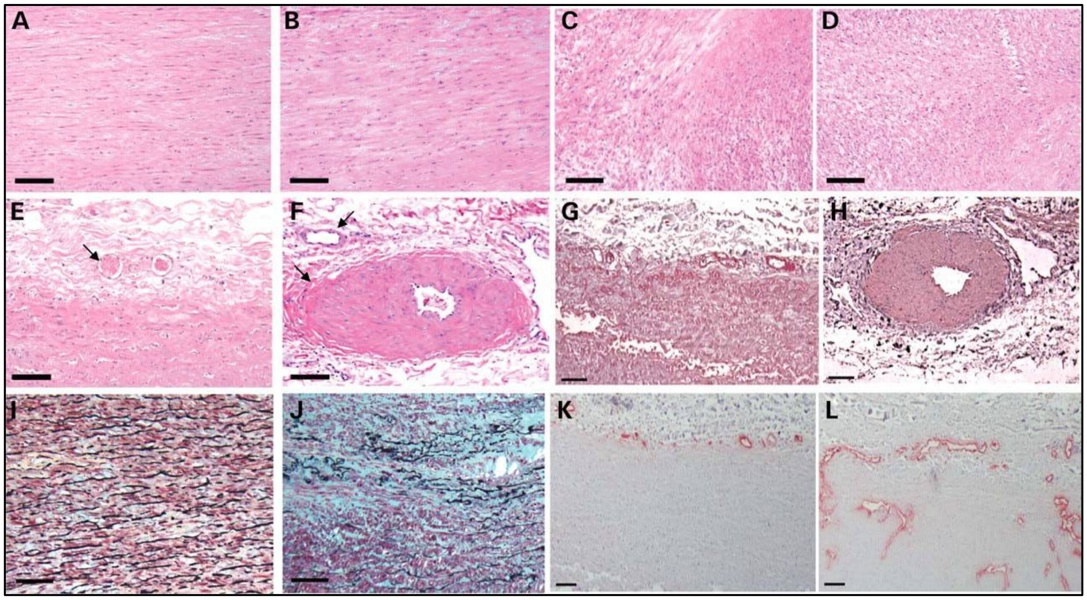

Figure II-1. Aortic pathology associated with *MYH11* mutations. H&E staining showed normal alignment of SMCs in control (A) and a Marfan patient (B), but focal areas of SMC hyperplasia and disarray in two *MYH11* patients (C, R712Q mutant and D, L1264P mutant). SMC hyperplasia was particularly apparent in the vasa vasorum of the *MYH11* patient. H&E staining of control (E) and *MYH11* L1264P mutant (F) aortic tissue showed enlargement of the vasa vasorum coupled with luminal narrowing in some vessels, whereas other vessels appeared normal, as indicated by arrows. SM α-actin staining revealed normal vasa vasorum in the control (G), and confirmed that vessel thickening in the *MYH11* patient was due to SMC hyperplasia (H). Movat staining of the aortic media from control (I) and patient (J) showed typical features of medial degeneration in the *MYH11* patient, including proteoglycan accumulation (blue), fragmentation and loss of elastic fibers (black), and focal areas of SMC loss. Von Willebrand factor staining showed that the *MYH11* patient had a dramatic increase in the number of small vessels penetrating deep into the medial layer (L)

compared with controls (K). Scale bars represent 100 µm. Reprinted by permission from Oxford University Press (36), copyright (2007).

****

Additionally, SMCs in areas of the media were oriented in random directions, in contrast to controls, which had SMCs and elastic fibers organized in concentric layers perpendicular to the axis of mechanical stretch. Although hyperplasia has been reported in TAA development, aneurysms are often characterized by SMC loss (19;80;82). The combination of hyperplasia and cellular disarray represent a novel aortic phenotype in TAAD patients.

In addition to cellular disarray and accumulation in the media, a number of vessels in the vasa vasorum of the *MYH11* patient heterozygous for an L1264P mutation showed enlargement and thickening, based on H&E staining. Staining for SM α-actin and counterstaining for nuclei confirmed that this thickening is due to SMC proliferation (**Figure II-1**). Thickening occurred in some, but not all, of the vasa vasorum, suggesting that the contractile mutation is the primary defect, and a secondary insult to the vessel wall triggers the hyperplastic response.

At the time of surgical aortic repair, the surgeons noted an unusual, visible increase in vascularity in this particular patient. Von Willebrand staining, specific for endothelial cells, was used to confirm the increased vascularity. In normal aortic walls, the vasa vasorum are mainly confined to the adventitia and the adventitia-media border. In sharp contrast to controls, the *MYH11* patient showed a dramatic increase in the number of small blood vessels penetrating into the medial SMC layer of the aortic wall (**Figure II-1**).

Increased proliferation and accumulation of SMCs in the MYH11 aorta

Counting of SM α-actin positive cells in aortic tissue sections from the ascending aorta of two controls, and sections taken from the sinuses of Valsalva and from the ascending aorta in the *MYH11* patient revealed a significant increase in cell number in the patient's aorta (**Figure II-2**).

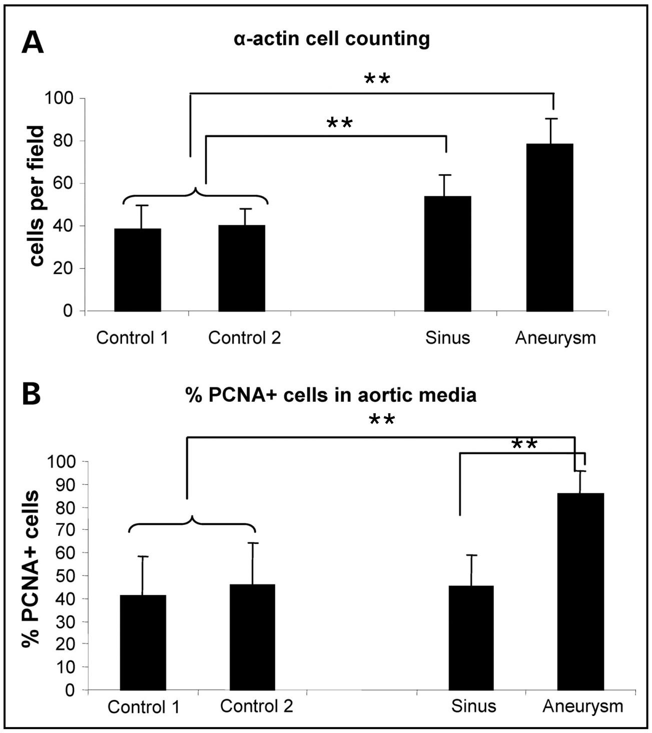

Figure II-2. SMC hyperplasia and increased SMC proliferation due to *MYH11* mutations. (A) Significantly greater numbers of SM α-actin positive cells were found in *MYH11* aortic tissue, and this was consistent for tissue taken either from the aneurysmal portion of the aorta or from the sinuses of Valsalva. (B) Immunostaining of tissues with PCNA, a proliferative marker, showed a significantly higher percentage of actively proliferating SMCs in the medial layer of the patient's aneurysmal tissue compared with controls and with the sinuses of Valsalva. Error bars represent S.D. **p<0.01. Reprinted by permission from Oxford University Press (36), copyright (2007).

****

This observation was significant both in the undilated aortic root (sinuses of Valsalva) and in the aneurysmal portion of the aorta (ascending). These data confirm that the increase in cellularity is due to increased numbers of SMCs rather than inflammatory cells or a different cell type. To determine whether these cells represented actively proliferating SMCs, we immunostained the cells for PCNA, a nuclear marker for actively proliferating cells, and counted the number of PCNA positive nuclei as well as the total number of nuclei under high power magnification. A significantly higher percentage of SMCs in the patient's ascending aorta, at the site of aneurysm formation, were actively proliferating, compared with the controls ($p<0.01$). However, although increased nuclei were present in the patient's sinuses of Valsalva, no significant difference in the percent of PCNA positive cells was found between the sinuses and the controls. There was a significantly higher percentage, however, in the number of actively proliferating cells in the patient's ascending aneurysm compared with the patient's sinuses of Valsalva ($p<0.01$). Although myocyte hypertrophy is one of the hallmark features of HCM, toluidine blue staining did not reveal any apparent differences in cell size in the *MYH11* patient compared with controls (data not shown).

Increased IGF-1 but not TGF-β1 or PDGF-B expression

Since TGF-β1, PDGF-B, and IGF-1 were all reported to be increased in tissues of HCM patients, we analyzed expression of these growth factors in our explanted SMCs, as well as in whole frozen aortic tissue samples (93-95). IGF-1 transcript levels were significantly increased in the patient's SMCs, and IGF-1 immunoreactivity was increased in the patient's aortic tissue compared with controls. TGF-β1 was not increased, and PDGF-B was decreased compared with the controls (**Figure II-3**).

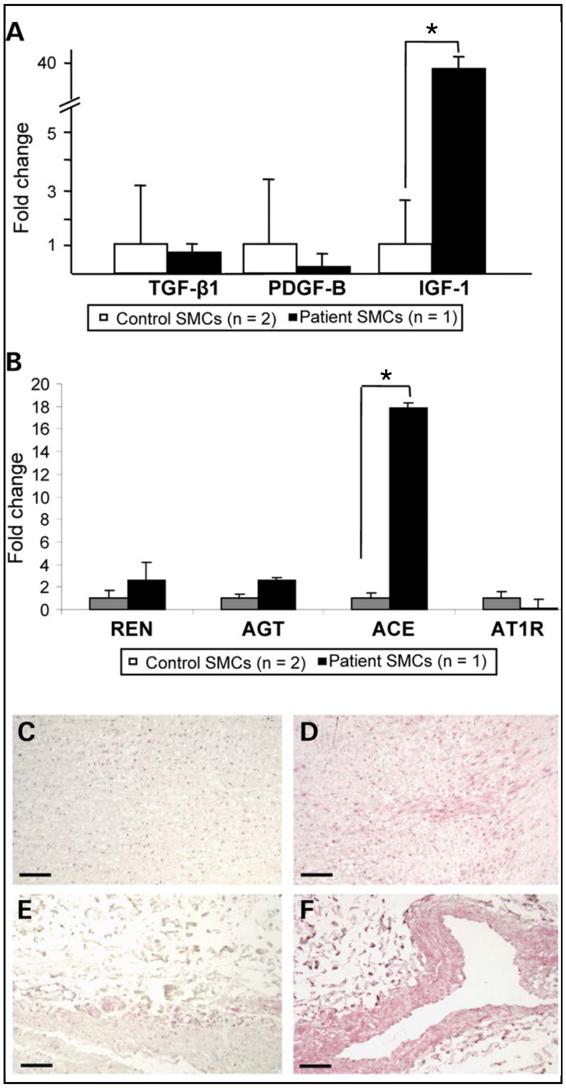

Figure II-3. IGF-1 and ACE expression are increased in *MYH11* mutant SMCs and tissues. (A) IGF-1 gene expression is significantly increased in SMCs explanted from the *MYH11* mutant aorta compared with controls. In contrast, TGF-β1 and PDGF-B levels are not significantly altered. (B) ACE gene expression is significantly increased in *MYH11* SMCs compared with controls. In contrast, other RAS components including renin (REN), angiotensinogen (AGT), and angiotensin II type I receptor (AT1R) are not significantly altered. Gene expression data are normalized to GAPDH, and error bars represent S.D. $^*p<0.05$. (C-F) IGF-1 immunoreactivity was increased in both the aortic media and

hyperplastic vessels in the adventitia in the *MYH11* tissue (D,F) compared with control (C,E). Reprinted by permission from Oxford University Press (36), copyright (2007).

****

Increased TGF-β1 activation has been reported in aneurysms in a mouse model of Marfan syndrome; therefore, we sought to determine whether pathways downstream of TGF-β1 were activated in the *MYH11* cells and tissue (10). Phosphorylated Smad2/3 is an early marker of activated TGF-β1 signaling; however, we did not find any difference in Smad2/3 phosphorylation in the patient aorta compared with controls (data not shown). Immunostaining for two other downstream markers of TGF-β1 signaling, CTGF and PAI-1, also failed to reveal any difference in TGF-β1 activation (data not shown). These data suggest that TGF-β1 signaling is not increased in the MYH11 aorta. However, IGF-1 immunoreactivity was increased in the patient's aortic tissue compared with controls (**Figure II-3**). Thus, IGF-1 but not TGF-β1 or PDGF-B, is increased in response to *MYH11* mutations.

Potential role for a local renin-angiotensin system in the disease process

Although the majority of IGF-1 in the body is produced in the liver and circulates throughout the body, IGF-1 can also be locally produced in an autocrine/paracrine manner. IGF-1 expression can be upregulated through multiple pathways in SMCs, including through mechanical stress, oxidative stress, growth factor signaling, and Ang II-mediated signaling (106). We also analyzed production of pro-angiogenic and pro-proliferative cytokines using a multiplex ELISA, and found striking increases in MIP-1-α and MIP-1-β. MIP-1-α is of particular interest because Ang II infusion results in increased MIP-1-α production in the aorta (104) (**Figure II-4A**).

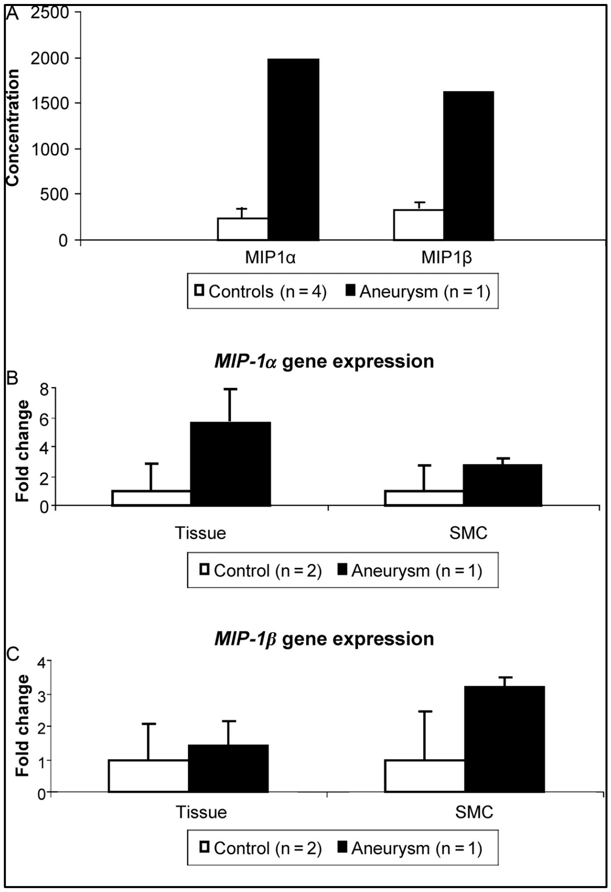

Figure II-4. MIP-1α and MIP-1β expression are increased in *MYH11* SMCs and tissues. (A) Organ culture followed by a Bio-Plex cytokine assay revealed increased secretion of MIP-1α and MIP-1β from the *MYH11* aorta (n=1) into the culture media compared with controls (n = 4). Concentrations are expressed in units of pg/mL. (B,C) MIP-1α and MIP-1β gene expression were increased in *MYH11* SMCs and aortic tissue, compared with controls. Error bars represent SD. Bio-Plex cytokine assay was performed by Dr.Yao-Zhong Liu in collaboration with The University of Texas Medical Branch at Galveston. Reprinted by permission from Oxford University Press (36), copyright (2007).

****

QPCR analysis of explanted SMCs and aortic tissues confirmed an increase in gene expression of these cytokines, suggesting that these are being produced specifically by SMCs rather than other cell types in the aortic wall (**Figure II-4B,C**). MIP-1α is expressed in response to angiotensin II signaling, leading us to hypothesize that a local renin-angiotensin system is contributing to the observed increase in IGF-1. Gene expression of renin-angiotensin system components in aortic tissue and explanted SMCs showed an increase in angiotensin-converting enzyme, but not renin, angiotensinogen, or angiotensin II type I receptor. Data from explanted SMCs are shown in **Figure II-3**; data from whole aortic tissue was consistent with the explanted SMCs. Due to the dramatic increase in ACE expression, we expected to also find increased secretion of angiotensin II by the *MYH11* SMCs. However, an angiotensin II ELISA, as well as angiotensin II immunostaining of aortic tissue, failed to show a difference in angiotensin II secretion by the whole aortic tissue section (data not shown).

Inflammation and MYH11 TAAD

Vascular wall inflammation is present in a subset of TAAD and may play an important role in pathogenesis. Since MIP-1α and MIP-1β are inflammatory cytokines and both the secreted cytokines as well as mRNA levels were increased in the *MYH11* patient, we hypothesized that inflammation is present in *MYH11* TAAD pathogenesis. MIP-1α is produced by macrophages; therefore, we hypothesized that medial tissue in the *MYH11* aorta would contain significant numbers of macrophages compared with control tissues. However, immunostaining for CD3, a T-cell antigen, and CD68, a macrophage marker, did not reveal any major inflammation. Counting of CD68 positive cells under high-powered fields failed to reveal a significant difference in the numbers of macrophages in the patient vs. the controls (data not shown).

Disruption of contractile filament assembly or stability

The missense mutation L1260P is predicted to disrupt the structure of MYH11. This mutation is located in the coiled-coil domain of the protein and is predicted to disrupt coiled-coil formation and/or stability (36). However, it was not known whether alterations in the myosin filaments disrupted the structure of other contractile proteins within the cell. Initial immunofluorescent staining did not show strong SM α-actin labeling; therefore, SMCs were treated with TGF-β1, a known inducer of SMC differentiation, to induce increased expression of contractile proteins. 72 hours post TGF-β1 treatment, *MYH11* SMCs expressed SM α-actin, but the actin was not organized into contractile filaments within the cell, in contrast with controls (**Figure II-5**). These data support the idea that disrupting one element of the contractile apparatus also disrupts other contractile elements within the cell and ultimately leads to decreased contractile function.

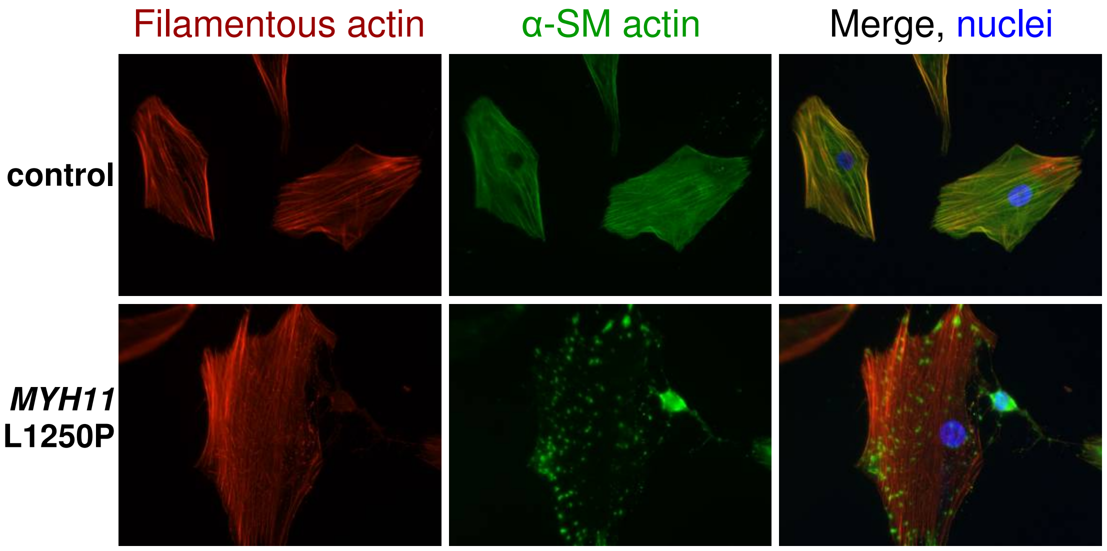

Figure II-5. Decreased SM α-actin polymerization in *MYH11* SMCs. Explanted control and *MYH11* mutant SMCs were treated with 5ng/mL TGF-β1 to enhance SM α-actin expression, after initial immunostaining for SM α-actin failed to yield results. Phalloidin-labeled actin filaments (red) remained unaltered in the mutant SMCs; however, SM α-actin filaments are disrupted in the *MYH11* mutant SMCs. Focal areas of SM α-actin staining were observed, suggesting that filaments begin to form but are prohibited by defective MYH11 from fully assembling by within the cell.

****

Discussion

We have described a novel pathology associated with *MYH11* mutations, including SMC hyperplasia and disarray in the aortic wall, hyperplastic vasa vasorum, and increased IGF-1 expression, in addition to typical features of medial degeneration. The observed disarray, growth factor production, and ECM accumulation were similar to findings in HCM patients, with the exception that proteoglycan rather than collagen was increased in the *MYH11* patient. In contrast to HCM, we observed SMC hyperplasia rather than hypertrophy. This hyperplasia is significant because some controversy exists over whether SMC loss or SMC hyperplasia occurs in aortic aneurysms (80-82). In one study, SMC loss was reported in approximately 50% of TAAs (19). Another study showed that SMC loss was important, but the study focused on abdominal aneurysms, which differ from TAA in their etiology and pathogenesis (80). More recently, a different study suggested that SMC hyperplasia is an initial adaptive response during early stages of aneurysm formation (82). This idea is supported by the fact that SMC hyperplasia was observed in the vasa vasorum of the *MYH11* patient, who had a rapidly expanding aneurysm at the time of surgical repair. Therefore, identifying the pathways leading to SMC hyperplasia is important for understanding familial TAAD.

Others have reported abnormal thickening of the vasa vasorum in thoracic aortic aneurysms, and blockage of the vasa vasorum renders the aorta more prone to dissection (19). The extent of vasa vasorum thickening appeared to be greater in the *MYH11* patient than in patients with *FBN1* or *TGFBR2* mutations, however. Future studies will determine whether an increased amount of vasa vasorum thickening is commonly present in individuals with mutations in other SMC-specific contractile genes.

In addition to SMC hyperplasia, the marked increase that we observed in IGF-1 warrants follow-up for several reasons. First, IGF-1 can be locally produced by SMCs, and multiple studies have demonstrated that this leads to an increase in cell proliferation. For example, treatment of rat vascular SMCs with exogenous IGF-1 induced an increase in proliferation, and this effect was inhibited with an IGF-1 neutralizing antibody. Additionally, exposing the rat SMCs to cyclic stretch caused both an increase in IGF-1 secretion and in cellular proliferation, which was also blocked by treatment with an IGF-1 antibody (107). Second, in addition to its role in SMC proliferation, IGF-1 plays an important role in regulating contractility. Aortas from mice that chronically overexpress IGF-1 generate more force when contracting than wildtype mouse aortas. Overexpression of an inhibitor of IGF-1 action, IGF binding protein 4 (IGFBP4), prevents this increase (108). Additionally, IGF-1 causes an increase in both α-actin and myosin expression in vascular SMCs (108;109) The dual role for IGF-1 in SMCs, together with data from the *MYH11* patient, suggest that IGF-1 may be increased in response to improper contractile filament assembly or stability, and may play a role in driving the observed SMC proliferation. Further, the fact that IGF-1 can be pathologically increased in response to vascular injury further emphasizes its potential importance in pathogenesis of TAAD in *MYH11* patients. For example, IGF-1 levels were increased in rat aortas that were surgically banded near the renal artery to induce hypertension (110). Also, IGF-1 levels are increased in response to arterial balloon injury (111;112). Additional studies have shown that increased IGF-1 levels are capable of causing increased proliferation in response to vessel injury. In mice that are genetically modified to overexpress IGF-1 in SMCs, disruption of the endothelium in the carotid artery leads to increased SMC proliferation and migration (113).

Unexpectedly, experimental evidence suggested a potential role for a local renin-angiotensin system in *MYH11* disease pathogenesis. The increase in ACE expression by explanted SMCs, along with increased secretion of MIP-1α, suggest that Ang II production and signaling are increased in the *MYH11* patient. Ang II is known to induce cardiac hypertrophy, as well as SMC proliferation. Additionally, Ang II infusion is an established model of abdominal aneurysms (114). However, contribution of a local renin-angiotensin system is difficult to assess, and conflicting data exist as to whether alterations in renin-angiotensin system components are associated with HCM. ACE is a circulating enzyme and is secreted by endothelial cells. Therefore, it is possible that ACE expression is due to the increased vascularity observed in the *MYH11* patient. However, the fact that explanted SMCs specifically express increased ACE does not support this possibility. Primary endothelial cells are technically difficult to isolate and culture, and as much endothelium and adventitia as possible are scraped away during SMC isolation; thus, the SMC explant protocol used is unlikely to result in contamination of SMC culture with endothelial cells. It is also possible that the increased ACE expression in the *MYH11* patient is due to a polymorphism coincidental with the *MYH11* mutation, similar to some cases of HCM (101). The ACE gene was not tested for polymorphisms in this individual.

In contrast to findings in mouse models of Marfan syndrome, we did not find evidence of increased TGF-β1 signaling in the MYH11 patient. TGF-β1 mRNA expression was not significantly altered. Phosphorylated Smad2/3, an early marker for activated TGF-β1 signaling, was not increased in the patient's aortic tissue. Additionally, the expression of CTGF and PAI-1, two proteins known to be increased in response to TGF-β1 signaling, remained unaltered. These data suggest that additional mechanisms other than dysregulated TGF-β1 signaling are driving the disease process due to *MYH11* mutations. The observed increase in IGF-1, together with the established roles for IGF-1 in promoting SMC contractility and proliferation, suggest a potential role for IGF-1 in *MYH11* disease pathogenesis.

Interestingly, in addition to TAAD and PDA, patients heterozygous for *MYH11* mutations are also more likely to develop major occlusive cardiovascular diseases than unaffected family members, in the absence of other cardiovascular risk factors. In our families with identified *MYH11* mutations and in the large French family originally used to identify the mutations, 19% of individuals heterozygous for the mutation (5 out of 26) developed either early onset stroke or early onset CAD, but these diseases were absent in the family members who did not carry the mutation (Pannu et al, manuscript submitted). Additionally, *MYH11* mutations have been identified in patients with other forms of vascular disease, including 3 different missense mutations in individuals with premature CAD, 5 alterations (3 novel and 2 present in CAD) in individuals with early onset stroke, and 7 alterations in individuals with Moyamoya disease, which is a pediatric-onset ischemic stroke syndrome due to intimal fibrocellular accumulation in arteries in the circle of Willis (Pannu et al, manuscript submitted) (115).

One advantage of this study is that we were able to gain insight into aneurysmal disease at its peak of progression, in contrast to many other tissue samples that are obtained when the disease is more in its end stages. Although the mutation is rare and the sample size for this study was very small, the fact that the tissue sample came from a very rapidly expanding aorta provided us with a unique opportunity to gain insight into the disease process, as well as generate new hypotheses for follow-up in other TAAD patients. While we were conducting this study, mutations in multiple other SMC-specific contractile genes were identified, and the data obtained from this study was able to provide a starting point for analysis of subsequent contractile gene mutations.

One limitation of this study is that we did not directly assess disruption of myosin contractile filaments in *MYH11* mutant SMCs, either by immunofluorescence, due to technical difficulties with antibody staining, or by assessing myosin motor activity through ATPase assays. However, several lines of evidence, including more recent studies on several *MYH11* mutants, exist that argue in favor of the mutation disrupting contractile filaments. First, both software-predicted evidence and *in vitro* data exist to suggest that contractile function is disrupted. COILS software predicted a decrease in the probability of coiled-coil formation in L1260P mutant *MYH11* (36). The R712Q mutation is paralogous to a myosin IIA mutation that has already been shown to uncouple ATPase activity from the myosin motor as well as disrupt the thermal stability of the protein, contractile filaments are highly likely to be disrupted by this mutation as well (36). Additionally, previous reports of *MYH11* mutations show a predicted disruption in coiled-coil formation as well as increased denaturation of *MYH11* filaments after formalin fixation, indicative of a less stable protein (33). More recent *in vitro* assays have shown that a number of *MYH11* mutations in the ATPase head domain have reduced ATPase activity compared to wildtype (Pannu et al, manuscript submitted). Second, immunofluorescence data suggest that SM α-actin filament formation and/or stability is disrupted in the *MYH11* mutant SMCs. The stoichiometry of components of the contractile apparatus is highly regulated, and disruption of one component easily leads to disruption of other components (116). This idea is supported by the observation that *Acta2*$^{-/-}$ mouse aortas display fewer myosin thick filaments than wildtype, as assessed by electron microscopy (117). Therefore, MYH11 contractile filaments are likely to be disrupted by the mutations described in this study.

It is still unknown whether the *MYH11* SMCs are inherently more proliferative due to structural alterations in the cell, or whether the observed proliferation is caused by increased cellular stress and release of growth factors secondary to loss of cellular contractility and loss of elastic fibers in the aortic wall. However, current data as well as previous studies suggest that cell proliferation may play a key role in disease formation in these individuals, and that IGF-1 may be a key factor in this process. While we cannot completely exclude the involvement of other growth factors in the progression of this disease, we propose that a decrease in SMC contractility and subsequent increase in cellular stress induces the SMCs to overproduce IGF-1. The primary defect in the contractile apparatus in the cell may hinder the ability of IGF-1 to increase contractility, while still allowing for IGF-1-induced proliferation. Future studies will provide insight into the mechanism and role of increased IGF-1 expression by aortic SMCs in the pathology of familial TAAD due to *MYH11* mutations, as well as other mutations that result in a similar vascular pathology.

CHAPTER III

CHARACTERIZATION OF THE VASCULAR AND CELLULAR PHENOTYPE IN TAAD PATIENTS HETEROZYGOUS FOR *ACTA2* MUTATIONS

Background

Six different actin isoforms have been identified: SM α-actin (*ACTA2*), cardiac α-actin (*ACTC*), skeletal α-actin (*ACTA1*), smooth muscle γ-actin (*ACTG2*), cytoplasmic γ-actin (*ACTG1*), and cytoplasmic β-actin (*ACTB*) (118;119). The various actin isoforms are highly homologous, with greatest variability found near the N-terminus, but are not functionally redundant. SM α-actin comprises approximately two thirds of total actin and 40% of total protein within SMCs, making it the single most abundant protein in this cell type (120;121).

Several studies have shown that actin isoforms can partially but not fully compensate for loss of one isoform. Expression of *Actg2* rescues the lethality in *Actc*$^{-/-}$ mice, and partially but does not fully restore cardiac structure and function. Expression of *Actc* but not *Actg1* rescues the early postnatal lethal phenotype in *Acta1*$^{-/-}$ mice, demonstrating that in some cases one actin isoform can potentially be substituted for another (122;123). Some cardiac α-actin is expressed in humans in the absence of skeletal α-actin; however, the cardiac α-actin expression is unable to prevent disease in these individuals. The exact mechanisms determining specificity of each actin isoform are not known. All of these studies provide support for the idea that defects in the SM α-actin protein cannot be compensated for simply by the presence of other actin isoforms within SMCs.

Acta2$^{-/-}$ mice demonstrate decreased vessel contractility, underscoring the indispensability of SM α-actin for proper SMC contraction (117). Surprisingly, complete deletion of SM α-actin does not disrupt development of the cardiovascular system. Increased expression of *Acta1* and *Actg2* in vascular SMCs in these mice was identified, presumably to compensate for the loss of ACTA2 (117;124).

Other actin isoforms play an important role in SMC contraction as well. β-cytoplasmic actin and γ-actin make up 21% and 13% of total actin in vascular SMCs, respectively (120). Some debate exists over whether the various actin isoforms in SMCs can polymerize into the same actin filaments, or whether actin isoforms are compartmentalized within the cell (125;126).

The discovery of *MYH11* mutations leading to TAAD, along with novel pathologic findings associated with these mutations, led to the following questions: Are additional SMC-specific contractile proteins altered in TAAD? If so, do mutations in these other contractile proteins lead to a similar vascular pathology? Subsequent identification of mutations in SM α-actin provided answers to some of these questions. *ACTA2* missense mutations in TAAD were identified through linkage analysis and positional cloning (34). A large family was recruited for study but did not have mutations in *FBN1*, *TGFBR2*, or *MYH11*, and was not linked to any other known TAAD loci. The putative gene was mapped to chromosome 10q23-24 using an Affymetrix array followed by microsatellite markers for fine mapping of the critical interval. Twelve candidate genes were sequenced in the identified region, and a missense mutation in *ACTA2*, R149C, was identified. Sequencing of other familial TAAD samples revealed missense mutations at a total of eight different residues, in fourteen families, with recurrent mutations at R149C in five families, and R258C/R258H in three families (34). Additional mutations were subsequently identified both by our lab group and by others, including previously identified as well as novel mutations (83;127;128). Recently, de novo mutation of R179C leading to an exceptionally severe systemic clinical phenotype was identified in 5 unrelated children and young adults

(Dianna Milewicz, personal communication). All of the currently identified ACTA2 mutations are predicted to produce a mutant protein from the altered allele.

ACTA2 mutations showed a dominant inheritance pattern with variable age of disease onset and decreased penetrance (34). A subset of *ACTA2* mutation carriers also have PDA, livedo reticularis, or iris flocculi. Livedo reticularis is a condition caused by persistent occlusion of dermal capillaries leading to a purplish, netlike rash mainly on the upper and lower extremities, and iris flocculi are neoplastic cysts found in the iris. Since SMCs are present in the iris, it is possible that mutations in *ACTA2* may both disrupt contractile function and enhance proliferation, leading to cyst formation (127). Surprisingly, the penetrance for TAAD caused by *ACTA2* mutations was relatively low (0.48), even though the LOD score indicating that *ACTA2* is indeed linked to TAAD was statistically significant, with a value of 4.17 (34).

The mutations in SM α-actin are located throughout the gene, and are predicted to have differing functional effects, with a common endpoint of disrupting actin polymerization (34). N117, R118, and V154 may disrupt either nucleotide binding or hydrolysis, and are located near the nucleotide binding cleft. Y135, R149, and T353 disrupt the binding site for various regulatory and end-capping proteins. R292 may disrupt actin polymerization due to its close proximity to residues involved in actin-actin interactions. R258 mutations are predicted to disrupt actin interactions with nebulin (34).

The presence of livedo reticularis in some *ACTA2* patients led to the hypothesis that *ACTA2* mutations cause vascular occlusive diseases in addition to TAAD. Upon examination of family medical histories, early onset CAD, stroke, and Moyamoya disease were found to segregate with *ACTA2* mutations in affected families, and this was highly statistically significant. Further, the disease penetrance rose from 0.48 to 0.80 when individuals with occlusive diseases were included in the analysis. When analyzed separately, each major vascular phenotype showed a positive LOD score for linkage to the *ACTA2* gene, and the combined LOD score for all of the vascular phenotypes rose from 4.17 to 10.62 (83). Therefore, it was concluded that *ACTA2* mutations cause vascular occlusive diseases in addition to TAAD. The fact that *ACTA2* mutations are predicted to disrupt normal SMC contractile function suggests that decreased aortic contractility contributes to aneurysm formation. Interestingly, certain *ACTA2* mutations are more highly associated with premature CAD than stroke, while other *ACTA2* mutations are more associated with premature strokes and Moyamoya disease. Moyamoya disease is a bilateral occlusion of arteries in the circle of Willis due to SMC hyperplasia in the intimal layer of the vessel, and leads to early onset strokes (115). The most notable difference is between individuals with R149C mutations, which caused mainly TAAD and CAD, and individuals with R258C/H mutations, which caused mainly TAAD and stroke, along with Moyamoya disease (83).

Studies of mutations in other actin isoforms have provided valuable insight into mechanisms that may be driving disease in individuals with *ACTA2* mutations. *ACTC* mutations cause idiopathic dilated cardiomyopathy and familial hypertrophic cardiomyopathy (129;130). Mutations in either *ACTB* or *ACTG1* lead to deafness, and *ACTB* mutations also lead to developmental abnormalities and dystonia (131;132). *ACTB* mutations were also reported to cause severe mental retardation and recurrent infections (133). *ACTA1* mutations cause skeletal myopathy, and more mutations have been found in *ACTA1* than any other actin isoform to date (134;135). Studies of *ACTC* and *ACTA1* mutations provide the most valuable insight for our study, because several mutations in these genes are homologous to a number of mutations identified in *ACTA2* patients. Five mutations are found at homologous residues in both *ACTA1* and in *ACTA2* (34;83;135). Each of these mutations are predicted to disrupt function of *ACTA1* (135). Due to the highly conserved nature of actins, these data, along with the fact that no polymorphisms have been identified in the *ACTA2* gene, indicate that the alterations in *ACTA2* are pathologic (34). Additionally, information gained from *ACTA1* myopathies provide evidence that mutations in actin isoforms act in a dominant negative manner to disrupt contractile function of the cell (136).

Based these previous studies, the identified mutations in *ACTA2* are predicted to disrupt structure and function of the protein in a dominant negative manner. However, little is known about the mechanisms underlying disease pathogenesis in these individuals. Dysregulation of TGF-β1 plays an important role in the pathogenesis of aneurysms in MFS (10). However mutations in *MYH11*, another contractile gene, did not lead to increased TGF-β1 signaling but did lead to SMC hyperplasia, suggesting that mutations in SMC-specific contractile genes may result in a different mechanism of disease pathogenesis than previously described mutations. Our data from *MYH11* SMCs and tissues suggest a novel proliferative pathology due to a contractile gene mutation, and subsequent studies identified early-onset vascular occlusive diseases in patients with *MYH11* mutations (Pannu et al., manuscript submitted). *ACTA2* is the second SMC-specific contractile gene identified leading to TAAD, and also causes early-onset occlusive diseases including CAD, stroke, and Moyamoya disease. As mentioned previously, Moyamoya disease results from a progressive stenosis of the internal carotid arteries due to intimal hyperplasia (115). Collectively, these data suggest that *ACTA2* mutations should also lead to a proliferative pathology.

In summary, damaging mutations exist in most other actin isoforms, and studies particularly in *ACTA1* patients have shown evidence that the mutant protein disrupts contractile filament structure and interferes with the functioning of the remaining wildtype protein. Based on existing data in *ACTA1* and *ACTC* mutant individuals and mice, and our pathologic findings in the aortas of patients with *MYH11* mutations, *we hypothesize that ACTA2 mutations disrupt SM α-actin filaments and lead to a proliferative vascular pathology similar to MYH11.*

Materials and Methods

SMC explant and culture

All studies involving human subjects were approved by the institutional review board at the University of Texas Health Science Center at Houston (UTHSCH), and informed consent was obtained from all study participants. SMC explant, culture, and plating were performed as described in Chapter II.

Histology, Immunofluorescence, and Microscopy

Aortic tissues from 9 patients heterozygous for *ACTA2* missense mutations and from 6 controls were obtained (**Table 2**).

Table 2. Tissue samples used for study

aortic tissue samples

pedigree ID	mutation	age	sex	ethnicity
TAA105 II:4	R258H	49	F	NE
TAA166 II:2	Y135H	52	M	NE
TAA174 III:3	R118Q	47	M	NE
TAA313 II:2	T353N	49	M	NE
TAA327 III:19	R149C	36	M	NE
TAA327 IV:4	R149C	28	F	NE
TAA327 IV:5	R149C	26	M	NE
TAA455 II:11	R185Q	42	M	H
sporadic	I250L	43	M	NE

coronary and cardiac samples

pedigree ID	mutation	age	sex	ethnicity
TAA441:IV:3	R118Q	28	M	NE
TAA441:III:6	R118Q	50	M	NE
TAA015:III:1	R292G	53	F	NE

controls

control ID	age	sex	ethnicity
6437	48	F	NE
6701	68	F	NE
6625	47	M	H
2664	48	F	NE
7234	35	M	H
6559	69	M	H

Table 2. Tissue samples used for study. Sample ID, *ACTA2* mutation, age, gender, and ethnic origin of patient and aortic and cardiac tissues, and control aortic tissues utilized for study are listed. (For ethnic origins, NE = Northern European descent; H = Hispanic).

****

Coronary artery tissue from one patient and cardiac tissue from two patients became available, and were also obtained and analyzed (**Table 2**). Histology and immunofluorescent staining were carried out as described in Chapter II. For high-resolution images of SM α-actin staining, deconvolution microscopy was performed using a DeltaVision Deconvolution microscope system (Applied Precision, Inc.). Images were acquired and deconvolved using SoftWoRx 3.5 software. Images were obtained using 40x and 60x oil immersion objectives.

Cell proliferation assays

SMCs explanted from two patients heterozygous for *ACTA2* missense mutations and from two controls were plated in triplicate at a density of 10,000 cells per well in a 9-well plate (**Table 3**).

Table 3. Cell strains used for cell proliferation studies

Smooth Muscle Cells							
Family	**Patient ID**	**mutation**	**age**	**sex**	**Control ID**	**age**	**sex**
TAA313	II:2	T353N	49	M	MG8131	36	M
sporadic	MG5875	I250L	43	M	MG8438	43	F
Fibroblasts							
Family	**Patient ID**	**mutation**	**age**	**sex**	**Control ID**	**age**	**sex**
TAA018	III:1	P72Q	27	F	MG3015	23	F
TAA174	III:3	R118Q	47	M	MG3032	26	M
TAA327	IV:4	R149C	30	F	MG3008	32	M
TAA041	II:3	R149C	37	M	MG3018	36	F
TAA041	II:6	R149C	32	M	MG3017	38	M
TAA455	II:12	R185Q	42	M	MG3019	41	F
TAA455	II:8	R185Q	50	M	MG3031	43	M
TAA105	II:3	R258H	36	F	MG3033	48	F
TAA105	II:4	R258H	49	F	MG3002	49	M
					MG3027	53	F

Table 3. Cell strains used for cell proliferation studies. Age denotes the age of the individual at the time that an aorta or skin biopsy was obtained. Reprinted from (83), with permission from Elsevier.

****

After 24 hours, cells were placed in SmBm containing 0.2% FBS, and 5-bromo-2-deoxyuridine (BrdU), which replaces thymidine during DNA synthesis, was added. 24 hours post BrdU treatment, cells were fixed, and a BrdU ELISA was carried out according to the manufacturer's instructions (Millipore). Absorbance of each plate was read at 450nm, and this optical density reading was proportional to the amount of BrdU incorporation. Experiments were repeated three independent times on SMCs between passage 2 and 5. A Student's T test was used to determine statistical significance, with $p<0.05$ considered significant.

Quantitative Gene Expression

Total RNA was isolated and QPCR was performed as described in Chapter II. Data are represented as mean ± S.D., and Student's T tests were used to determine statistical significance, with $p<0.05$ considered significant.

Results

Histologic features of ACTA2 TAAD

Initially we examined the histology of the ascending aorta in patients with ACTA2 mutations who underwent aortic surgical repair. We had access to nine aortas from patients with the following mutations: R258H, Y135H, R118Q, T353N, R149C, R185Q, and I250L (**Table 2**). Similar to the *MYH11* aorta in Chapter II, we used Movat staining to visualize multiple components of the vascular wall. Movat staining of aortic tissue revealed features of typical medial degeneration as indicated by the accumulation of proteoglycans (blue) and loss of elastic fibers (black) (**Figure III-1A**).

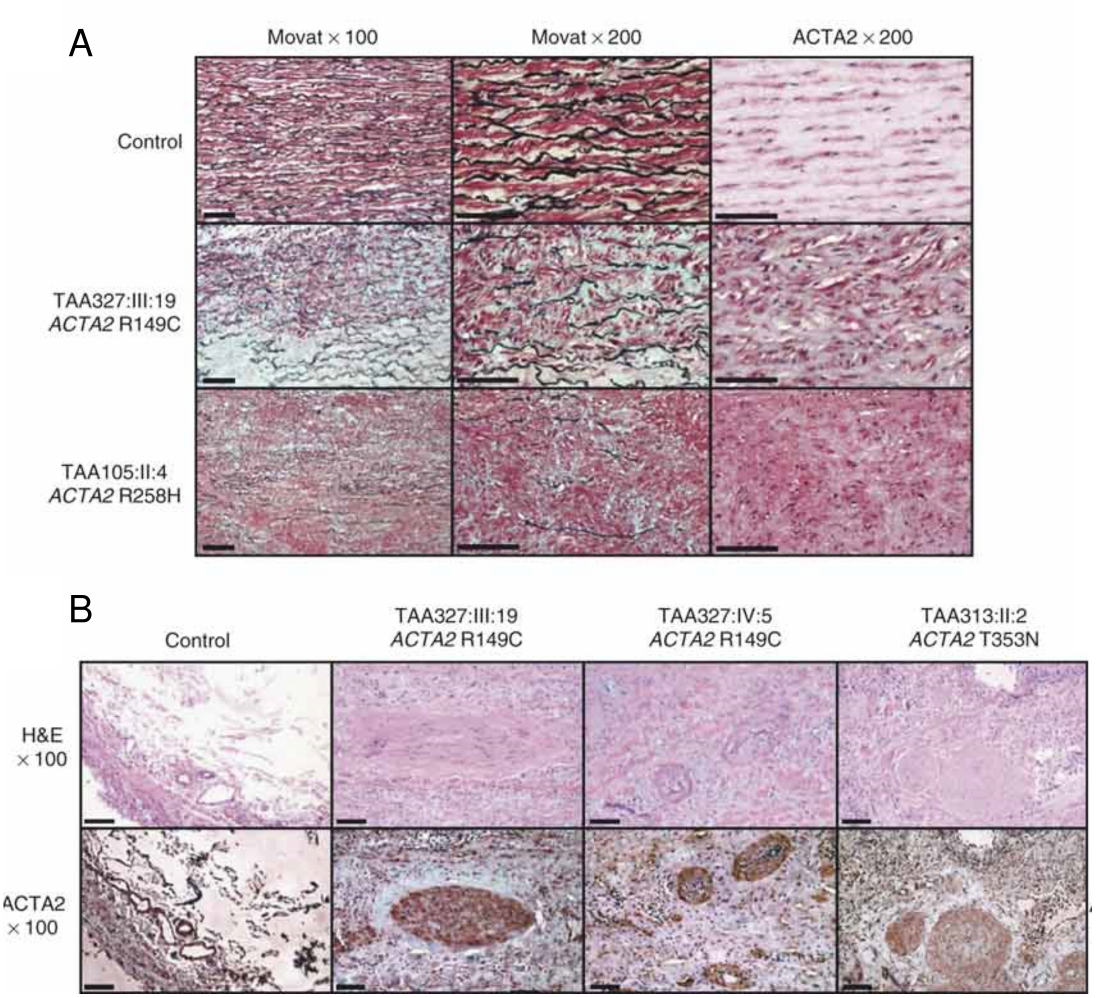
A
Movat × 100
Movat × 200
ACTA2 × 200
Control
TAA327:III:19
ACTA2 R149C
TAA105:II:4
ACTA2 R258H
B
Control
TAA327:III:19
ACTA2 R149C
TAA327:IV:5
ACTA2 R149C
TAA313:II:2
ACTA2 T353N
H&E
× 100
ACTA2
× 100

Figure III-1. Aortic pathology associated with *ACTA2* mutations. (A) Movat and SM α-actin immunostaining of the media from control and *ACTA2* mutant aortic tissues. Movat staining revealed typical features of medial degeneration in *ACTA2* mutant tissue compared with control, including areas of SMC loss, proteoglycan accumulation (blue), lack of collagen accumulation (yellow) and fragmentation and loss of elastic fibers (black). SM α-actin immunostaining revealed areas of SMC hyperplasia and disarray compared with control. (B) Both H&E staining and SM α-actin immunostaining showed hyperplastic vessels were present in the adventitia in *ACTA2* mutant aortic tissue but absent in control. The hyperplastic vessels were both enlarged in size and showed luminal narrowing, and in some

cases were completely occluded. SM α-actin immunostaining, along with von Willebrand factor staining (not shown) confirmed that these were blood vessels and that the hyperplasia was due to increased numbers of SMCs. Scale bars represent 100μm, and magnification for each panel is indicated. Reprinted by permission from Macmillan Publishers Ltd: [Nature Genetics] (34), copyright (2007). http://www.nature.com/

****

We also examined the aortas to determine whether features similar to the *MYH11* aorta were present, including disarray, focal areas with increased SMCs, and thickened vasa vasorum. Similar to *MYH11* mutations, aortas from *ACTA2* patients showed increased SMCs in focal areas, and we confirmed this by SM α-actin immunostaining (**Figure III-1A**). SMCs in the patients' aortas also displayed areas of random orientation with respect to each other, similar to the disarray observed in the *MYH11* aorta. The arteries in the vasa vasorum were also enlarged and thickened in *ACTA2* patients compared with similar arteries in control aortas. Despite the enlargement, the vessels were stenotic, and in some cases were completely occluded. We stained for an endothelial specific marker (von Willebrand factor, not shown) and α-SM actin to confirm that these were blood vessels (**Figure III-1B**). Immunostaining confirmed the identity of these structures as vessels, and also showed SMC hyperplasia. Data from two R149C mutant aortas and one T353N mutant aorta are shown, and these are representative of the enlarged vessels that were present in every *ACTA2* mutant aorta where adventitial tissue was visible (the adventitial layer was completely missing in one tissue sample). We also used Movat-stained tissue samples to examine the integrity of the internal elastic lamina, and determine whether the proliferation in the vessels was confined to the media, to a neointimal layer, or a combination of both. Movat staining confirmed that the internal elastic lamina of these vessels remained intact, and that vessel thickening was due to increased SMCs in the medial layer, rather than neointimal formation (not shown).

SMC proliferation and occlusion in other arteries

During the course of our study, coronary artery and/or cardiac tissue from three individuals with ACTA2 mutations became available for pathologic examination (**Table 2**). Coronary artery tissue was obtained from a 28 year old male of Northern European descent heterozygous for an R118Q mutation who died from an acute aortic dissection. He did not have any known risk factors for cardiovascular disease or any diagnosis of CAD prior to death. Initial H&E staining showed 70% narrowing of the vessel due to an atherosclerotic lesion combined with increased cellularity in both the medial and intimal layers of the vessel. We used a Movat stain to determine which ECM components were increased in the vessel wall, and immunostained with SM α-actin to confirm that the increased cellularity was due to increased SMCs. We observed that the lesion in this individual was due to an accumulation mainly of cells rather than lipids, in contrast to typical atherosclerotic plaques. SM α-actin immunostaining confirmed that the accumulated cells were SMCs (**Figure III-2A**).

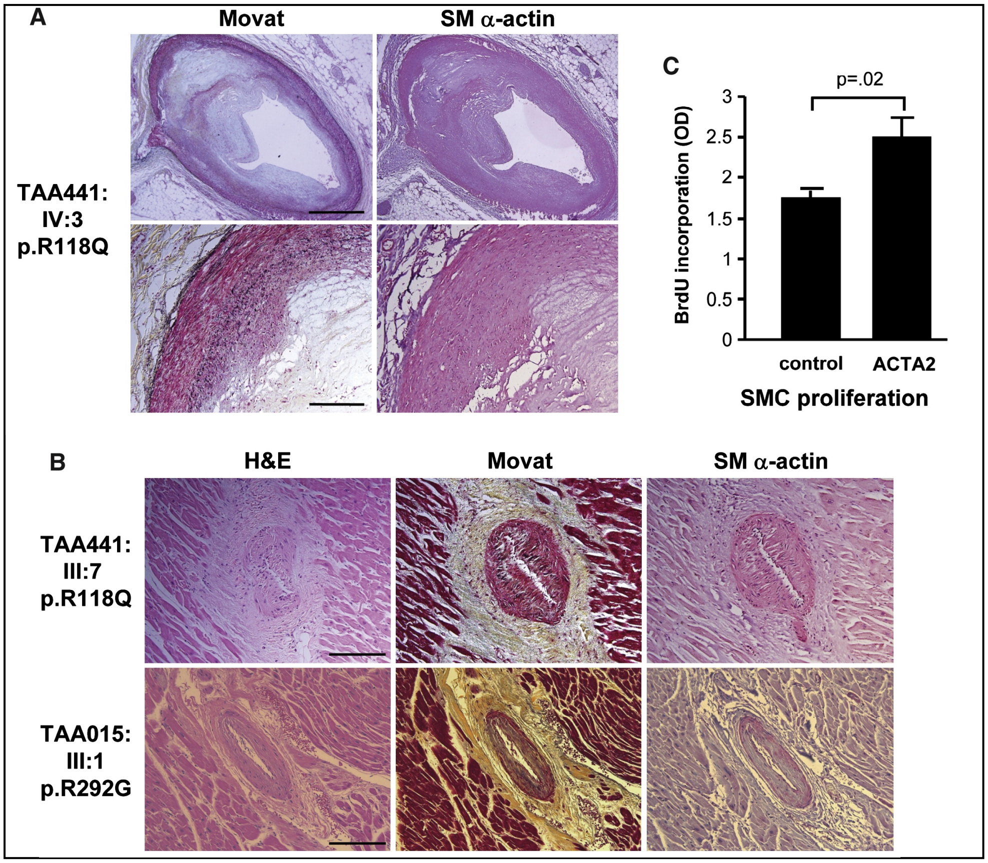
A
Movat
SM α-actin
TAA441:
IV:3
p.R118Q
C
p=.02
BrdU incorporation (OD)
3
2.5
2
1.5
1
0.5
0
control
ACTA2
SMC proliferation
B
H&E
Movat
SM α-actin
TAA441:
III:7
p.R118Q
TAA015:
III:1
p.R292G

Figure III-2. *ACTA2* mutations are associated with SMC hyperplasia and SMC proliferation in culture. (A) Coronary artery tissue from a 28-year-old male heterozygous for an R118Q *ACTA2* mutation showed 70% narrowing of the vessel, and this was due to a fibrocellular atherosclerotic plaque. Movat staining showed that this lesion was due mainly to accumulation of cells, and SM α-actin staining confirmed that these were SMCs. Scale bars represent 1.0mm in the top two panels (magnification 40x) and 200μm in the bottom two panels (magnification 200x). (B) Epicardial arteries from two individuals heterozygous for *ACTA2* mutations showed abnormal thickening. H&E, Movat, and SM α-actin staining are shown. The first individual (TAA441:III:6) had an R118Q mutation, and the second individual (TAA015:III:1) had an R292G mutation. (C) Cell proliferation assays showed that SMCs explanted from patients heterozygous for *ACTA2* mutations (n = 2) proliferated

significantly more rapidly than matched control SMCs (n = 2), as quantified by ELISAs for BrdU incorporation. Error bars represent S.E.M. and p-value is indicated. Reprinted from (83), with permission from Elsevier.

****

Cardiac tissue was obtained from two patients, neither of whom were at high risk for CAD. The first sample was from a male of Northern European descent heterozygous for an R118Q mutation, who first had an acute aortic dissection at age 50, diagnosed with CAD at age 54, and died at age 59 after having a chronic aortic dissection surgically repaired. Pathologic examination of the tissue showed abnormal thickening of epicardial arteries. We used SM α-actin and MOVAT staining to confirm that this thickening was due to SMC accumulation in the medial layer. The second sample was from a 53 year old Northern European female heterozygous for an R292G mutation, who died of unknown causes. Similar to the first tissue sample, abnormal thickening of epicardial arteries was found and noted at autopsy (**Figure III-2B**). Together, these data support the idea that pathologic changes due to *ACTA2* mutations are not just confined to the aorta but are present in multiple vascular beds, including coronary arteries.

SM α-actin expression, polymerization, and localization

Based on predicted structural alterations due to *ACTA2* mutations, we hypothesized that SM α-actin filament formation would be impaired. To test this hypothesis, we immunolabeled SMCs explanted from *ACTA2* patients and matched controls with both SM α-actin and phalloidin, which binds to all polymerized actin within the cell. Filaments in control SMCs extended across the cell body and colocalized with total actin filaments within the cell. *ACTA2* patients also showed filaments composed of other actin isoforms, but little to no SM α-actin-containing filaments. These data indicate that *ACTA2* mutations result in a decrease in formation and/or stability of SM α-actin filaments (**Figure III-3**).

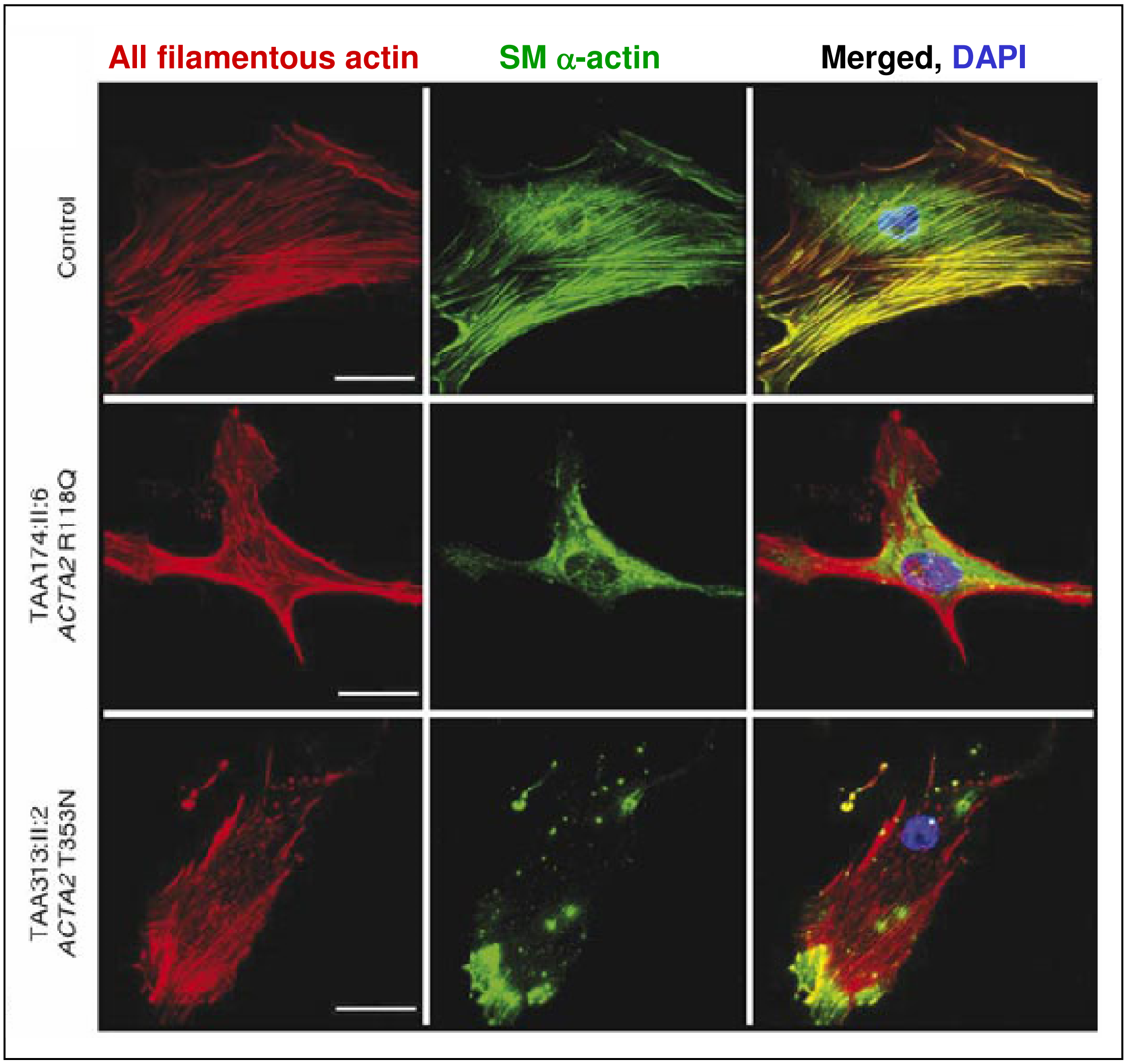
All filamentous actin
SM α-actin
Merged, DAPI
Control
TAA174:II:6
ACTA2 R118Q
TAA313:II:2
ACTA2 T353N

Figure III-3. SM α-actin filament disruption due to *ACTA2* mutations. Analysis of actin stress fibers in SMCs explanted from control (top row) and *ACTA2* mutant aortas (bottom two rows). The left panels show phalloidin staining of total filamentous actin (red), the middle panels show SM α-actin (green), and the right panels show a merged image. SM α-actin filaments were greatly reduced in *ACTA2* mutant SMCs. Double labeling of the SMCs for total actin filaments showed that filamentous actin and SM α-actin were colocalized in

the control SMCs. Little to no colocalization was observed in the *ACTA2* mutant SMCs. Scale bars represent 40µm; magnification = 400x. Reprinted by permission from Macmillan Publishers Ltd: [Nature Genetics] (34), copyright (2007). http://www.nature.com/

****

Interestingly, in the two samples available for study, actin filaments were disrupted to differing degrees. In SMCs heterozygous for an R118Q mutation, actin accumulated in the perinuclear region of the cell, and little to no filament assembly was observed. A T353N mutation resulted in formation of rodlike structures at the cell periphery. However, SM α-actin filament formation was still greatly impaired, and filaments did not extend across the cell as in the controls (**Figure III-3**). Explanted SMCs from a third individual, heterozygous for an I250L mutation in *ACTA2*, showed too little *ACTA2* expression initially to adequately analyze by immunofluorescence. We treated SMCs from this patient and from matched controls with TGF-β1, since it is a well known and potent stimulator of SMC differentiation. Expression of *ACTA2* was increased upon TGF-β1 treatment; however, no SM α-actin filament formation was observed in these cells, and actin was accumulated mainly in the perinuclear region (**Figure III-4**). Findings in this patient were similar to the R118Q mutant SMCs in **Figure III-3**.

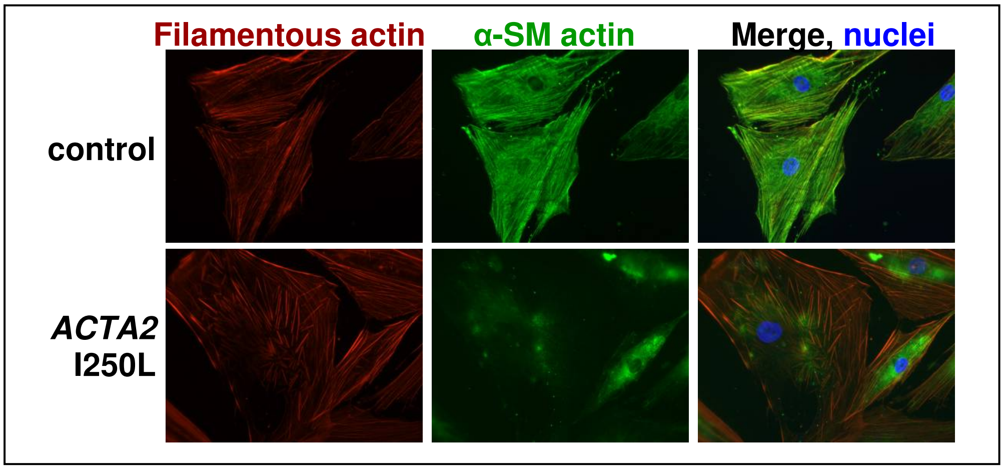

Figure III-4. SM α-actin expression in TGF-β1 treated *ACTA2* SMCs. Since SMCs from a patient heterozygous for an *ACTA2* I250L mutation expressed very low levels of SM α-actin, these SMCs and matched controls were treated with 5 ng/mL TGF-β1. The left panels show phalloidin staining of total filamentous actin (red), the middle panels show SM α-actin (green), and the right panels show a merged image. 72 hours post TGF-β1 treatment, SM α-actin expression was increased but failed to form filaments (green). In contrast, the SM α-actin in controls formed filaments that colocalized with total actin in the cells.

****

Increased proliferation of ACTA2 mutant SMCs

Since multiple vessels from *ACTA2* patients showed focal areas of SMC hyperplasia, we hypothesized that this was due to an increase in SMC proliferation within the vascular wall. We used BrdU incorporation assays to quantify DNA synthesis and determine whether explanted SMCs from these individuals proliferate more rapidly *in vitro*. We found that proliferation, as assessed by BrdU incorporation, was significantly increased in SMCs explanted from patients with heterozygous *ACTA2* mutations (n=2) compared with age and gender matched controls (n=2) (**Figure III-2C**). These data are consistent with the histologic data, both from aortic tissues and from coronary and epicardial arteries from affected individuals, and indicated that *ACTA2* mutations are associated with a proliferative vascular pathology, similar to *MYH11* mutations. These data are also consistent with histologic findings in the *MYH11* patient.

Increased IGF-1 but not TGF-β1 or PDGF gene expression and immunostaining

Due to the similar proliferative pathology in tissues and SMCs from both *MYH11* and *ACTA2* patients, we hypothesized that IGF-1 would also be increased in *ACTA2* mutant tissues and SMCs similar to *MYH11* tissues and SMCs. IGF-1 transcript levels were significantly increased in two out of three SMC samples. The increase in IGF-1 was slightly variable, however, since a third SMC sample also displayed a slight increase in IGF-1 gene expression but this increase was not statistically significant (**Figure III-5A**).

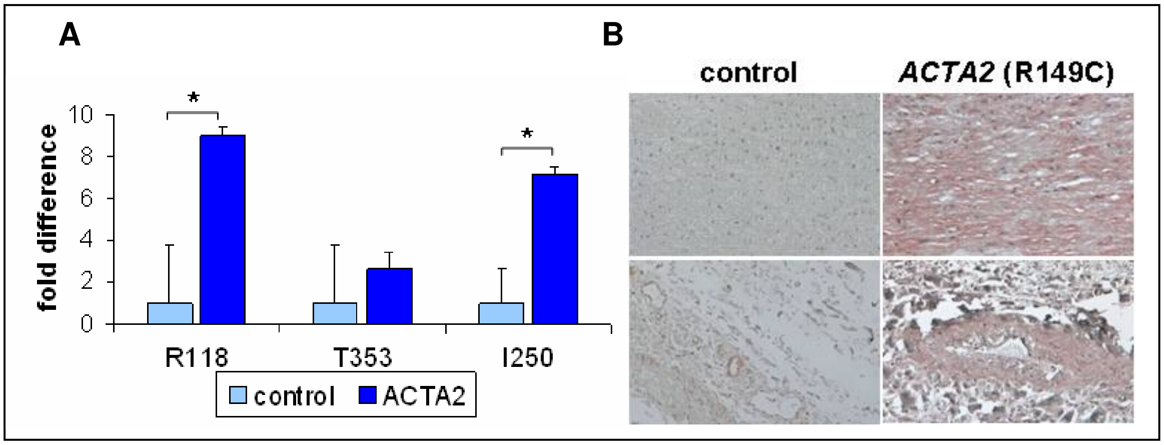

Figure III-5. IGF-1 expression is increased in *ACTA2* SMCs and tissues.

(A) IGF-1 gene expression is increased in *ACTA2* mutant SMCs compared with matched controls, and increases in two out of three of these samples were statistically significant. Data are normalized to GAPDH. Experiments were performed in triplicate (control n=2; *ACTA2* patient n=1 for each separate mutation). Labels indicate the specific *ACTA2* missense mutations, and error bars represent ± S.D. *p<0.05. (B) IGF-1 protein expression in aortic media (B, top two panels) and adventitia (B, bottom two panels) is increased in patients heterozygous for *ACTA2* mutations. Immunostaining of IGF-1 in aortic tissues produced variable results overall, but was consistently increased in patients with R149C mutations.

****

We also performed immunostaining using an IGF-1 antibody to determine whether IGF-1 protein expression in the aortic tissue was increased. Similar to findings in our QPCR analysis, we observed increased immunoreactivity to IGF-1 in some but not all *ACTA2* aortas. Despite some variability among samples, however, IGF-1 immunostaining was consistently more intense in the aortas of patients heterozygous for R149C mutations and was present in both the aortic media and in the hyperplastic vasa vasorum in these tissues (**Figure III-5B**).

Discussion

In Chapter II we described a novel proliferative pathology due to *MYH11* mutations, and we hypothesized that additional mutations in SMC-specific contractile genes would both disrupt the contractile filament structure within the cell and lead to a vascular pathology similar to what we observed in the *MYH11* aortic tissue. Consistent with our hypothesis, heterozygous missense mutations in *ACTA2* led to disruption of SM α-actin filament formation in explanted SMCs, compared with controls. These data were also consistent with structural predictions based on the locations of the various mutations within *ACTA2*. In addition to disruption of SM α-actin filaments, *ACTA2* aortas displayed a vascular pathology similar to the *MYH11* patient, with focal areas of increased SMC hyperplasia and disarray, in both the media and in the vasa vasorum. We also found increased proliferation of *ACTA2* mutant SMCs *in vitro* in static culture, compared with controls. These data suggest that a contractile defect in SMCs leads to increased proliferation even in the absence of mechanical stress, and further confirms our hypothesis that contractile mutations in *ACTA2* and *MYH11* lead to a common proliferative pathology.

The incidence of early-onset CAD and stroke in *ACTA2* mutant individuals raised the question of whether this proliferative pathology was present in other vascular beds, contributing to occlusive disease. We had the opportunity to analyze two cardiac tissue samples and one coronary artery tissue sample from patients heterozygous for *ACTA2* mutations, and we observed similar patterns of SMC hyperplasia, abnormal vessel thickening, and luminal narrowing in all of these samples. These data indicate that the proliferative pathology is indeed present in other vascular beds in affected individuals, and suggest that inappropriate proliferation of SMCs may be involved in the premature CAD and stroke due to *ACTA2* mutations. Thickening and luminal narrowing of small vessels within the heart has previously been reported in cases of hypertension(137;138).

In addition proliferative pathology similar to *MYH11*, *ACTA2* patients' SMCs and tissues displayed increased IGF-1 gene and protein expression. As previously discussed, IGF-1 is a regulator of both SMC contractility and proliferation (107;108;108;109). IGF-1 is also upregulated in response to vascular injury (110-113). All of these studies suggest that the observed increase in IGF-1 may be contributing to the hyperplasia in *ACTA2* mutant aortas. IGF-1 expression in some of the aortic tissues was variable, however. This variability may be due either to the specific mutation in *ACTA2* or due to the unavoidable fact that tissue samples were collected at various stages of disease progression. Individuals heterozygous for R149C mutations consistently had higher levels of IGF-1 in aortic tissue than individuals with other mutations. Unfortunately, explanted SMCs from R149C mutant individuals were not available for study. Further experiments are necessary to determine whether IGF-1 is driving SMC proliferation, particularly in the patients' samples with the highest levels of IGF-1 expression.

One distinct advantage of this study is the availability of clinical data, which enabled correlations of the *in vitro* cellular phenotype to be made with the clinical presentation of disease. Pathologic analysis of blood vessels from *ACTA2* mutant individuals suggested that vessel occlusion also played an important role in the disease process, and this finding correlated with the early onset CAD and stroke present in families carrying *ACTA2* mutations. Conversely, particularly in the case of livedo reticularis (LR), the clinical findings were able to inform the direction of research. In the family originally used to map and identify the first *ACTA2* mutations, LR was a near-100% predictor of which individuals carried the mutant allele(34). The presence of LR, a known vascular occlusive condition, also prompted further analysis of occlusive diseases in *ACTA2* mutant individuals and families.

Similar to the experiments using *MYH11* SMCs and tissues, this study was limited by sample size and the availability of aortic tissues and explanted SMCs. Development of specific model systems for studying the cellular effects of *ACTA2* mutations will allow for a better assessment of the *in vitro* cell proliferation and the specific molecular mechanisms driving the proliferation, and should be particularly useful in elucidating the role of IGF-1 in this process.

Our data from this study support both a decrease in SMC contractile function and an increase in proliferation due to *ACTA2* mutations. SM α-actin filaments were disrupted in mutant SMCs, providing evidence that the mutations lead to disruption in SMC structure. Analyses of *ACTA1* and *ACTC* mutations support the idea that missense mutations disrupting formation of actin filaments also lead to decreased contractility (139;140). Study of *Acta2*-/- mice shows that total loss of *Acta2* decreases SMC contractility; the development of transgenic and knock-in mouse models will aid in determining whether aortic contractility is altered due to mutation of *Acta2* (117). Therefore, although the evidence is indirect rather than a direct measurement of contractile function, our results indicate a probable loss of SMC contractile function. Both the SMC hyperplasia in multiple vascular beds and the increased SMC proliferation *in vitro* support a gain of proliferative function due to *ACTA2* mutations.

Individuals with early onset CAD or stroke in *ACTA2* families lacked any of the major risk factors for cardiovascular disease, including hypercholesterolemia, severe and uncontrolled hypertension, or diabetes. These clinical data, along with the SMC accumulation *in vivo* within blood vessels in multiple vascular beds, along with the increased SMC proliferation *in vitro*, suggest that single missense mutations are capable of triggering a proliferative response leading to vessel stenosis and occlusion. This represents a novel pathway for development of occlusive vascular disease development due to a genetic defect. Further, the increase in IGF-1 and the established roles of IGF-1 in SMCs suggest that IGF-1 may be a key factor in driving proliferation and vessel occlusion. However, the specific role of IGF-1, as well as the mechanism(s) driving increased IGF-1 expression in the mutant tissues and SMCs, remain unknown.

In conclusion, *ACTA2* mutations lead to disruptions in SM α-actin filament assembly, increased SMC proliferation, and increased IGF-1 expression. Future studies will focus on 1) developing a model system to overcome the difficulties with small sample size, 2) elucidating the specific roles that IGF-1 plays in driving proliferation in *ACTA2* SMCs, and 3) determining whether the increase in proliferation can be prevented, to delay the progression of disease in affected individuals.

CHAPTER IV

ESTABLISHMENT AND CHARACTERIZATION OF A MODEL SYSTEM FOR DETERMINING MAJOR PATHWAYS DRIVING PROLIFERATION

Background

Myofibroblasts are cells with biochemical and morphologic features of both fibroblasts and SMCs and can arise from multiple cell types in numerous different organs (141). The complex regulation of this transition is complex but has been studied extensively. One of the hallmarks of myofibroblast differentiation is the expression of SM α-actin, but myofibroblasts also express multiple other SMC-specific contractile genes (142). Many different factors are capable of inducing myofibroblast differentiation *in vitro* and *in vivo*. *In vitro,* mechanical force due to stretching, composition and rigidity of the substrate can induce myofibroblast differentiation (143-145). Chemical modulators including TGF-β1 and heparin can also induce differentiation (141;146). Antimitotic agents have also been found to increase SM α-actin production (147). Cell density has also been shown to modulate the effects of various treatments and external forces on myofibroblast differentiation, and cells plated at low density gain a myofibroblast phenotype upon reaching confluence (148). *In vivo*, latent TGF-β1 is released from its inactive form in the extracellular matrix after mechanical stretch or injury, driving differentiation of myofibroblasts, which aid in wound healing. It is not completely known whether the disappearance of myofibroblasts is due to de-differentiation back into fibroblasts, apoptosis, or a combination of both (144;149).

Early events in myofibroblast differentiation involve TGF-β1/Smad signaling. TGF-β1 binds to type II TGF-β receptors, which form heterotetramers with type I receptors, and are phosphorylated following TGF-β1 binding. Following receptor internalization, Smad anchor for receptor activation (SARA) aids in recruiting Smad2 and Smad3 to the receptor (150). Smad2 and Smad3 are phosphorylated, and the activated Smad2/3 complex translocates to the nucleus and activates transcriptional targets, including SM α-actin, through a TGF-β control element (TCE) in the *ACTA2* promoter (151). TGF-β1 also induces the expression of integrins and ECM, including fibronectin and collagen, driving autophosphorylation of FAK and subsequent activation of FAK signaling (152).

Later signaling events leading to SM α-actin protein accumulation within the cell are dependent on cell adhesion, ECM production, and signaling through FAK. Expression of the ED-A splice variant of fibronectin is required for TGF-β1-induced myofibroblast differentiation (153). Since maintenance of the myofibroblast phenotype is dependent on a stiff ECM, the sustained expression of SM α-actin may be dependent on cell adhesion-dependent FAK signaling. In one study, a correlation was found between SM-α-actin levels and both autophosphorylated and total FAK (152). In contrast, another group reported that myofibroblast differentiation was enhanced in FAK$^{-/-}$ mouse embryonic fibroblasts (MEFs), suggesting that at least in MEF cells, TGF-β1 is capable of activating additional pathways to compensate for the loss of FAK in promoting SM α-actin expression (154). Together, these studies show that myofibroblast differentiation is adhesion-dependent and is regulated by FAK, but that other pathways are involved as well. Studies in 10 T1/2 cells have shown that the PI3K/Akt pathway is involved in transformation of these cells to SMCs upon treatment with TGF-β1 (155).

Differentiated myofibroblasts possess several distinct advantages as a model system for studying the cellular effects of *ACTA2* mutations: 1) samples could more readily be obtained from affected individuals as well as normal controls, 2) samples heterozygous for a wider range of *ACTA2* mutations could be tested, and 3) dermal fibroblasts exhibit phenotypic plasticity in certain culture conditions and can be induced to differentiate into myofibroblasts that synthesize SMC-specific contractile proteins.

Although preliminary data suggested that both *ACTA2* and *MYH11* mutations lead to increased SMC proliferation, we chose to focus on *ACTA2* mutations since they represent a larger percentage of all familial TAAD. Insight gained from these studies should be applicable to TAAD caused by mutations in other contractile proteins as well. The goals of this study are to 1) establish myofibroblasts as a model system for studying *ACTA2* mutations, 2) utilize this model system to confirm an increase in IGF-1 in a larger sample of patients with *ACTA2* mutations, and 3) determine the role of IGF-1 in cell proliferation due to *ACTA2* mutations. The importance of IGF-1 in SMC differentiation, as well as the ability of IGF-1 to induce SMC proliferation, has been discussed previously (see Discussion, Chapter II). Also, an extensive body of literature suggests that myofibroblasts expressing SM α-actin are an adequate model system for our study. *We hypothesize that ACTA2 mutant myofibroblasts proliferate more rapidly than controls, similar to the cultured SMCs, and that the proliferation occurs in an IGF-1 dependent manner.*

Materials and Methods

Dermal fibroblast explant and culture

All studies involving human subjects were approved by the institutional review board at the University of Texas Health Science Center at Houston (UTHSCH), and informed consent was obtained from all study participants. Dermal fibroblasts were explanted from 9 patients heterozygous for *ACTA2* mutations and from 10 controls matched for age and gender, using a previously established protocol. None of the controls had a known history of vascular disease. All samples used for study are listed in **Table 3** of Chapter III. Small biopsies of dermal tissue were obtained from the forearm. Tissue was briefly washed in 70% ethanol, PBS, and DMEM, and epidermal and fatty layers of tissue were removed. Tissues were minced and placed in 60mm dishes. A glass coverslip was placed over the tissue pieces, and 3mL DMEM containing 10% FBS was added to the dish, and media was changed twice a week. Cells were allowed to migrate out of the tissue, and were trypsinized and seeded into flasks once multiple areas of confluence were apparent under the coverslips. Fibroblasts were cultured in DMEM containing 10% FBS, and were used for experiments at passage 2 through 5.

Myofibroblast protocol 1: Low density/high density plating

Low density and high density plating of dermal fibroblasts was done using a published protocol, with minor modifications (148). Dermal fibroblasts were grown to confluence in T75 flasks, and were plated at either 5 or 500 cells/mm^2 in DMEM containing 10% FBS. Culture medium was replaced every three to four days. Upon reaching confluency, cells were serum-starved for 24 hours and harvested for RNA and protein analysis. Cells plated at high density reached confluence within 1 day or less, while cells plated at low density did not reach confluence for nearly 2 weeks, and this time frame varied somewhat among samples.

Myofibroblast protocol 2: TGF-β1 treatment

Dermal fibroblasts cultured in T75 flasks were allowed to remain at confluency for 4-5 days prior to each experiment. Cells were plated in duplicate at 80-100% confluency in a final volume of 2mL into 60-mm dishes, to allow for both RNA and protein analysis. Cells were allowed to settle overnight (20-24 hours). Culture medium was removed, and 2 mL

DMEM containing 0.2% FBS was added to each dish. After 24 hours of serum starvation, two plates were harvested for RNA and protein analysis. This was time zero, and was used as an untreated control. 2mL fresh DMEM containing 0.2% FBS ± TGF-β1 (10ng/mL; R&D Systems, Inc.) was added to the remaining plates. A 10 ng/mL dose was used because others had shown that it was an optimal dose for differentiating primary fibroblast cultures (149). For initial analysis, cells were washed 1x in PBS and harvested 24, 48, and 72 hours post treatment ± TGF-β1, to determine the best time point for analyzing SM α-actin protein (**Figure IV-1A**). For all subsequent experiments, cells were analyzed 72 hours post treatment ± TGF-β1.

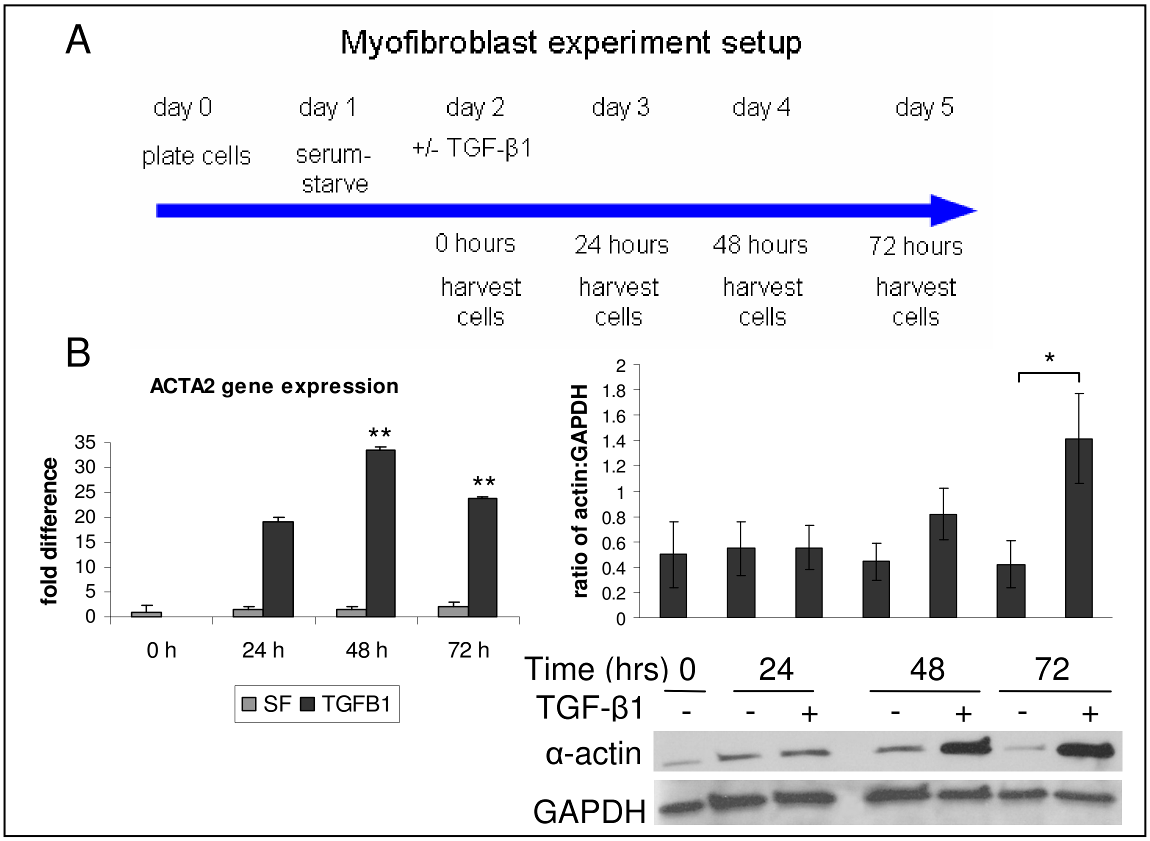

Figure IV-1. Myofibroblast time-course experiment. (A) Control myofibroblasts (n=4) were differentiated from dermal fibroblasts through TGF-β1 treatment, and a time course experiment was performed to determine the best timepoint for harvesting myofibroblasts for

our study. Fibroblasts were plated at confluence. 20-24 hours after plating, fibroblasts were serum-starved for 24 hours. Quiescent fibroblasts were either harvested at a zero-hour timepoint or treated ± TGF-β1 and incubated for an additional 24, 48, or 72 hours. (B) *ACTA2* transcript levels (left panel) and SM α-actin protein expression (right panel) were increased upon TGF- β1 stimulation. Transcript levels were normalized to GAPDH, and the fold change relative to serum starved controls is shown. *ACTA2* transcript levels were slightly greater after 48 hours than 72 hours; however, the greatest amount of SM α-actin protein was expressed at 72 hours, consistent with previously published results. Representative immunoblots from three experiments are shown. Densitometry is a composite from different fibroblast strains (right panel). Data are shown ± S.D. * p=0.05, **p<0.01.

****

Protein isolation and immunoblotting

Protein was harvested in RIPA buffer containing 50 mM Tris-HCl pH 7.4, 1% NP-40, 0.25% Na-deoxycholate, 150 mM NaCl, 1 mM EDTA, 1 mM PMSF, 30μL/mL protease inhibitor cocktail (Sigma), and phosphatase inhibitors (10 mM NaF and 1 mM Na_3VO_4). Samples were incubated at 4°C for 30 minutes and vortexed 3x periodically throughout the incubation period, followed by centrifugation at 13,000 rpm for 30 minutes. Pellets were discarded, and supernatant was quantified using a Bradford assay. Equal amounts (10μg) of protein were boiled for 5 minutes in loading buffer, and loaded onto 4-20% acrylamide gels (Bio-Rad). Protein was transferred to PVDF membranes and immunoblotted using standard techniques. Briefly, membranes were blocked in 5% nonfat dry milk in TBS-T for 1 hour, followed by primary antibody for either 1-2 hours at room temperature, or overnight at 4°C.

Secondary antibodies were used at a concentration of 1:5000 for one hour at room temperature. Antibodies used are listed in **Table 1** of Chapter II.

RNA isolation and quantitative gene expression analysis

RNA isolation and QPCR analysis were performed as previously described.

Immunofluorescence

Dermal fibroblasts were seeded onto 22mm glass coverslips at a density of 5,000 cells per coverslip and allowed to attach overnight. Myofibroblast differentiation was carried out as described. 72 hours post TGF-β1 treatment, cells were fixed in 4% paraformaldehyde, and immunofluorescent labeling was carried out as previously described for SMCs. **Table 1** lists the antibodies and concentrations used.

Cell proliferation assays

Dermal fibroblasts were seeded in triplicate at a density of 20,000 per well, and were allowed to attach overnight before serum-starving in DMEM containing 0.2% FBS. 24 hours after serum deprivation, cells were treated ± TGF-β1 (10 ng/mL) and allowed to incubate for 72 hours, followed by incubation with BrdU reagent for an additional 24 hours. Cells were fixed, and BrdU ELISAs were carried out according to the manufacturer's instructions. Assays were repeated three separate times (*ACTA2* patients, n=9; controls, n=10). Statistical significance was determined using Student's t-tests.

For the IGF-1 receptor inhibitor and neutralizing antibody assays, fibroblasts were plated in triplicate at 10,000 cells per well, serum-starved, and treated with TGF-β1 (10 ng/mL) as described above. 72 hours post TGF-β1 treatment, cells were pre-treated for 30 minutes ± two different doses (0.1 μM and 1 μM) of PQIP (*cis*-3-[3-(4-methyl-piperazin-l-yl)-cyclobutyl]-1-(2-phenyl-quinolin-7-yl)-imidazo[1,5-*a*]pyrazin-8-ylamine), a specific IGF-1R inhibitor (OSI Pharmaceuticals, Inc.) before BrdU reagent was added (156). Cells were also treated ± 200 nM IGF-1 as a positive control for inhibitor specificity. Cells were incubated with BrdU reagent for 24 hours and fixed, and BrdU incorporation was quantified through ELISA, according to the manufacturer's instructions (Millipore, Billerica, MA). Data are representative of three independent experiments. For the neutralizing antibody assay, cells were plated in duplicate and treated ± α-IR3, an IGF-1R neutralizing antibody (2 μg/mL; Abcam) instead of PQIP. This concentration was chosen because concentrations of 1 μg/mL and 2.5 μg/mL have been shown inhibit proliferation in MCF7 cells and in metastatic non-small cell lung cancer cells, respectively (157;158). Student's t-tests were used to determine statistical significance.

Analysis of IGF-1 secretion

To quantify IGF-1 secretion by *ACTA2* mutant and control cells, myofibroblasts, an IGF-1 ELISA (R&D Systems, Inc., Minneapolis, MN) was used. Cell culture supernatant from 9 *ACTA2* myofibroblast and 10 control myofibroblast samples were assayed, and the IGF-1 ELISA was performed according to the manufacturer's instructions. To better concentrate the IGF-1 in the tissue culture supernatant, samples were concentrated using Amicon Ultra centrifuge tubes (Millipore, Billerica, MA).

Results

Establishment of a myofibroblast model system

To determine the best method for myofibroblast differentiation, we tested two different methods that were previously described in the literature. The first method involved plating fibroblasts at low density and allowing them to grow to confluence, and the second method involved treating confluent, serum-starved fibroblasts with TGF-β1 (148;149). Plating fibroblasts at high vs. low density yielded variable and inconsistent results (data not shown). Another disadvantage is that this method was time-consuming. Low density plated cells took several weeks to reach confluency, and often did not survive well from being plated so sparsely. In contrast, TGF-β1 treatment yielded far better and more consistent results. One study showed that TGF-β1 treatment resulted in significantly increased SM α-actin gene and protein expression as early as 24 hours, and another study showed that the optimal amount of incubation time after TGF-β1 stimulation was 72 hours (149;151). We tested several different timepoints to confirm the optimal incubation time in our fibroblast system. SM α-actin mRNA was increased significantly 24 hours after TGF-β1 treatment, and remained elevated at 48 and 72 hours ($p<0.01$). Immunoblot analysis showed that SM α-actin protein expression was increased by 48 hours, with the greatest expression most consistently at 72 hours ($p<0.05$; **Figure IV-1B**). A representative immunoblot from one out of three independent controls is shown. Therefore, a 72-hour timepoint was used for the remainder of experiments.

Dermal fibroblasts express SM α-actin in addition to other SMC contractile proteins upon differentiation into myofibroblasts. Therefore we hypothesized that the myofibroblasts would be a good model system for determining whether inducing SM α-actin expression had a proliferative effect on patients' myofibroblasts. Assays for SM α-actin expression, actin polymerization, and cell proliferation showed that myofibroblasts displayed similar characteristics to SMCs and are a valid model system. Treatment of fibroblasts explanted from controls (n=10) and from patients heterozygous for *ACTA2* mutations (n=9) all showed increased SM α-actin mRNA and protein expression at 72 hours following TGF-β1 treatment, consistent with published results (**Figure IV-2A,B**) (149).

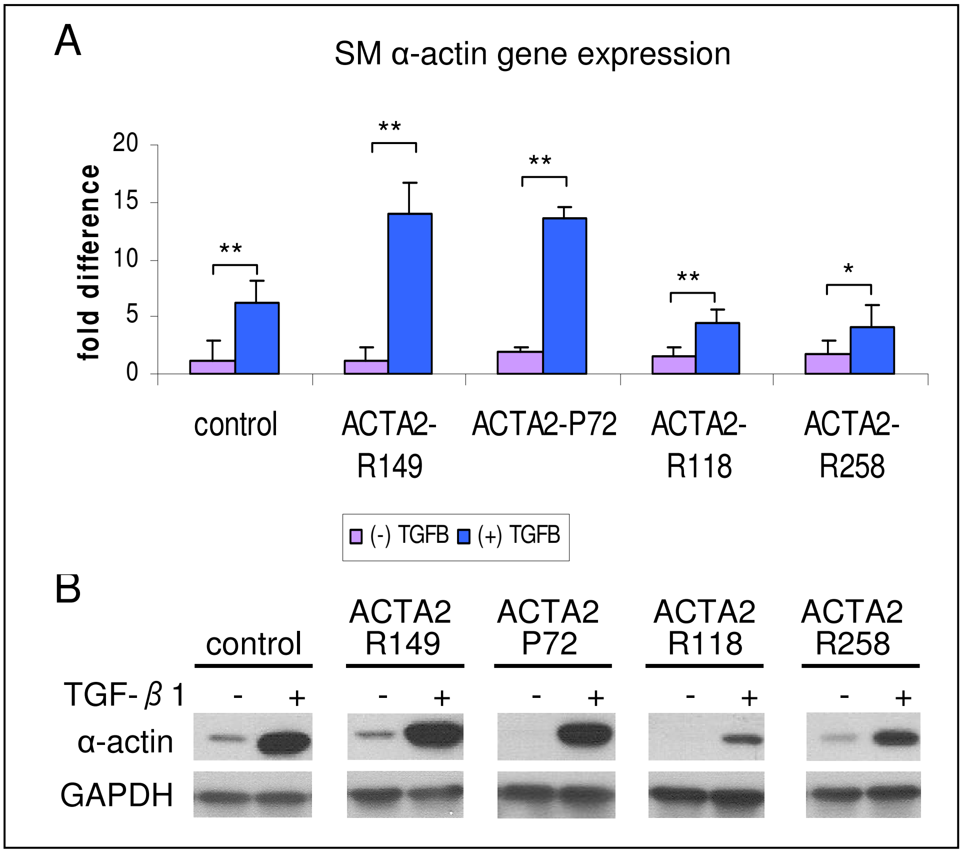

Figure IV-2. SM α-actin expression in *ACTA2* mutant and control myofibroblasts. Both *ACTA2* mutant and control dermal fibroblasts significantly increase SM α-actin transcript levels (A) and protein expression (B) 72 hours post TGF-β1 treatment (10ng/mL). Samples with less of an increase in *ACTA2* gene expression also displayed less SM α-actin protein expression following TGF-β1 treatment. Gene and protein expression levels varied, with the

most notable differences between R149 and R258 mutations. Error bars represent ± S.D. QPCR data are normalized to GAPDH and are a composite of three experiments, and representative immunoblots are shown. *p<0.05, **p<0.01.

****

Interestingly, the level of *ACTA2* mRNA expression varied depending on the mutation, even though all samples displayed a significant increase in mRNA expression upon TGF-β1 stimulation. The most marked difference was between R149C and R258H mutant samples. SM α-actin protein expression was increased in all samples that were studied, and followed a trend similar to that observed in mRNA levels.

Next, we used two different methods to determine whether SM α-actin filament structure was disrupted in *ACTA2* mutant myofibroblasts compared with controls: immunofluorescent labeling of SM α-actin, and an ultracentrifugation assay to separate polymerized vs. unpolymerized actin, followed by immunoblotting for SM α-actin. Immunofluorescent staining showed that SM α-actin filaments were disrupted in patients' myofibroblasts compared with controls (**Figure IV-3A**).

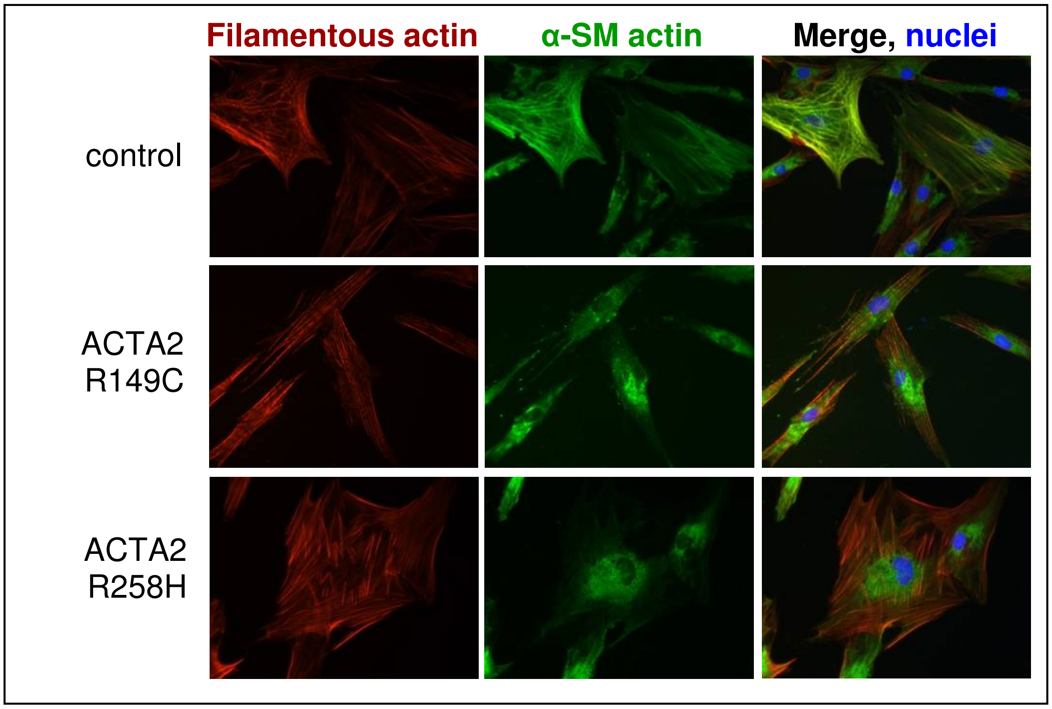

Figure IV-3. SM α-actin polymerization is disrupted in *ACTA2* mutant myofibroblasts. Immunofluorescent labeling of total actin filaments (red) and SM α-actin (green) showed normal total actin as well as α-actin filaments in control myofibroblasts, and these filaments colocalized within the cell. In contrast, patients' myofibroblasts lacked SM α-actin filaments, and α-actin localized mainly in the perinuclear region, similar to results obtained in *ACTA2* explanted SMCs.

****

As a final step both in testing myofibroblasts as a model system and in confirming that *ACTA2* mutations lead to increased proliferation, we quantified the amount of DNA synthesis in *ACTA2* mutant vs. control myofibroblasts. 72 hours post TGF-β1 treatment, we added BrdU reagent to the myofibroblasts and allowed cells to incubate an additional 24 hours. *ACTA2* mutant myofibroblasts showed significantly faster proliferation, as assessed by BrdU incorporation, in culture than age and gender matched controls (**Figure IV-4, Table 3**).

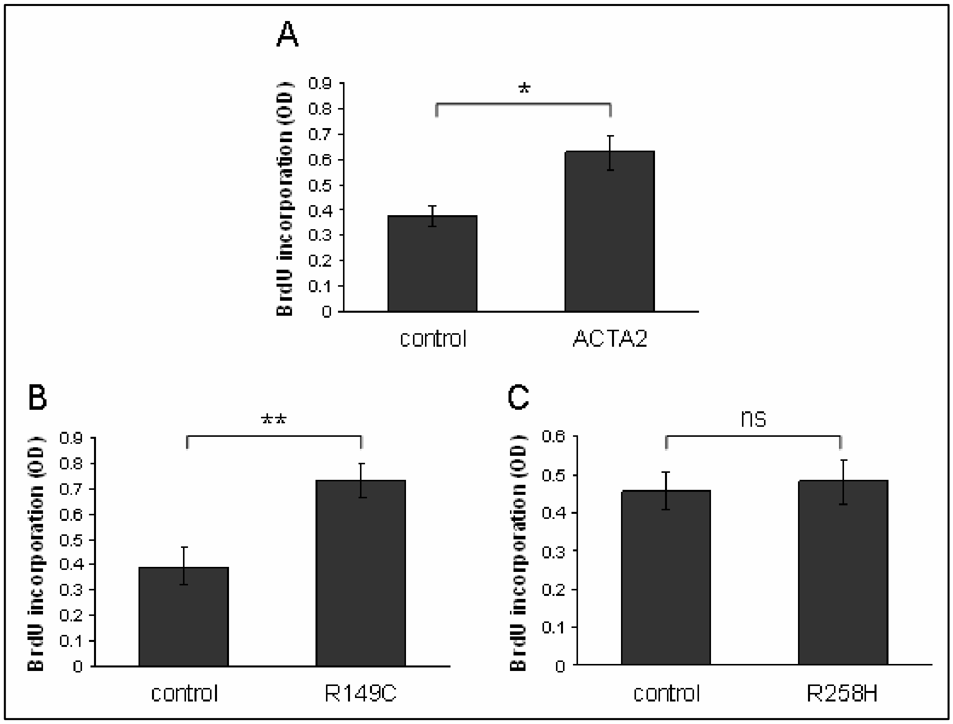

Figure IV-4. Increased proliferation in *ACTA2* mutant myofibroblasts. (A) *ACTA2* mutant myofibroblasts (n=9) proliferated significantly more rapidly than controls (n=10) 72 hours post treatment with TGF-β1. (B,C) Some variability was observed in the amount of proliferation of R149C vs. R258H myofibroblasts. R149C mutant cells (n=3) proliferated nearly twice as rapidly as matched controls, while R258H mutant cells (n=2) showed only a marginal increase in proliferation. Data shown are a composite of three experiments, and error bars represent ± S.E.M. *p<0.05, **p<0.01, ns = not significant.

****

These data further confirm our hypothesis that disruption in *ACTA2* causes an increase in proliferation. These data also indicate that myofibroblasts are a suitable model for studying the mechanisms driving increased proliferation due to *ACTA2* mutations. However, similar to the variability in SM α-actin expression, the amount of cell proliferation also appeared to be dependent on the mutation. The largest difference was observed between myofibroblasts harboring an R149C vs. R258H mutations (**Figure IV-2, Figure IV-4**). While R149C mutant myofibroblasts proliferated nearly twice as rapidly as controls, R258H myofibroblasts displayed only a marginal increase in proliferation that failed to reach statistical significance.

Increased IGF-1 gene expression but not systemic IGF-1 production

We quantified IGF-1 gene expression in myofibroblasts to determine whether 1) IGF-1 gene expression was increased similar to *ACTA2* mutant SMCs, 2) whether sample-to-sample variations in the levels of IGF-1 expressions existed, and 3) whether TGF-β1 induced myofibroblast differentiation would be suitable for elucidating the role of IGF-1 in *ACTA2* SMC proliferation. IGF-1 gene expression was significantly increased in *ACTA2* mutant myofibroblasts but not in controls upon TGF-β1 treatment. Similar to SM α-actin expression and proliferation, the increase in IGF-1 expression varies based on the mutation and cell strain. The R149C myofibroblasts expressed more IGF-1 than R258H myofibroblasts (**Figure IV-5**).

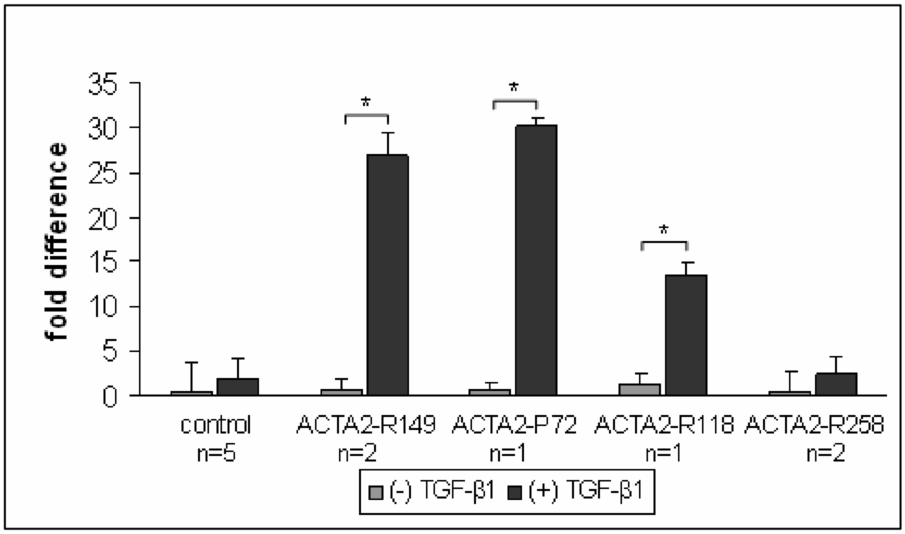

Figure IV-5. Increased IGF-1 gene expression in *ACTA2* mutant myofibroblasts.

IGF-1 gene expression was significantly increased 72 hours post TGF-β1 treatment in four out of six *ACTA2* mutant myofibroblast samples tested (three out of four different *ACTA2* mutations) compared with controls (n=5). The amount of IGF-1 overexpression was variable in the patients, similar to *ACTA2* gene expression results and appears somewhat proportional to *ACTA2* expression levels seen in Figure IV-3a. Notably, a stark contrast between IGF-1 expression in R149C vs. R258H mutant cells existed. The variable expression is similar to results obtained in explanted *ACTA2* SMCs. Data are normalized to GAPDH mRNA, and error bars represent S.D. *p<0.05.

****

Since IGF-1 mRNA levels were increased, we made multiple attempts to quantify IGF-1 secretion by the myofibroblasts in culture. However, ELISAs performed on tissue culture supernatant (R&D Systems, Inc.) failed to yield detectable levels of IGF-1, even after centrifugation to concentrate media samples, and we were unable to determine whether the increased IGF-1 mRNA corresponded with an increase in protein expression and secretion.

Partial inhibitory effect of IGF-1R neutralizing antibodies or IGF-1R blocker on proliferation

The goal of this study was both to establish a model cell system, and to utilize the model to study the pathways driving proliferation in *ACTA2* mutant cells. IGF-1 transcript levels were increased in *MYH11* SMCs, *ACTA2* SMCs, and *ACTA2* myofibroblasts, and IGF-1 immunoreactivity was increased in *MYH11* and *ACTA2* aortic tissues. Since IGF-1 has known roles in promoting proliferation, we determined whether preventing IGF-1 signaling through the IGF-1 receptor would prevent the observed increase in proliferation. To accomplish this, we used two different inhibitors: a small molecule inhibitor of IGF-1R (PQIP), and an IGF-1R neutralizing antibody (α-IR3). Previously published data using PQIP showed an IC_{50} within a nanomolar range, and that the IC_{50} for blocking cell proliferation in a number of cancer cell lines was between 0.023-0.6 μM (156). Based on these data, we used doses of 0.1 uM and 1 μM for our studies. PQIP blocked all IGF-1-induced proliferation in both control and *ACTA2* mutant myofibroblasts; however, the patients' myofibroblasts continued to proliferate significantly more rapidly than the control cells even after PQIP treatment (**Figure IV-6A**).

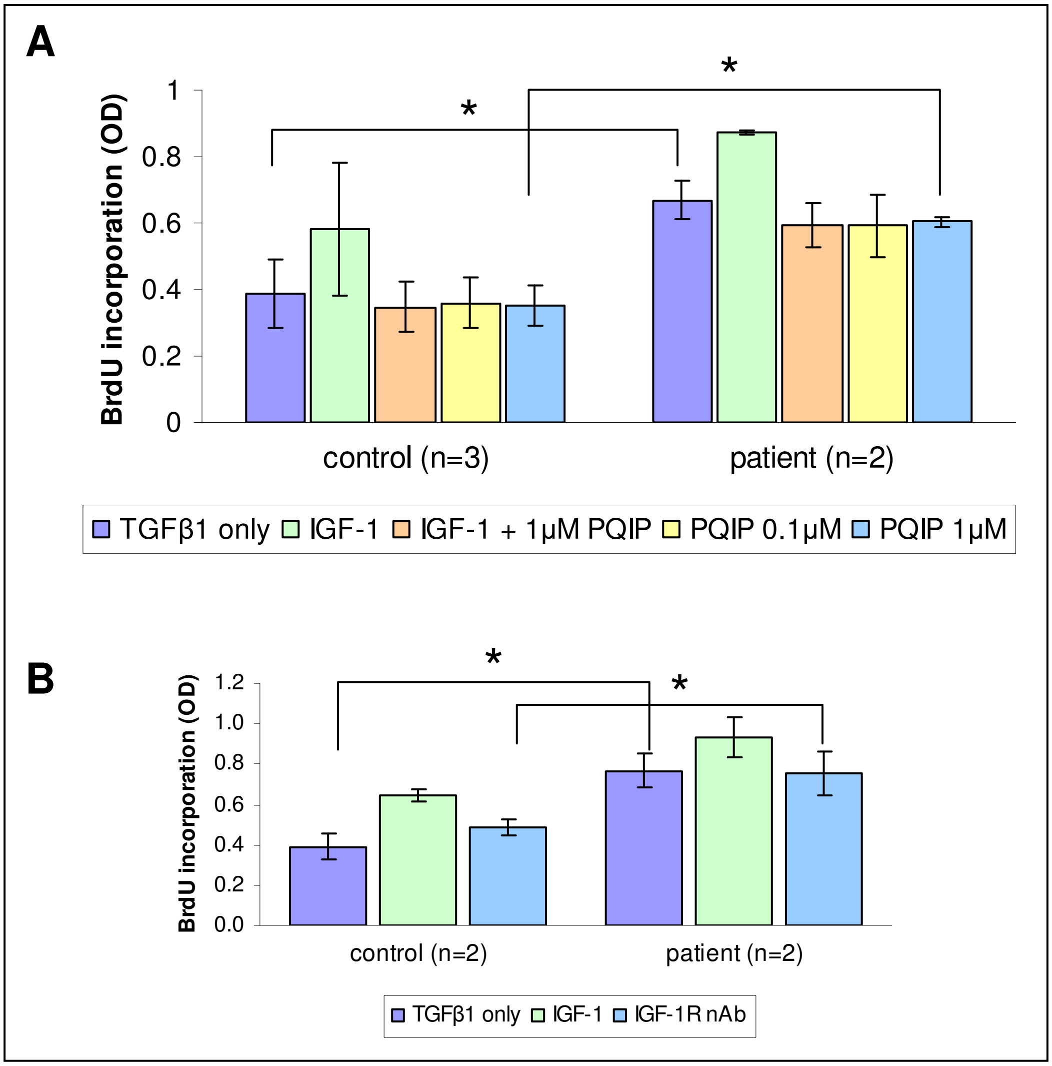

Figure IV-6. *ACTA2* mutant myofibroblast proliferation *in vitro* is not dependent on IGF-1. (A) A specific IGF-1 receptor kinase inhibitor (PQIP; OSI Pharmaceuticals, Inc.) completely prevents IGF-1 induced proliferation; however, in patients' cells, proliferation is still significantly greater than in controls after treatment with 1 µM PQIP, suggesting that increased proliferation in these cells *in vitro* is not IGF-1 dependent. IGF-1 + PQIP treatment served as a control to confirm inhibitor specificity. Data are representative of three independent experiments. Error bars represent mean ± S.E.M. *$p<0.05$. (B) Similar results were obtained using an IGF-1 receptor neutralizing antibody (α-IR3) at a concentration of 2µg/mL. Error bars represent mean ± S.E.M. *$p<0.05$.

****

Similar results were obtained using an IGF-1R neutralizing antibody at a dose similar to inhibitory doses used in two different cancer cell lines (**Figure IV-6B**). These data suggest that at least *in vitro*, factors other than (or in addition to) IGF-1 are driving proliferation in the *ACTA2* mutant cells.

Discussion

The goals of this study were to develop a model for studying *ACTA2* mutations, and to use this model to determine whether the observed increase in proliferation is dependent on IGF-1. *ACTA2* mutant myofibroblasts express SM α-actin, have disrupted α-actin filaments, increased proliferation, and increased IGF-1 expression compared with controls, similar to explanted SMCs. These data all suggest that myofibroblasts are a good model for studying the pathways leading to increased proliferation in the mutant SMCs.

Since IGF-1 is capable of driving both contractility and proliferation in SMCs, we hypothesized that proliferation in these cells is dependent on IGF-1, and utilized the myofibroblast model to address this question. However, the inability of the specific IGF-1 receptor inhibitor PQIP, an IGF-1 receptor neutralizing antibody, and additionally an ERK inhibitor to completely block proliferation in these cells suggest that mechanisms other than IGF-1 are driving proliferation *in vitro*. These mechanisms are likely complex, involving input from multiple signaling pathways.

In addition to characterizing myofibroblasts as a model system and assessing whether IGF-1 is driving proliferation in this system, we made some unexpected observations, which may have clinical relevance. Some differences existed in SM α-actin and IGF-1 expression as well as proliferation in the mutant myofibroblasts. Based on the consistency of the results from the controls, and the different clinical phenotypes observed associated with R149C vs. R258H mutations, we hypothesize that these differences may indicate slightly different disease mechanisms. R149C mutations are more frequently associated with premature CAD, while R258C/H mutations are more associated with premature stroke, along with Moyamoya disease. Some of the mutant myofibroblasts, particularly those heterozygous for R258H mutations, showed less of an increase in *ACTA2* upon TGF-β1 stimulation than other patients and controls, suggesting that either these particular cell strains do not produce as much SM α-actin in response to TGF-β1 stimulation, or that some SM α-actin RNA and/or protein may be degraded. The same myofibroblast samples (R149C vs. R258H mutant samples) also showed distinct differences in proliferation after TGF-β1 treatment. Future studies will determine whether the differences in R149C and R258H cells are clinically relevant, or are merely due to inherent differences between primary fibroblast cell strains.

Myofibroblasts have proved useful as a model system, but they have several inherent disadvantages. One drawback is that even after TGF-β1 stimulation, these cells are not fully differentiated SMCs. Myofibroblasts express, but do not show SMC-specific splicing of, SMC terminal differentiation markers (159). Also, myofibroblasts and SMCs contract using different cellular mechanisms. Myofibroblasts contract mainly through Rho/ROCK activation and subsequent inhibition of myosin light chain phosphatase (144). This pathway leads to increased Ca2+ sensitization in SMCs, but contraction and maintenance of vascular tone are also regulated by Ca2+ influx via stretch-dependent ion channels and voltage dependent Ca2+ channels (160). Ca2+ binds to calmodulin and activates myosin light chain kinase. Phosphorylated myosin light chain allows for myosin to interact with actin and generate contractile force (160). Also, contractile force generation is reversible in SMCs but irreversible in myofibroblasts (144). Therefore, while myofibroblasts may help provide insight into some cellular pathways, these cells may not be a good model system for studying SMC contractility directly. In addition, the use of myofibroblast strains from multiple individuals raises the possibility of genetic variability among patients and controls. Another shortcoming of both the myofibroblast model and the SMCs used in Chapters II and III is that all of these cells were grown in static culture, whereas SMCs *in vivo* are subjected to mechanical strain due to pressure from blood flow. Finally, in the current study, the TGF-β1 treatment protocol created difficulties with accurately assessing IGF-1R activation. The time frames for IGF-1R activation after myofibroblast differentiation through TGF-β1, the length of the activation, and time of IGF-1 production are not known. Additionally, the mechanism by which a specific contractile defect causes upregulation of IGF-1 is still not known.

Despite these disadvantages, the myofibroblast model system still has some advantages. The system is inducible in that the expression of SMC contractile genes can be switched "on" and "off" based on a combination of the presence of TGF-β1 and the density at which the cells are plated (149), An inducible model is advantageous because it has the potential to reveal defects in the ability of SMCs to maintain a differentiated, contractile phenotype in response to external stimuli. Current data obtained using the myofibroblast model do not indicate that *ACTA2* mutant SMCs have an impaired ability to maintain a differentiated SMC phenotype, as shown by their robust upregulation of SM α-actin mRNA and protein. However, this myofibroblast system is currently being utilized to show defects in SMC differentiation caused by *TGFBR2* and *COL3A1* mutations (Inamoto S. et al, manuscript submitted; Dianna Milewicz, personal communication).

In conclusion, we have developed a myofibroblast model system that proved to be useful in confirming a proliferative phenotype in *ACTA2* mutant cells. However, due to the inherent differences between myofibroblasts and SMCs, a SMC-specific model is needed for further study of the specific mechanisms driving proliferation. Since actin filaments are disrupted in both *ACTA2* mutant SMCs and myofibroblasts, pathways that regulate both actin polymerization and cell proliferation are excellent candidate pathways. Future work will focus on 1) developing an SMC-specific cell culture model, 2) determining whether pathways with a dual role in regulating actin polymerization and contractility drive proliferation in this model and 3) confirming results in *ACTA2* mutant SMCs. Additionally, once these studies are completed, a transgenic or knock-in mouse model of *Acta2* mutations is needed to elucidate the specific role of increased proliferation *in vivo*. Although IGF-1 does not appear to be driving proliferation *in vitro* in R149C mutant myofibroblasts, increased IGF-1 expression may still contribute to proliferation *in vivo*, and mouse models of vascular injury and/or IGF-1 overexpression support this idea (110-113). Transgenic mouse models with *Acta2* mutations will be essential for addressing this question. These mice could either be crossed with mice that overexpress or underexpress IGF-1, or IGF-1R inhibitors could be used *in vivo* in these mice, to aid in determining whether IGF-1 drives proliferation and is ultimately involved in disease pathogenesis.

CHAPTER V

IDENTIFICATION OF PROLIFERATIVE PATHWAYS ACTIVATED BY LOSS OR MUTATION OF *ACTA2*

Background

While myofibroblasts have some advantages and usefulness as a model system, these cells also possess a number of limitations that complicate the determination of proliferative mechanisms (see Discussion, Chapter IV). Based on the myofibroblast studies, we concluded that a SMC-specific model system is needed. In the absence of transgenic or knock-in mouse models of *Acta2* mutations, we considered three different model cell lines or cell strains: transformed SMC lines transfected with vectors containing mutant *ACTA2,* similarly transfected primary SMCs, or *Acta2*$^{-/-}$ SMCs.

Based on all of the available information about other cell strains, we chose to utilize primary smooth muscle cells explanted from *Acta2*$^{-/-}$ mice as a model system. These cells have several distinct advantages. First, unlike the myofibroblasts, they are genetically uniform and should yield consistent results. Any differences between wildtype and *Acta2*$^{-/-}$ SMCs are less likely to be due to extraneous genetic factors. Second, they are primary SMCs rather than SMC lines that may have acquired other mutations or chromosomal alterations since undergoing transformation. Third, these cells provide an ideal model for studying a complete loss of SM α-actin filaments. Since α-actin filaments are disrupted in all of the mutant cells that were assessed, we hypothesize that a complete loss of SM α-actin should result in a similar phenotype and provide valuable insight into the mechanisms driving proliferation and vascular occlusive disease associated with *ACTA2* mutations in humans.

Acta2$^{-/-}$ mice were generated by Dr. Robert Schwartz and colleagues in 2000 by inserting a vector containing the *Acta2* gene with a Pol2neobpA cassette at the transcriptional start site into embryonic stem cells, disrupting transcription of the *Acta2* gene. Successfully targeted cells were injected into blastocysts of C57 mice to generate a chimeric mouse, and offspring were bred and genotyped for the presence or absence of *Acta2* (117). Major findings in the *Acta2*$^{-/-}$ mice included decreased contractility of isolated aortic ring segments, decreased systolic blood pressure, inability to increase blood flow in response to elevated body temperature, and impaired ability to raise blood pressure back to normal levels after infusion with sodium nitroprusside, a compound that lowers blood pressure. *Acta2*$^{-/-}$ mice showed a flattened appearance of elastic fibers in the aorta, which is also indicative of decreased contractility. However, these mice were viable and the vascular system developed normally. Other findings included increased mRNA and protein expression of skeletal α-actin, presumably a compensatory response due to the complete loss of SM α-actin. Endogenous skeletal α-actin overexpression, however, was unable to completely restore contractility in the *Acta2*$^{-/-}$ vessels (117). Additionally, electron microscopy revealed decreased formation of myosin thick filaments, providing evidence that disruption of one element of the contractile apparatus leads to disruption of other components as well (117).

In 2004, Zimmerman et al reported that *Acta2*$^{-/-}$ mice displayed decreased bladder contractility *in vitro* and *in vivo*. Although this finding was significant *in vitro*, it was not statistically significant *in vivo*, potentially because SM γ-actin is more abundant than SM α-actin in the bladder. A third study showed that loss of *Acta2* does not cause major morphologic changes in retinal structure, but increased permeability of the blood-retinal barrier, which resulted in decreased retinal function (161). A fourth study reported increased kidney myofibroblast proliferation in *Acta2*$^{-/-}$ mice, using a unilateral ureteral obstruction model of kidney injury (124). *Acta2*$^{-/-}$ mice showed increased fibrosis compared to wildtype post-injury, as well as increased myofibroblast proliferation and procollagen-1 expression both *in vitro* and *in vivo*. These defects were rescued by transfection with an adenovirus containing wildtype *Acta2*, providing evidence that the proliferation as well as the increased injury response were due to an inability of the *Acta2*$^{-/-}$ kidney myofibroblasts to produce smooth muscle α-actin (124). Additionally, FA proteins including phosphorylated FAK, total FAK, paxillin, and vinculin were increased in *Acta2*$^{-/-}$ myofibroblasts (124). The authors suggested that disruption of *Acta2* leads to alterations in FAs, and that this disruption may play an important role in disease development in their model (124). However, the exact nature of the role of FAs in this disease process remains undefined.

From studies with the *Acta2*$^{-/-}$ mice, it is clear that both proliferation and SMC contractility are altered due to the complete loss of a contractile protein. Others have demonstrated that SM α-actin expression slows the growth of tumors and immortalized cell lines, providing support for our argument that loss of contractile filaments can result in either a loss or a gain of function depending on the location of the vascular bed (162;163). Additionally, SM α-actin has a p53 response element within the promoter region, and is a transcriptional target of p53 (147). We have shown that mutations that either disrupt or are predicted to disrupt *Acta2* polymerization lead to an increase in SMC and myofibroblast proliferation, suggesting that total loss of *Acta2* as well as deletion of *Acta2* may drive proliferation via similar cellular mechanisms (83). Therefore, SMCs explanted from *Acta2*$^{-/-}$ mice should yield valuable insight into proliferative pathways in *ACTA2* mutant SMCs.

As mentioned in the previous chapter, pathways and molecules that regulate both SMC contractility and proliferation are excellent candidates for our study. One such pathway is Rho/ROCK signaling. In SMCs, Rho is activated in response to contractile agonists including endothelin-1 and Ang II that activate G-protein coupled receptors (160).

Rho/ROCK signaling can also be activated in response to growth factor stimulation, mechanical stretch, or through cell-ECM interactions (164). Rho activates ROCK, which inactivates myosin phosphatase, allowing for myosin light chain to remain active (phosphorylated) and increasing the cell's sensitivity to calcium (160). Rho also plays an essential role in driving actin polymerization by activating multiple effector proteins within the cell. Increased actin polymerization in turn drives the expression of SMC-specific markers including SM22, SM α-actin, SM myosin heavy chain, and calponin (165). In addition to its roles in actin polymerization and SMC-specific gene expression, multiple studies suggest that elevated Rho/ROCK signaling promotes SMC proliferation. Rho/ROCK signaling leads to reduced p27 levels through increased Skp2 production, as well as elevated cyclin D1 levels, resulting in cell cycle progression (166;167). Constitutively active Rho promoted BrdU incorporation into NIH3T3 cells (168). HMG CoA reductase inhibitors (statins) decreased the amount of Rho present at cell membranes and prevented Rho-induced reduction of p27 levels, thereby reducing SMC proliferation (169). Although one study reported that Rho activation did not induce SMC proliferation, this study was done on SMCs from saphenous veins (170). Others have shown that arteries and veins are structurally and functionally different, and that SMCs explanted from arteries vs. veins respond differently *in vitro*, which could account for the disparity in results obtained (171). Overall evidence suggests that Rho/ROCK activation is capable of driving SMC proliferation.

SRF-dependent regulation of SMC phenotypic switching may also contribute to the increase in proliferation, and a general overview of SMC phenotypic switching is provided in Chapter I. SRF acts as a molecular "switch" between contractile and growth-responsive gene expression in SMCs, and that this switching is regulated in part through actin polymerization and nuclear localization of myocardin-related transcription factors (MRTFs) (172;173). SRF phosphorylation at Ser162 leads to inhibition of myogenic genes, while still allowing for expression of proliferative genes (174). Experimental evidence from multiple sources shows that levels of unpolymerized actin (G-actin) within the cell control SRF activation through regulation of MRTFs (175). There are two main classes of SRF cofactors: MRTFs, which control muscle-specific differentiation, and TCFs that control growth factor responsive genes (175). When G-actin levels increase in the cell, MRTF-A is exported from the nucleus and binds to G-actin. MRTFs, which are normally found in the nucleus in differentiated SMCs, are localized in the cytoplasm in fibroblasts but translocate to the nucleus upon stimulation of RhoA-mediated actin polymerization (176). MRTFs and TCFs compete with each other for binding to SRF (177). Removal of MRTF from the nucleus increases the amount of SRF that binds to TCFs, allowing for greater smooth muscle cell proliferation and growth. Activation of TCF/SRF transcription complexes is also promoted by factors including mechanical stretch, vascular injury, and exogenous growth factor stimulation, leading to increased ERK activation (175). Thus, changes in actin polymerization coupled with vascular injury and/or the presence of excess growth factors could potentially lead to a switch between MRTF/SRF and TCF/SRF mediated transcription and subsequent proliferation.

Both Rho/ROCK and SRF mediated pathways are plausible candidates for driving proliferation in *ACTA2* mutant SMCs due to decreased SM α-actin polymerization. However, this presents a potential dilemma in *Acta2*$^{-/-}$ SMCs, since there are no pools of unpolymerized SM α-actin. Although conflicting evidence exists over whether SM α-actin and other actin isoforms directly interact in SMCs, loss of a contractile protein may lead to disruption of cytoskeletal proteins as well. Therefore it is also possible that pools of other unpolymerized actin isoforms in the *Acta2*$^{-/-}$ SMCs are increased, leading to proliferation through either of the two mechanisms described.

A third candidate for study is focal adhesion (FA) dependent signaling, which represents a group of pathways rather than a single pathway that regulate actin expression and polymerization as well as cell proliferation (65). Multiple factors regulate the size, specific composition, and the function of FAs, including the specific cell type being studied, the ECM composition and stiffness, the activation state of associated integrins, and the amount of contractile force generated by the cell (178). Integrin clustering is essential for FA formation and is one of the early molecular events in this process (67). The focal complexes formed by initial integrin clustering are short-lived structures, and contain αvβ3 integrin, talin, paxillin, phosphorylated proteins, and FAK (179). Early FAs contain zyxin as well as greater quantities of the proteins recruited to focal complexes. Classical or "mature" FAs are 2-6 µm in length, and contain little or no tensin or α5β1 integrin (180). "Supermature" FAs are 8-30 µm long and contain increased amounts of vinculin and paxillin, in addition to tensin and α5β1 integrin (180). In contrast to FAs, fibrillar adhesions are mainly involved in organizing ECM and coordinating cell attachment to ECM. Fibrillar adhesions contain large amounts of tensin and α5β1 integrin, but vinculin, paxillin, and αvβ3 integrin are almost entirely absent (180).

Following FA formation, SM α-actin filament formation is a critical step in the process of FA development and maturation in myofibroblasts. Supermature FAs that are connected to SM α-actin stress fibers are required for maximal contractile force generation by myofibroblasts (180;181). Inhibition of α-actin expression during myofibroblast differentiation prevents FAs in these cells from developing into supermature FAs (182). When SM α-actin is expressed, but depolymerization is induced, FAs are destabilized and disassembled (181). Conversely, the length of the FAs formed regulates both the force generated by the cell and the recruitment of SM α-actin to stress fibers (180).

In SMCs, FA regulation is vital for maintaining SMC contractile function (178). FAK is an integral part of the FA complex, acting as a mechanosensor, a scaffold for recruitment of other proteins to these complexes, and a regulator of FA turnover (67;68). Knockdown of FAK expression in tracheal muscle strips resulted in decreased smooth muscle contractile force generation (69). SM α-actin expression in response to external forces is mediated in part through FAK activation (183). FAK signaling activates multiple cellular pathways including Rho, Rac, PI3K, and Ras/ERK, and contributes to proliferation and migration in adherent cells (184;185). Increased FAK signaling also leads to increased proliferation and migration in multiple types of cancer (186). Expression of FRNK, an alternative splice variant of the FAK gene that inhibits FAK activity, prevents SMC proliferation (187-189). FAK is also overexpressed in diseased arteries and veins that display intimal hyperplasia (190). In one study, FAK promoted SMC proliferation by stabilizing Skp-2, an F-box protein that recognizes and degrades p27 (191). Thus, FAK is a key molecule at FA sites, and activates multiple major pathways to regulate cell contractility and proliferation.

Based on our data that actin filaments are disrupted in *ACTA2* mutant cells, either a Rho/ROCK dependent or SRF dependent mechanism, or a combination of both, may drive increased SMC proliferation. Also, mutation or loss of SM α-actin is likely to alter FA structure and function, disrupting multiple signaling pathways. *We hypothesize that* *pathways with dual roles affecting both SMC contractility and proliferation are upregulated in Acta2$^{-/-}$ SMCs, driving increased proliferation.*

Materials and Methods

Mouse SMC isolation and culture

Acta2$^{+/+}$ and *Acta2*$^{-/-}$ mice were anesthetized with 400mg/kg 2.5% Avertin (2-2-2 Tribromoethanol; Sigma-Aldrich). The ascending portion of the aorta distal to the heart and just proximal to the innominate artery, and the descending portion of the aorta between the left subclavian artery and the renal bifurcation were carefully removed. Adventitial fat was dissected away using a scalpel and forceps. Aortas of two mice from each genotype were pooled, and SMCs were explanted as previously described in Chapter II. Cells were cultured in SmBm supplemented with growth factors (insulin, fibroblast growth factor, and epidermal growth factor; Lonza), 20% FBS (Atlanta Biologicals), 1x antibiotic/antimycotic (Invitrogen), 2mM L-glutamine, 20mM HEPES, and 1mM sodium pyruvate.

Cells were plated at 70-80% confluence (100,000 cells per 35mm dish, 350,000 cells per 60mm dish, or 5,000 cells per 22mm round coverslip) and allowed to attach overnight in complete media. Prior to protein or RNA isolation, cells were placed in lower-serum medium without growth factors, and with 5% FBS, for 24 hours. For inhibitor assays, cells were treated with inhibitor at the time of serum starvation, and were incubated with inhibitor for 24 hours prior to harvesting cells.

For a subset of experiments, dishes and wells were coated with either fibronectin-1 (20 µg/mL; Sigma) or collagen IV (0.1 mg/mL; Sigma). Dishes and wells were allowed to dry at room temperature overnight before cells were plated, and Collagen IV coated dishes were sterilized with UV light for 20 minutes prior to performing the experiment. Plating SMCs on fibronectin-1 drives a more proliferative phenotype, and plating cells on collagen IV drives a differentiated, contractile phenotype (192). We coated plates with both of these matrices separately to determine whether driving either proliferation or differentiation had differential effects on FAK activation and localization of FA components in the wildtype vs. *Acta2*$^{-/-}$ SMCs.

Protein isolation and immunoblotting

Protein isolation and immunoblotting were carried out as previously described, with the exception that phosphatase inhibitor cocktails I and II (10 μL/mL; Sigma-Aldrich) were substituted for the 10 mM NaF and 1 mM Na_3VO_4. Antibodies and dilutions used are listed in **Table 1** in Chapter II.

RNA isolation and quantitative gene expression analysis

RNA isolation and quantitative PCR were performed using Trizol, RNeasy purification, and Taqman gene expression assays as previously described in Chapter II. All data were normalized to 18S and Gapdh separately, with similar results. Data shown in graphs are normalized to 18S.

Microarray analysis

Duplicate samples of total RNA isolated from explanted descending aortic SMCs from wildtype and *Acta2*$^{-/-}$ mice was used for study. An Agilent Bioanalyzer was used to confirm RNA quality. After initial amplification, RNA was labeled and hybridized to an

Illumina MouseWG-6 v2.0 beadchip. Illumina BeadStudio software was used to extract the data and confirm data quality. Genes with a differential expression score of ≥ ± 30 ($p<0.001$) were filtered for analysis. Ingenuity Pathways Analysis software was utilized to determine whether major canonical signaling pathways were altered in the *Acta2*$^{-/-}$ SMCs compared with controls (193). Genes with a twofold or greater change in expression and a p-value ≤ 0.001 on the array were uploaded into the Ingenuity program, the altered genes were compared against Ingenuity's library of canonical pathways, and statistical significance was automatically determined by the software using Fischer's exact tests. Validation of selected genes was performed using Taqman assays on an independent set of RNA samples, as previously described.

Cell proliferation assays

Cells were plated 10,000 cells/well in triplicate. Preliminary experiments were performed using different serum concentrations (0.2% and 5%) for different amounts of time in low-serum media before BrdU was added (0 hours and 24 hours), in order to determine optimal conditions for quantifying cell proliferation.

For treatment with inhibitors, cells were plated 5,000 cells/well (80-90% confluence) and allowed to attach overnight. 20-24 hours after plating, cells were placed in SmBm containing 5% FBS ± inhibitor. After 30 minutes of pre-treatment with inhibitor, cells were incubated with BrdU reagent for 24 hours, and a BrdU ELISA was carried out as previously described. The following inhibitors were used for study: U0126 (ERK), Y27632 (Rho kinase), PF-532,278 (FAK), and PF-562,271 (FAK/Pyk2). Experiments were performed in triplicate, and p-values were obtained using a Student's t-test.

Histology and immunofluorescence

Ascending and descending aortas from wildtype and *Acta2*$^{-/-}$ mice were isolated, formalin-fixed and paraffin-embedded. Tissue sections were stained with H&E for analysis. ImageJ software (NIH) was used to measure the circumference (C) around the inner layer of the aortic wall, and aortic diameter was calculated by dividing C/π (77). Medial thickness was also measured using ImageJ. Immunofluorescence was carried out as previously described, with the following modifications: For phospho-FAK staining, cells were fixed in ice cold 50/50 methanol/acetone for 5 minutes at -20C. Following fixation, coverslips were rinsed 3x in PBS. For all other immunofluorescence, cells were fixed in 4% paraformaldehyde in 0.1M phosphate buffer, as previously described. Cells were permeabilized in PBS containing 0.2% saponin and 10% FBS for 10 minutes, and washed 3x in PBS prior to blocking and staining. 5% normal donkey serum in PBS was used for blocking and for all antibody dilutions. **Table 1** in Chapter II lists the antibodies and concentrations used.

Transwell migration assays

Cells were plated 50,000 per well 0.2% FBS, in transwells containing membranes with 8 μm pores (BD Biosciences). The final volume in each well was 500 μL, and cells were plated in duplicate. Transwells were inserted into wells of a 24-well plate, containing 5% FBS + PDGF-B (10 ng/mL), with a final volume of 750 μL per well. Plates were incubated for 6 hours. Transwells were washed in PBS, and cotton swabs were used to gently remove non-migrated cells from the upper portion of each membrane. Cells were fixed in 4% paraformaldehyde for 10 minutes, washed 3x in PBS, stained with 0.5% crystal violet for 10 minutes, washed 3x in PBS and allowed to dry overnight. Membranes containing stained cells were cut from the transwell chambers and mounted onto slides using Permount (Fisher). Five high-powered fields from each transwell membrane were photographed by a blinded observer, and the cells per high-power field were counted.

Rho activation assay

A Rho pulldown assay was performed to determine whether more active RhoA was present in the *Acta2*$^{-/-}$ SMCs. SMCs were seeded at 80-90% confluence in a T75 culture flask and allowed to adhere overnight. Cells were serum-starved for 24 hours, and were stimulated with complete media containing 20% FBS one hour prior to the assay. Assay components were purchased from Cell Biolabs, Inc. (San Diego, CA). All work was performed in a coldroom. Cells were washed 2x in PBS, and flasks were incubated on ice 1mL lysis buffer for 10 minutes and then scraped. Cell lysates were passed through a 27½ gauge needle to shear genomic DNA, and 60 µL of total lysate was set aside for protein quantification and for immunoblotting of total RhoA. Lysates were centrifuges at 13,000 x g for 10 minutes. Agarose beads conjugated to a Rho binding domain were resuspended, 40 µL of beads was added to each tube, and samples were incubated for 1 hour at 4ºC with gentle shaking. Samples were centrifuged at 13,000 x g for 10 seconds, supernatant was carefully removed and discarded, and samples were washed in 500 µL lysis buffer. The wash was repeated a total of 3 times. After the final wash, the bead pellet was resuspended in 2x reducing sample buffer, boiled for 5 minutes, and centrifuged at 13,000 x g for 10 seconds. Equal volumes of the pull-down assay supernatant, along with the total protein samples, were separated on a 10% polyacrylamide gel, transferred to a PVDF membrane, and immunoblotted for RhoA.

Results

Characterization of the aortic phenotype in Acta2$^{-/-}$ mice

ACTA2 mutations cause aneurysms in humans; however, an aneurysm phenotype had not been previously described in *Acta2*$^{-/-}$ mice. Therefore we wanted to determine whether loss of SM α-actin in *Acta2*$^{-/-}$ mice also led to aneurysm formation. Ascending aortas from *Acta2*$^{-/-}$ mice were significantly larger than wildtype at 10-12 weeks of age, indicating the beginnings of aneurysm formation. Gross examination of the aortic tissue showed enlargement of the ascending aortas in *Acta2*$^{-/-}$ mice compared with wildtype. No obvious enlargement of the descending aorta was present (**Figure V-1A**).

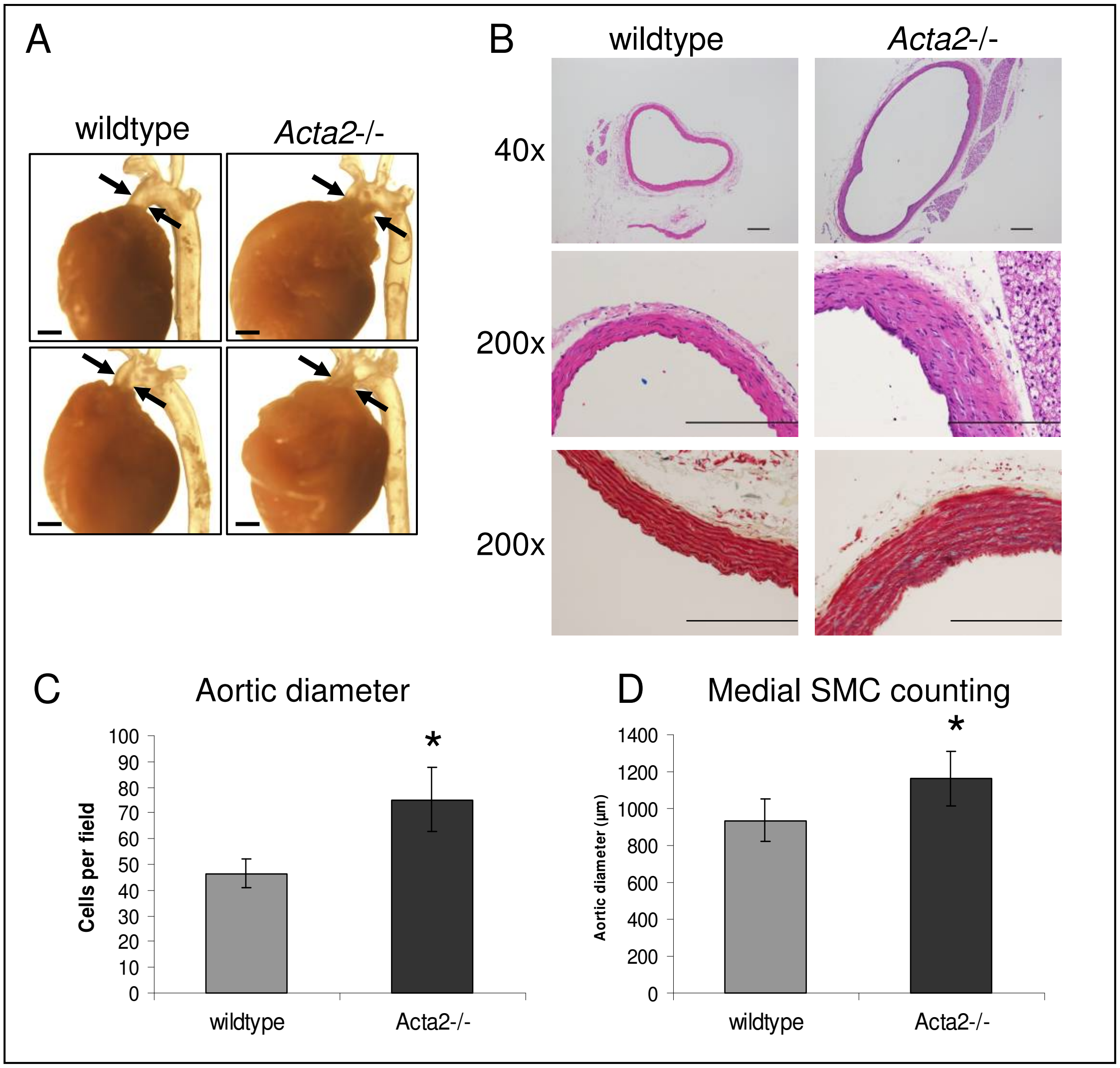
A
wildtype
Acta2-/-
B
wildtype
Acta2-/-
40x
200x
200x
C
Aortic diameter
Cells per field
100
90
80
70
60
50
40
30
20
10
0
*
wildtype
Acta2-/-
D
Medial SMC counting
Aortic diameter (μm)
1400
1200
1000
800
600
400
200
0
*
wildtype
Acta2-/-

Figure V-1. Aortic aneurysms in *Acta2*$^{-/-}$ mice. *Acta2*-/- mice display ascending aortic enlargement accompanied by increased proteoglycans and increased thickening and cellularity in the vessel wall. (A) Upon gross examination, formalin-fixed ascending aortas of 10-12 week old *Acta2*-/- mice appeared larger than age matched wildtype. There were no apparent differences in the descending aorta. Scale bars represent 1.0mm. (B) H&E staining (top two panels) revealed enlargement of the ascending aorta in *Acta*2-/- mice, along with asymmetric thickening of the vessel wall and increased SMCs in the aortic media. Movat staining (bottom panel) showed some proteoglycan accumulation (blue) in the *Acta2*-/- aorta. Top panel is magnified 40x and middle and bottom panels are magnified 200x. Scale

bars represent 500 µM. (C) Aortic diameter was measured using ImageJ analysis software, and is significantly larger in 8-12 week old *Acta2*-/- mice (n=6) than age matched wildtype (n=6). (D) Counting of medial SMCs showed increased SMCs in *Acta2*-/- aortas (n=6) compared with wildtype (n=6). Cells in five high powered fields were counted for each aortic tissue sample. Data for (C) and (D) are shown ± S.D. *p<0.05.

****

Histologic examination of ascending aortic tissue confirmed this enlargement (**Figure 1B**). We used ImageJ software to measure the inner circumference of the aortic wall and then calculated aortic diameter (**Figure 1C**). The diameter was significantly enlarged in 8-12 week old *Acta2*$^{-/-}$ mice (n=6) compared with age matched controls (n=6), and this change was visibly apparent in the tissue in mice as young as 8 weeks.

Aortic aneurysms are associated with medial degeneration of the aorta, characterized by proteoglycan accumulation and elastic fiber loss and fragmentation. We used Movat staining to visualize ECM components in the aorta to determine whether medial degeneration was present in the dilated aortas from Acta2$^{-/-}$ mice. Proteoglycan expression was slightly increased in *Acta2*$^{-/-}$ compared with wildtype aorta (**Figure V-1B**). The aortic wall also appeared asymmetrically thickened in *Acta2*$^{-/-}$ mice. To determine whether this thickening was associated with increased numbers of SMCs in the medial layer, we counted cells under high powered fields (400x; n=4 mice per genotype) and found that *Acta2*$^{-/-}$ aortas had increased SMCs (**Figure V-1D**).

Overall, these data show a previously undescribed aneurysm phenotype in *Acta2*$^{-/-}$ mice, accompanied by an increase in the number of SMCs present in the vascular wall, and minimal changes typical of medial degeneration. Based on these data and on previously published data, *Acta2*$^{-/-}$ mice are likely to be a suitable model for our studies of SMC proliferation in association with aneurysm formation.

Increased proliferation and migration in Acta2$^{-/-}$ *SMCs*

Previous studies reported increased proliferation in *Acta2*$^{-/-}$ renal myofibroblasts (124). Based on these data and on our data showing increased proliferation in *ACTA2* mutant SMCs and myofibroblasts, we hypothesized that the *Acta2*$^{-/-}$ SMCs would also demonstrate increased proliferation and would provide a suitable model system. Our initial experiments to test culture conditions showed that serum deprivation using 5% FBS at the time of BrdU incubation yielded the best and most consistent results. Therefore, this experimental setup was used for the remainder of the cell proliferation assays. Similar to *ACTA2* mutant SMCs and myofibroblasts, *Acta2*$^{-/-}$ SMCs explanted from both the ascending and descending aorta proliferate significantly more rapidly than wildtype *in vitro* (**Figure V-2A**).

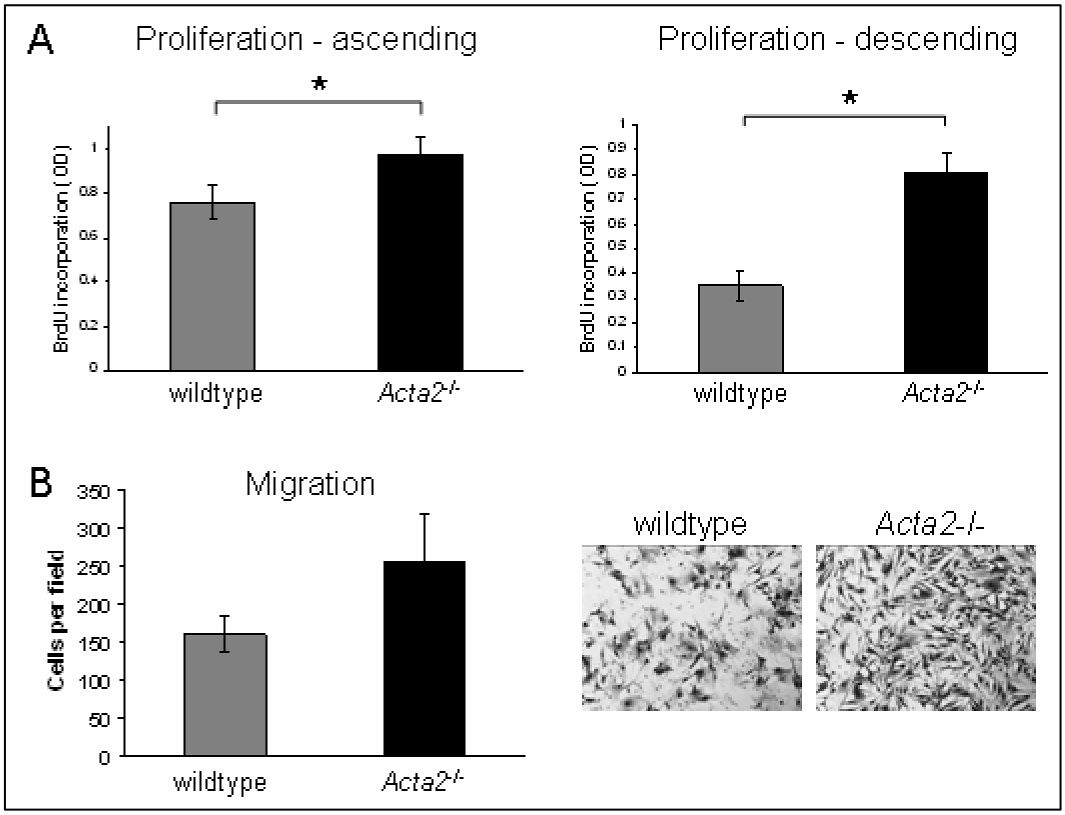

Figure V-2. Increased proliferation and migration in *Acta2*$^{-/-}$ SMCs. (A) SMCs explanted from both the ascending and descending aortas of *Acta2*-/- mice proliferated significantly more rapidly than wildtype. (B) Transwell migration assays showed that *Acta2*-/- SMCs in 0.2% FBS migrated more rapidly toward a gradient of 5% FBS + 10ng/mL PDGF than wildtype. The experiment was performed in duplicate wells and repeated three times. Results were quantified by counting the number of migrated cells per high powered microscope field on the transwell membrane. Five separate fields were counted per sample, and representative images of cells on the transwell membrane are shown. Interestingly, *Acta2*-/- SMCs display slightly elongated morphology compared with wildtype. Error bars represent ± S.E.M. *p<0.05

****

Since increased migration was also described in *Acta2*$^{-/-}$ myofibroblasts, we performed transwell migration assays to determine whether *Acta2*$^{-/-}$ SMCs also displayed increased migration (124). We used a transwell assay rather than a scratch or wounding assay because it allowed for assessment of cell migration in response to a chemotactic gradient (10 ng/mL PDGF-B). However, one disadvantage was that we were unable to monitor changes in cell shape during migration. Descending *Acta2*$^{-/-}$ SMCs migrated more rapidly than wildtype toward the PDGF-B gradient (**Figure V-2B**). These data indicate that *Acta2*$^{-/-}$ SMCs are a suitable model for studying SMC proliferation in response to a contractile protein defect, and suggest that increased SMC migration may be important as well.

ROCK and ERK inhibitors partially but not completely block proliferation

Based on the role that Rho/ROCK plays in actin polymerization and also in SMC proliferation, we hypothesized that Rho was overactivated in *Acta2*$^{-/-}$ mice, in response to the inherent contractile defect. Treatment of *Acta2*$^{-/-}$ SMCs with a ROCK inhibitor, Y27632, resulted in decreased proliferation in both *Acta2*$^{-/-}$ and wildtype SMCs, although only the decrease in *Acta2*$^{-/-}$ SMC proliferation was significant (**Figure V-3A**).

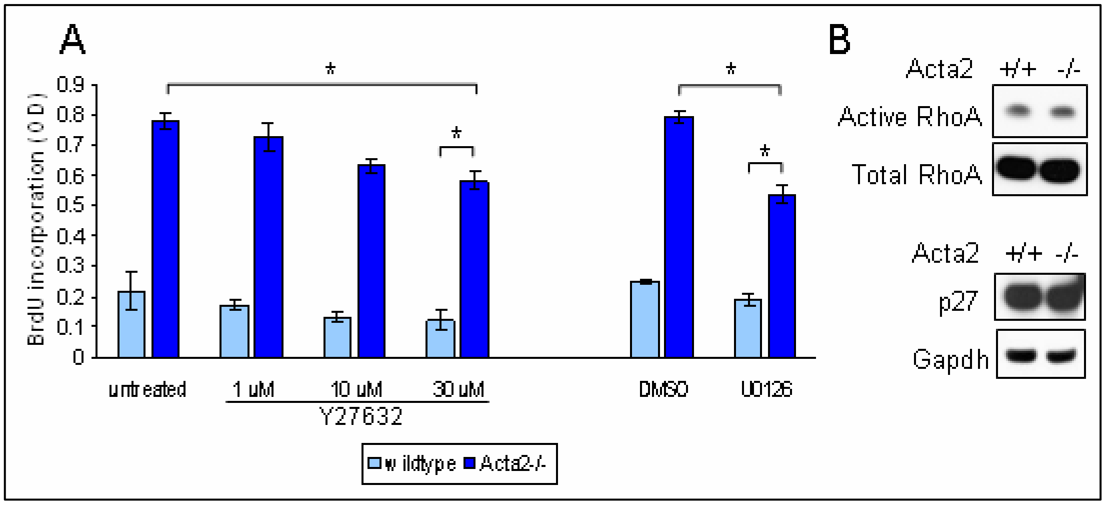

Figure V-3. Rho and ERK inhibitors partially block *Acta2*$^{-/-}$ SMC proliferation. (A) Treatment of SMCs with either a Rho kinase inhibitor (Y27632) or an ERK inhibitor (U0126) caused a significant decrease in proliferation in *Acta2*$^{-/-}$ SMCs but failed to completely block the proliferation compared to wildtype. For the ERK inhibitor, DMSO was added to the untreated cells to control for the DMSO present in the inhibitor solution. Data shown are a mean of three observations and error bars represent ± S.D. *$p<0.05$. (B) A Rho pulldown assay failed to show a difference in GTP-bound RhoA in *Acta2*$^{-/-}$ mice compared to wildtype. Additionally, p27 expression remained the same. Since p27 is degraded in response to RhoA activation, these data suggest that a Rho/p27 mediated mechanism is not likely driving proliferation.

****

Since doses of 10, 20, and 30 μM were used to block Rho activation and proliferation in *TSC2*$^{-/-}$ cells, we treated *Acta2*$^{-/-}$ SMCs with the same doses (194). However, even the highest dosage of 30 μM failed to completely prevent increased proliferation. Since the ROCK inhibitor partially inhibited proliferation, we used a Rho pulldown assay to determine whether RhoA activation was increased. We did not observe any difference in Rho activity between the *Acta2*$^{-/-}$ and wildtype SMCs (**Figure V-3B**). Since small changes in RhoA can be difficult to detect using this assay, we immunoblotted for p27, since it is known to be degraded in response to Rho activation (169). However, p27 levels were not altered. Together, these data suggest that Rho/ROCK activation plays a role in overall SMC proliferation, but is not the main pathway driving proliferation in the *Acta2*$^{-/-}$ SMCs.

We also hypothesized that a switch between SRF/MRTF and SRF/TCF mediated gene expression, in concert with growth factor stimulated ERK activation, might be driving proliferation. We labeled SMCs with MRTF-A to determine subcellular localization. We expected to find increased cytoplasmic localization; however, immunofluorescent labeling failed to yield interpretable results. QPCR analysis of c-fos, a gene known to be induced by SRF/TCF, showed that steady state expression levels were not increased in the *Acta2*$^{-/-}$ SMCs (not shown). We hypothesized that an increase in G-actin leads to increased cytoplasmic localization of MRTFs. We also hypothesized that in the complete absence of SM α-actin, β-actin filaments would be disrupted. However, immunofluorescent labeling of β-actin did not reveal an appreciable difference in β-actin filaments between the wildtype and *Acta2*$^{-/-}$ SMCs. Overall, we were unable to conclusively determine whether SRF mediated signaling contributes to the proliferation. Since IGF-1 was increased in *ACTA2* mutant SMCs and myofibroblasts, and is also known to activate ERK signaling, we hypothesized that IGF-1 along with ERK activation would be increased and potentially drive proliferation. However, in contrast to *ACTA2* mutant SMCs and myofibroblasts, we did not find any change in IGF-1 gene expression in *Acta2*$^{-/-}$ SMCs, suggesting that either other growth factors or other cellular pathways may be more important in the proliferative phenotype. Similar to the ROCK inhibitor, an ERK inhibitor, U0126, partially blocked but did not fully prevent increased proliferation in the *Acta2*$^{-/-}$ SMCs (**Figure V-3A**). Additionally, untreated *Acta2*$^{-/-}$ SMCs failed to show consistent increases or decreases in phosphorylated ERK (not shown). Taken together, these data suggest that although ERK activation may drive part of the increased proliferation, additional cellular pathways are involved.

Gene expression analysis in Acta2$^{-/-}$ SMCs

We used Ingenuity Pathway Analysis software to determine whether canonical pathways were altered in the *Acta2*$^{-/-}$ SMCs, leading to proliferation. Interestingly, the top canonical pathway identified by Ingenuity was Hepatic Fibrosis/Hepatic Stellate Cell Activation (p = 5.72E-10). Hepatic stellate cells are capable of transitioning to a myofibroblast-like proliferative phenotype and producing excessive ECM proteins (particularly collagen) in response to injury, and both the proliferation and ECM production are dependent on FAK signaling (195). Since both FAK and procollagen 1 expression were increased in *Acta2*$^{-/-}$ renal myofibroblasts, we would expect to find increased collagen production as well as FAK in the *Acta2*$^{-/-}$ SMCs (124). Since FAK is an integral part of FAs, we also looked for alterations in any genes known to be associated with focal adhesions (196). We found alterations in genes associated with ECM production and FAs, as well as genes associated with the SMC contractile complex and cell adhesion. A summary of these genes is listed in **Table 4**.

Table 4. FA, ECM, adhesion, and contractile genes altered in *Acta2*-/- SMCs.

Contractile apparatus

Gene	Protein name	Fold change
Actg2*	actin, gamma 2, smooth muscle, enteric	24.78
Myh11*	myosin, heavy polypeptide 11, smooth muscle	8.44
Smtn	smoothelin	2.26
Tagln	transgelin	3.81
Tpm2	tropomyosin 2, beta	2.12
Tpm1	tropomyosin 1, alpha	1.58
Acta2*	actin, alpha 2, smooth muscle	-8.96

Extracellular Matrix

Gene	Protein name	Fold change
Eln	elastin	8.09
Col12a1	procollagen, type XII, alpha 1	7.99
Col18a1	procollagen, type VIII, alpha 1	7.03
Col6a3	procollagen, type VI, alpha 3	6.76
Col3a1	procollagen, type III, alpha 1	4.36
Col15a1	procollagen, type XV	3.88
Col7a1	procollagen, type VII, alpha 1	3.57
Col6a2	procollagen, type VI, alpha 2	2.95
Col5a1	procollagen, type V, alpha 1	2.79
Col10a1	procollagen, type X, alpha 1	2.75
Col4a1	procollagen, type IV, alpha 1	2.51
Col4a2	procollagen, type IV, alpha 2	2.38
Fn1	fibronectin 1	2.08
Col6a1	procollagen, type VI, alpha 1	2.01
Col1a2	procollagen, type I, alpha 2	1.94
Col5a2	procollagen, type V, alpha 2	1.52
Col16a1	procollagen, type XVI, alpha 1	1.33
Col4a5	procollagen, type IV, alpha 5	-1.36
Col8a1	procollagen, type VIII, alpha 1	-1.75
Col4a6	procollagen, type IV, alpha 6	-5.62
Col28a1	collagen, type XXVIII, alpha 1	-6.26

Cadherins

Gene	Protein name	Fold change
Cdh5	cadherin 5 (VE-cadherin)	6.15
Cdh13	cadherin 13 (T-cadherin)	4.83
Pcdh9	protocadherin 9	-3.79
Pcdh21	protocadherin 21	-3.80
Gm1010	cadherin-like 26	-3.99
Cdh3	cadherin 3 (P-cadherin)	-4.77

Focal adhesion-related genes

Gene	Protein name	Fold change
Itga5	integrin alpha 5 (fibronectin receptor alpha)	2.24
Itga11	integrin, alpha 11	3.98
Itgb4	integrin beta 4, transcript variant 2	4.83
Lims2	LIM and senescent cell antigen like domains 2 (pinch2)	3.58
Fhl2	four-and-a-half LIM domains 2	3.25
Palld	palladin	3.43
Bmx	BMX non-receptor tyrosine kinase (Etk)	3.06
Csrp1	cysteine and glycine-rich protein 1	3.01
Flnb	filamin B	2.15
Cav1	caveolin, caveolae protein 1	1.96
Vim	vimentin	1.77
Rac3	RAS-related C3 botulinum substrate 3	1.65
Nck2	non-catalytic region of tyrosine kinase adaptor protein 2	1.61
Sorbs1	ponsin	1.58
Actn1	actinin, alpha 1	1.57
Tgfb1i1	TGF-β1 induced transcript 1	1.49
Sdcbp2	syntenin 2	1.44
Rapgef1	Rap GEF 1	1.42
Ptk2b	protein tyrosine kinase 2 beta	1.37
Itgb1bp1	integrin beta1 binding protein 1	1.36
Vcl	vinculin	1.22
Parva	parvin, alpha	-1.25
Zyx	zyxin	-1.30
Ppfia1	liprin	-1.46
Sdcbp	syntenin 1	-1.54
Vil2	ezrin	-1.57
Pfn2	profilin 2	-1.58
Tln2	talin 2	-1.64
Prkcm	polycystin-1	-1.69
Pfn2	profilin 2	-1.78
Pak4	p21 protein-activated kinase 4	-2.42

Other

Gene	Protein name	Fold change
Pip5k1b*	PIP5 kinase, type 1 beta	13.49
Srpx2	Sushi repeat protein X-linked 2	11.40

*denotes validation by Q-PCR

Table 4. FA, ECM, adhesion, and contractile genes are altered in *Acta2*$^{-/-}$ SMCs. *Acta2*$^{-/-}$ SMCs displayed increased ECM production, including elastin, fibronectin 1, and fifteen different collagen genes. Multiple FA-associated and adhesion genes are also altered, suggesting that these SMCs are fibrogenic and have altered adhesive properties. The fold change listed is the relative expression level in *Acta2*$^{-/-}$ SMCs compared with wildtype. An asterisk denotes validation via QPCR.

****

FAK gene expression was unaltered, and this was confirmed via QPCR; however, fifteen different collagen genes were upregulated, and twelve of these were increased by twofold or more. Only four collagen genes were downregulated, and two were decreased by more than twofold. Elastin and fibronectin also were upregulated eightfold and twofold, respectively. Since ECM overproduction is a characteristic feature of de-differentiated SMCs and ECM accumulation is evident in the intimal lesions in humans, we hypothesized that *Acta2*$^{-/-}$ SMCs exhibit a de-differentiated phenotype. However, expression of multiple terminal SMC differentiation markers were either unaltered or were increased in the *Acta2*$^{-/-}$ SMCs. Out of these genes, we validated increased expression of *Myh11* and *Actg2*. Calponin 1 is an additional marker of differentiated SMCs: although this gene was not listed in the array results, QPCR analysis showed that this gene was also increased in *Acta2*$^{-/-}$ SMCs. All of these gene expression data suggest a differentiated, contractile SMC phenotype rather than a de-differentiated phenotype. Additional evidence that these SMCs are not de-differentiated is S100A4 expression. S100A4 is a marker for de-differentiated SMCs in culture, but was not increased in *Acta2*$^{-/-}$ SMCs (197). The most highly upregulated gene on the array was *Actg2*, encoding SM γ-actin, and was increased 24.78-fold. These data are consistent with SM γ-actin increases reported by Takeji et al (124).

A number of genes encoding proteins that are known to be associated with FAs were altered in the *Acta2*$^{-/-}$ SMCs. Out of these alterations, twenty-two genes were upregulated, and nine of these genes were increased by twofold or greater. Ten genes were downregulated, and only one gene was downregulated by more than twofold. Of note, several integrin receptor levels are increased in the *Acta2*$^{-/-}$ SMCs: β4, α5, and α11. Several kinases, either associated directly or potentially associated with FAs, were also increased, including Etk, FAK2, and Pip5k1b. Although not directly localized to FAs under normal conditions, Pip5k1b has the potential to localize to the cell membrane when overexpressed (198). Also, Pip2 production within the cell has the potential to influence and regulate FA dynamics (198). Therefore, although not included in the final count of upregulated FA-related genes, Pip5k1b may be relevant for the study of FA alteration in the *Acta2*$^{-/-}$ SMCs.

Other adhesion-related genes were also altered in *Acta2*$^{-/-}$ SMCs. Cadherin 13 was upregulated 4.83-fold and is of particular interest because this protein, unlike other cadherins, has anti-adhesive properties, and its expression is associated with increased cell migration and proliferation, as well as alterations in FA localization with the cell (199). SMCs from *Acta2*$^{-/-}$ mice are generally more elongated in culture, and this change is particularly evident in the descending SMCs (**Figure V-2B**). The elongated phenotype, coupled with overexpression of cadherin-13, is consistent with reports of cells that have been transfected with cadherin-13 or that have been plated on a cadherin-13-containing substrate(199). *Srpx2* (Sushi repeat containing protein, X-linked 2) gene expression was also highly upregulated (11.4-fold). Recently, this protein was found to increase FAK activation in gastric cancer (200). Collectively, these microarray data suggest that FAs are altered in *Acta2*$^{-/-}$ SMCs.

Focal adhesions are altered in Acta2$^{-/-}$ *SMCs*

Vinculin is a marker for mature FAs, and tensin is a general marker for fibrillar adhesions. Since tensin and vinculin colocalization is an indicator of supermature FAs in differentiated myofibroblasts, we double-immunolabeled *Acta2*$^{-/-}$ and wildtype SMCs with these markers to determine if FA maturation was altered in the *Acta2*$^{-/-}$ SMCs (180). Tensin immunofluorescence showed a small amount of tensin-vinculin colocalization in the wildtype compared to *Acta2*$^{-/-}$ SMCs, possibly due to vinculin localization more at the cell periphery in the *Acta2*$^{-/-}$ SMCs than in wildtype (**Figure V-4A**).

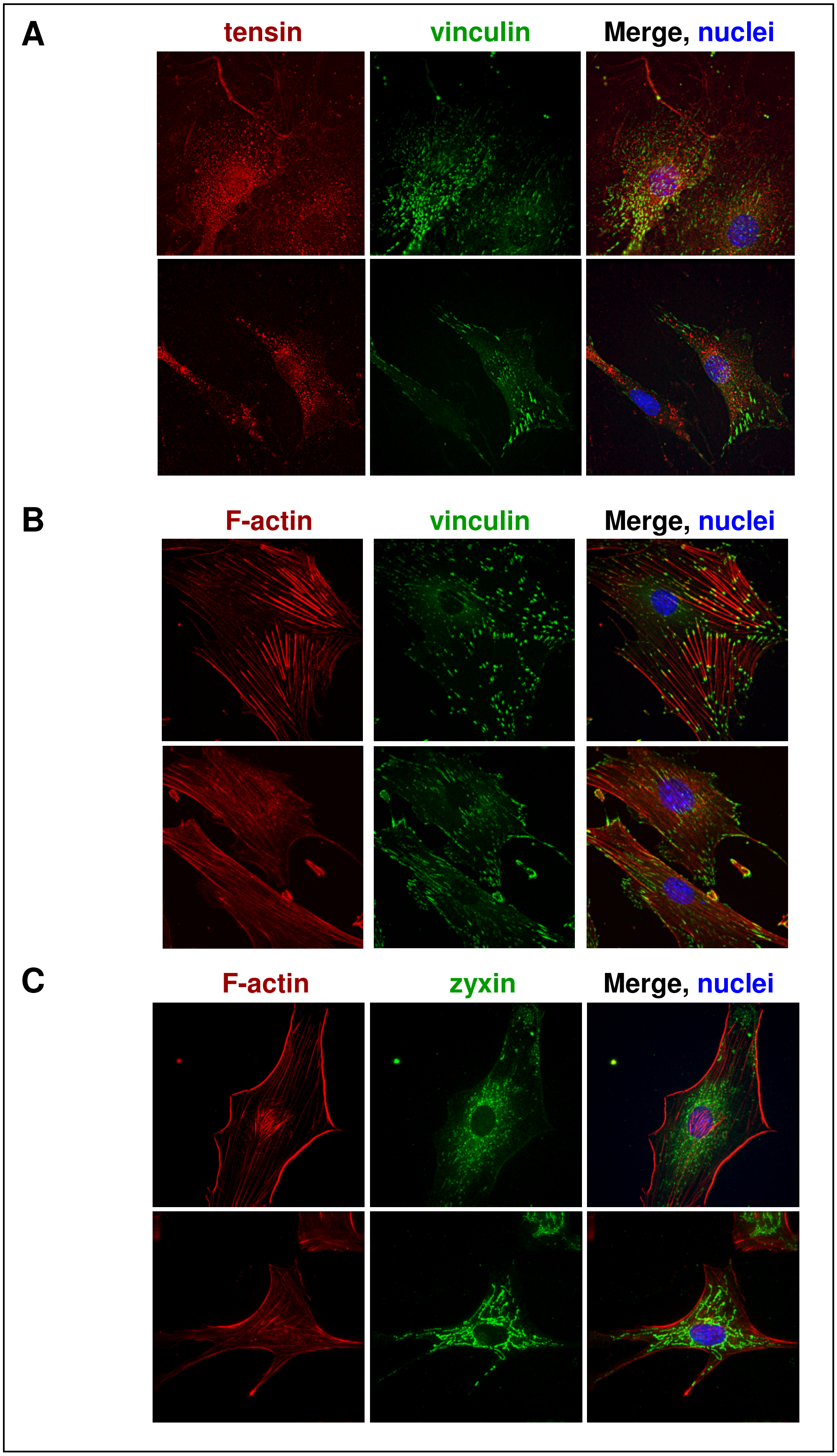
A
tensin
vinculin
Merge, nuclei
B
F-actin
vinculin
Merge, nuclei
C
F-actin
zyxin
Merge, nuclei

Figure V-4. Altered localization of FA components in *Acta2*$^{-/-}$ SMCs.

(A) Since tensin and vinculin colocalize in supermature FAs, we double labeled *Acta2*$^{-/-}$ and wildtype SMCs with tensin and vinculin. A small amount of tensin and vinculin colocalization is present in the wildtype but not *Acta2*$^{-/-}$ SMCs, possibly due to vinculin localization more at the cell periphery in *Acta2*$^{-/-}$ SMCs. (B) Vinculin-containing FAs (green) are localized more to the cell periphery in *Acta2*$^{-/-}$ SMCs than in wildtype SMCs. Results are representative of cells plated on collagen IV coated, fibronectin-1 coated, or uncoated coverslips, from two separate experiments. This staining pattern can also be seen in panel A. Staining of actin stress fibers (red) confirmed vinculin localization at adhesion sites at the ends of the actin fibers. Since vinculin is a definitive marker for FAs, these data confirm that FAs are altered in *Acta2*$^{-/-}$ SMCs compared to wildtype. (C) Since zyxin localizes to FAs but translocates to actin stress fibers or to the nucleus when cells are exposed to mechanical force, we immunofluorescently labeled SMCs with zyxin (green) and observed consistent alterations in zyxin staining patterns. In wildtype SMCs zyxin was localized to some adhesion sites at the cell periphery, and also localized in a punctate pattern within the perinuclear region of the cell. In *Acta2*$^{-/-}$ SMCs, zyxin exhibited a distinct, tubular staining pattern that was neither perinuclear nor localized to actin stress fibers. The subcellular structure(s) that zyxin is localizing to in these cells has not yet been determined; however, together these data support that FAs are altered in *Acta2*$^{-/-}$ SMCs. Cells shown were plated on fibronectin-1; similar and consistent results were obtained for cells plated on collagen IV and on uncoated coverslips.

****

Since vinculin is a widely used marker for FAs, we double immunolabeled cells with vinculin along with phalloidin, so that both FAs and actin filaments within the cell could be visualized. We observed that vinculin is consistently localized more to the cell periphery in the *Acta2*$^{-/-}$ SMCs than in wildtype (**Figure V-4A,B**). Similar localization patterns have been observed in fibroblasts that lack integrin-linked kinase (another FA-associated protein) and in SMCs that overexpress cadherin 13 (199;201).

Zyxin localizes to mature FAs, but also acts as a sensor and transducer of mechanical force in SMCs and moves from the FAs to the actin filaments with the application of mechanical force to cells (202;203). Since *Acta2*$^{-/-}$ mice have decreased aortic contractility, we hypothesized that localization of a mechanosensitive FA marker would be altered in these cells compared with wildtype. Whereas in wildtype mice zyxin was present in FAs at the cell periphery and in more punctate patterns in the perinuclear region, in *Acta2*$^{-/-}$ SMCs zyxin was formed into long, tortuous rodlike structures that do not localize with the β-actin filaments or in the nucleus (**Figure V-4C**). Based on these studies, zyxin localization is altered in the *Acta2*$^{-/-}$ SMCs but the etiology of the rod shaped structures that appear with zyxin staining in the null cells has not been determined.

Fibronectin-coated coverslips were used for all of the immunofluorescence studies for several reasons: 1) fibronectin drives FA formation in SMCs and therefore should highlight any problems with FA formation in the *Acta2*$^{-/-}$ SMCs, and 2) the most consistent inhibition of cell proliferation with two different FAK inhibitors (described below) was obtained using cells plated on fibronectin. While all results shown are from SMCs plated on fibronectin coated coverslips, SMCs plated on both collagen IV and uncoated coverslips produced similar results.

Since FAK is important for scaffolding as well as regulating FA formation and turnover, we immunostained and immunoblotted for phosphorylated FAK. Immunoblotting showed a slight increase in FAK in the descending but not the ascending SMCs, and immunoblot results from the descending SMCs are shown in **Figure V-5A**.

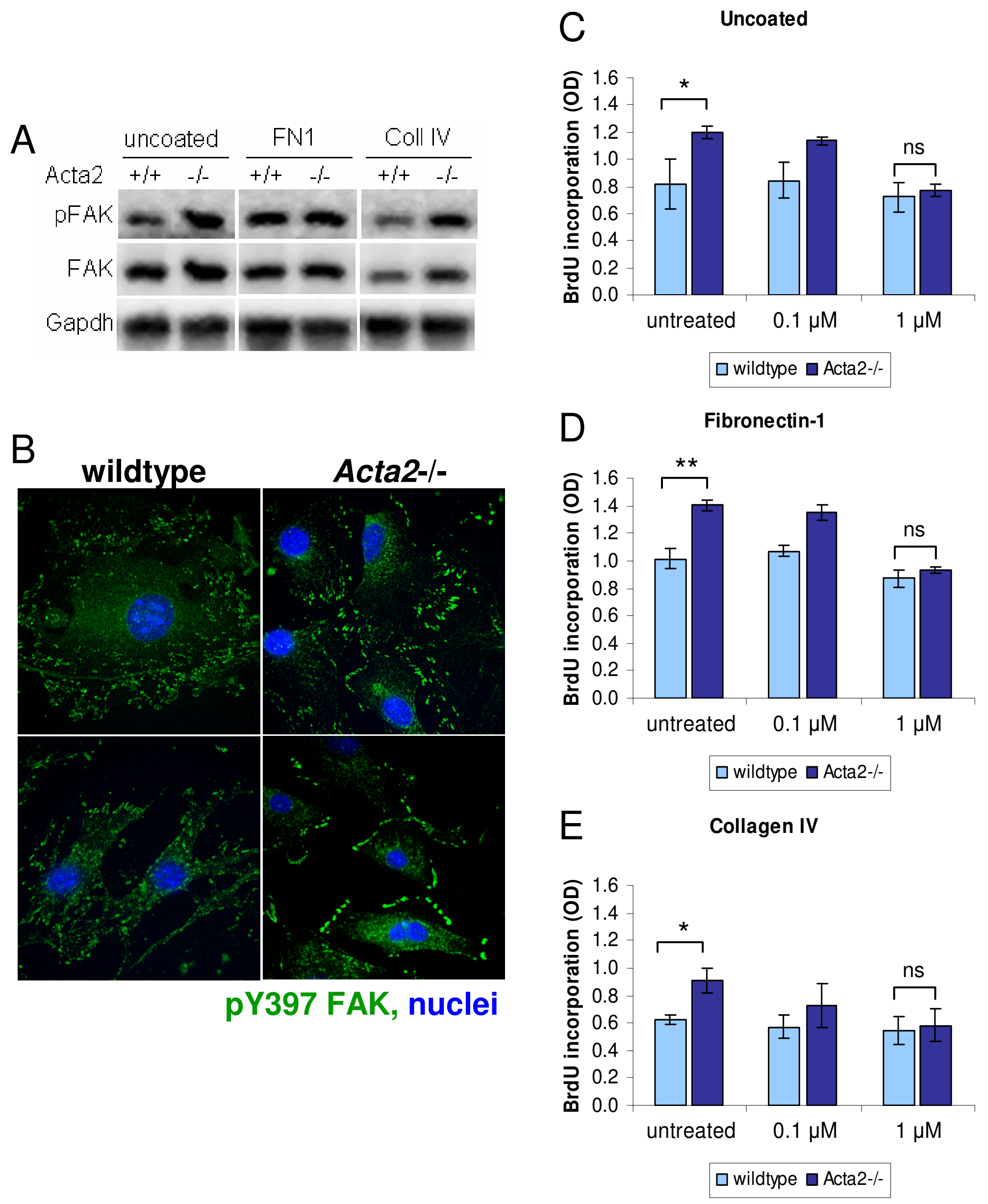

Figure V-5. FAK dependent proliferation in *Acta2*$^{-/-}$ SMCs. (A) Immunoblotting showed that pY397 FAK and total FAK are increased in descending *Acta2*$^{-/-}$ SMCs when plated on

uncoated or collagen IV coated matrices. The difference was less apparent in cells plated on fibronectin-1. (B) pY397 FAK is localized more to FAs at the cell periphery in *Acta2*$^{-/-}$ SMCs. This was consistent for both ascending (top two panels) and descending (bottom two panels) SMCs. Additionally, pY397 FAK staining at FAs appears more intense in *Acta2*$^{-/-}$ SMCs than in wildtype. (C-E) The FAK inhibitor PF-562,271 completely blocked increased proliferation in *Acta2*$^{-/-}$ SMCs plated on uncoated plates (C), and fibronectin-1 or collagen IV coated plates (D and E, respectively). A second FAK inhibitor, PF-532,278, completely blocked proliferation on fibronectin-1 coated surfaces but not uncoated or collagen IV coated surfaces (not shown). Together, these data indicate that *Acta2*$^{-/-}$ proliferation is dependent on FAK signaling. Experiments were performed in triplicate, and data are shown ± S.D. *p<0.05, **p<0.01, ns = not significant.

****

Densitometry did not yield a statistically significant difference in increased FAK between the *Acta2*$^{-/-}$ and wildtype SMCs. However, immunofluorescent staining revealed alterations in the localization of phosphorylated FAK in *Acta2*$^{-/-}$ compared with wildtype SMCs. Phosphorylated FAK is concentrated at focal adhesions at the cell periphery (**Figure V-5B**). Although FAK can be autophosphorylated within the cytoplasm, FAK that is actively signaling is only found in FAs (204). Therefore, the stronger localization of phosphorylated FAK at the cell periphery in FAs in *Acta2*$^{-/-}$ SMCs suggests that FAK signaling is increased, even though total levels of FAK are not dramatically altered.

Multiple FAK inhibitors block increased proliferation in Acta2$^{-/-}$ *SMCs*

SMCs plated on collagen, fibronectin, or uncoated 96-well plates were treated ± either of two FAK inhibitors, PF-532,278 or PF-562,271. We initially chose to use PF-532,278 because of its availability and specificity (205). This inhibitor completely blocked proliferation of the *Acta2*$^{-/-}$ SMCs plated on fibronectin-1 but only partially blocked proliferation in cells plated on collagen IV or uncoated plates (data not shown). To confirm the results, we obtained PF-562,271, a molecule that is currently in clinical trials for treatment of cancer (206). In contrast to the first FAK inhibitor, PF-562,271 completely prevented increased proliferation in *Acta2*$^{-/-}$ SMCs plated on all of the three matrices. Results are shown for fibronectin-plated cells treated ± PF-562,271 (**Figure V-5C**). Similar results were obtained for cells plated on uncoated or fibronectin-1 coated matrices ± PF-562,271, and also for cells plated on fibronectin-1 coated matrices ± PF-532,278 (not shown). Together, these data suggest that FAK dependent signaling is at least in part driving the observed proliferation in *Acta2*$^{-/-}$ SMCs.

Discussion

Acta2$^{-/-}$ mice are the first mouse model of aortic disease caused by disruption of a SMC-specific contractile protein. Additional characterization of these mice and *in vivo* quantification of the increases in aortic diameter should confirm this finding. Aortas in mice as young as 8 weeks are enlarged compared with wildtype, and aortas were previously shown to display decreased contractility, suggesting that these mice are a good model for studying aneurysm formation due to an inherent SMC contractile defect. Since other existing mouse models of aortic aneurysms focus on the contribution of TGF-β1 signaling and/or extracellular matrix proteins, a mouse model with an SMC contractile defect represents a unique opportunity to define novel pathways leading to aneurysm formation. Establishment of this model is important for our understanding of thoracic aortic disease. The *FBN1* mouse recapitulates the aneurysms found in MFS, which involve initially the sinuses of Valsalva. In contrast, aneurysms in patients with *ACTA2* mutations are the more common form of aneurysm, sparing the sinuses of Valsalva and involving the ascending aorta. These are also the type of aneurysms that form due to chronic hypertension. The *Acta2*$^{-/-}$ mice showed enlargement of the ascending aorta and should be particularly useful in determining the differences in pathogenesis between aneurysms due to MFS and aneurysms caused by either hypertension or *ACTA2* mutations.

Increased SMC numbers in aortic tissue indicate that *Acta2*$^{-/-}$ mice are a good model for studying the contribution of cell proliferation to aortic aneurysm formation as well. We observed increased SMCs and expansion of the vessel wall were found prior to significant medial degeneration in *Acta2*$^{-/-}$ mice. This is in contrast to aneurysm formation in MFS mouse models, where medial degeneration occurs at an early stage and increased SMCs in the medial layer are not observed (10). The observation that one of the initial pathologic features in the *Acta2*$^{-/-}$ aortas is SMC proliferation suggests a potential role for proliferation in aneurysm formation in this mouse, and raises the question of whether SMC proliferation drives aneurysm formation in *ACTA2* mutant aortas. Recent pathologic examination of aortic tissues from patients with an exceptionally severe *ACTA2* mutation, R179C, support this idea (Dianna Milewicz, personal communication). Aneurysmal tissue from these patients showed minimal medial degeneration coupled with subintimal SMC hyperplasia.

Through study of *Acta2*$^{-/-}$ SMCs, we have made several important observations: alterations in expression of FA-associated genes, peripheral localization of FAs, increased pFAK localization in FAs, and increased proliferation that is dependent at least in part on FAK. Altered vinculin localization in *Acta2*$^{-/-}$ SMCs provides evidence of disruption of both FAs and contractile force generation by the cell. Vinculin incorporation into FAs is required for generation of force by SMCs and is thought to be proportional of the amount of force being generated by the cell (207). This idea is consistent with the decrease in vinculin-containing adhesions across the cell body of *Acta2*$^{-/-}$ SMCs, and also agrees with previously published data that *Acta2*$^{-/-}$ aortas (and by implication also, *Acta2*$^{-/-}$ SMCs) have decreased ability to contract in vivo (117). Further, the stability of focal complexes at the cell periphery may be altered, and future work will determine whether FA turnover is increased in *Acta2*$^{-/-}$ compared to wildtype SMCs. The increased migration observed in the *Acta2*$^{-/-}$ SMCs is consistent with a rapid rate of FA assembly and disassembly (179).

Changes in localization of zyxin suggest that *Acta2*$^{-/-}$ SMCs have an altered ability to transduce force signals. Zyxin is a mechanosensitive component of FAs that is translocated to either actin stress fibers or to the nucleus when the cell is placed under mechanical stress, and may also act to reinforce the cell cytoskeleton (202;203). Future work will identify the subcellular structure that zyxin is localizing to within *Acta2*$^{-/-}$ SMCs.

In addition to the observed alterations in other FA proteins, FAK expression and localization is also altered. In the descending SMCs, FAK expression is increased, consistent with data from *Acta2*$^{-/-}$ myofibroblasts (124). However, unlike the myofibroblasts, this increase was not nearly as pronounced, and was not statistically significant. This could be due to inherent differences between myofibroblasts and SMCs.

Similar to patterns of vinculin immunofluorescent staining, phosphorylated FAK is localized more at FAs at the cell periphery in *Acta2*$^{-/-}$ SMCs compared to wildtype. Since these cells also migrate more rapidly in culture, these data are consistent with other reports of FAK localization to peripheral FAs during cell migration (204). FAK is found primarily at FAs but can be localized in the cytoplasm or nucleus as well. Phosphorylated FAK (Y397) is found mainly at FA sites along the cell periphery, but can also be autophosphorylated while still in the cytoplasm and/or localized to FAs further away from the edge of the cell (204). Transfecting cells with a C-terminal fragment of FAK displaced FAK from FAs and reduced proliferation and migration, showing that localization of FAK to FAs is required for fully functional signaling (185). Thus, despite the fact that immunoblotting did not reveal large differences in FAK phosphorylation, the immunofluorescence data show more FAK localization at the cell periphery, suggesting that FAK is altered in *Acta2*$^{-/-}$ SMCs.

Multiple FAK inhibitors were successful in blocking proliferation in *Acta2*$^{-/-}$ but not wildtype SMCs plated on fibronectin-1, suggesting that *Acta2*$^{-/-}$ proliferation is at least in part dependent on FAK. However, both of the kinase inhibitors used target FAK as well as several other nonspecific targets (205;206). PF-562,271 also inhibits Pyk2 (FAK2), which also localizes to the cell membrane and can drive proliferation when activated (208). Although Pyk2 is not nearly as highly expressed as FAK in SMCs, Pyk2 mRNA expression is marginally increased (1.37-fold) in *Acta2*$^{-/-}$ SMCs. This increase in expression has not yet been validated, and the role of Pyk2 in *Acta2*$^{-/-}$ SMC proliferation remains unknown. PF-562,271 appears to be a more potent inhibitor of Pyk2 than PF-573,228, which may explain why only partial inhibition of proliferation was achieved on uncoated and collagen-coated matrices using this inhibitor. Thus, while localization of phosphorylated FAK is clearly altered in the null SMCs, we cannot rule out the possibility that the complete inhibition of proliferation is due to the dual inhibition of FAK and Pyk2 (205;206).

Microarray analysis revealed increased SMC contractile gene expression, increased collagen gene expression, and alterations in a number of FA-associated genes. Since *Acta2*$^{-/-}$ SMCs were more proliferative and showed increased levels of ECM genes, we expected these cells to have a more de-differentiated phenotype. However, contrary to our expectations, *Acta2*$^{-/-}$ SMCs had increased expression of multiple markers of mature SMCs, including *Myh11* and *Cnn1*. Additionally, these SMCs did not display increased expression of S100A4, a marker of dedifferentiated, proliferative SMCs. These data indicate that *Acta2*$^{-/-}$ SMCs are proliferating in the absence of phenotypic switching, and agree with other observations that contractile and synthetic SMCs do not necessarily represent two mutually exclusive SMC phenotypes (56).

Multiple genes on the microarray suggest that FAs and potentially cell adhesion are altered, and future study will determine whether these alterations play a role in regulating proliferation. Cadherin-13 is of particular interest because of its anti-adhesive properties and the fact that its expression correlates with SMC proliferation (209). Another potential gene for follow-up is caveolin-1, which was upregulated 1.96-fold in *Acta2*$^{-/-}$ SMCs. Phosphorylated caveolin-1 is necessary but not sufficient to stabilize FAK within FAs and promote FA turnover (210). A third gene that deserves further study is Pip5k1b. The observation of increased Pip5k1b expression in the *Acta2*$^{-/-}$ SMCs raises the question of whether Pip2 production is altered at FAs in these cells. Although the α and β isoforms of Pip5k1 are not directly associated with FAs, the γ isoform is, and all of the Pip5k1 isoforms are responsible for some of the Pip2 production within the cell. Pip2 promotes the nucleation of new actin filaments by causing the release of gelsolin from actin (211). Pip2 also plays a role in FAK activation; however, localization within the cell is important. It remains to be determined whether Pip5k1b protein levels are increased, and whether increased Pip2 production within the cytoplasm plays a role in FA signaling in the *Acta2*$^{-/-}$ SMCs. A fourth adhesion-related gene, *Srpx2* (Sushi repeat containing protein, X-linked 2), may be interesting for follow-up as well. As previously mentioned, this protein is capable of activating FAK and promoting cell adhesion and migration in gastric cancer (200). All of these genes have potential relevance to both FAK and cell proliferation, and support a role for FAK regulation of proliferation in *Acta2*$^{-/-}$ SMCs. Future work will elucidate the role of these genes in *Acta2*$^{-/-}$ SMC proliferation.

In these studies, we have described for the first time alterations in both FA gene expression and protein localization in *Acta2*$^{-/-}$ SMCs, along with a role for FAK in driving increased proliferation in these cells. Since SM α-actin stabilizes FAs to allow for generation of contractile force, an inability to form SM α-actin filaments could result in increased FAK-mediated turnover of FAs and/or inability of the cells to form fully mature FAs capable of transducing mechanical force and responding to mechanical stress. Our data showing altered vinculin, zyxin, and phospho-FAK localization supports the idea that the *Acta2*$^{-/-}$ SMCs are unable to generate sufficient tension. The fact that FAK inhibitors reduced proliferation in *Acta2*$^{-/-}$ SMCs to levels equal to wildtype SMCs suggests a role for FAK signaling in driving *Acta2*$^{-/-}$ SMC proliferation. Thus, the altered FAK localization and signaling may be a compensatory mechanism resulting from the inability of *Acta2*$^{-/-}$ SMCs to generate sufficient intracellular tension.

Our data suggest *Acta2*$^{-/-}$ SMCs have decreased ability to respond to mechanical stress; therefore, stretching the SMCs *in vitro* may reveal even more pronounced alterations in FAs. Future studies will determine whether this is the case, by exposing the cells to cyclic mechanical strain on a Flexcell apparatus. Additionally, the specific downstream pathways activated by FAK to induce proliferation in *Acta2*$^{-/-}$ SMCs remain undefined, and future work will determine whether a specific downstream pathway or a combination of pathways are driving proliferation. Based on our current data, we predict that multiple pathways are likely to contribute.

In addition to these *in vitro* studies, we also plan to determine SMC proliferation *in vivo* in the *Acta2*$^{-/-}$ mice is dependent on FAK, using an established carotid injury model. Data generated using this model show that *Acta2*$^{-/-}$ mice have a greater proliferative response to vascular injury than wildtype mice, and we expect that a FAK inhibitor will prevent this proliferation *in vivo*. Finally, it will be exciting to determine whether FA alterations and FAK signaling are altered in patients heterozygous for *ACTA2* or *MYH11* mutations. Disruption of an SMC-specific contractile protein leading to an increase in FAK-dependent proliferation may represent a novel pathway leading to the combined phenotype of familial TAAD and vascular occlusive disease.

CHAPTER VI

DISCUSSION

We have identified a novel vascular pathology caused by mutations in the SMC-specific contractile genes *MYH11* and *ACTA2*. These studies provide the pathologic and cell biology data to support the hypothesis that a single gene defect can cause diverse vascular diseases in multiple arteries throughout the body. Furthermore, our data suggest two differing effects of *ACTA2* mutations on SMCs: a loss of function, leading to decreased SMC contraction, and a gain of function, leading to increased SMC proliferation (**Figure VI-1**).

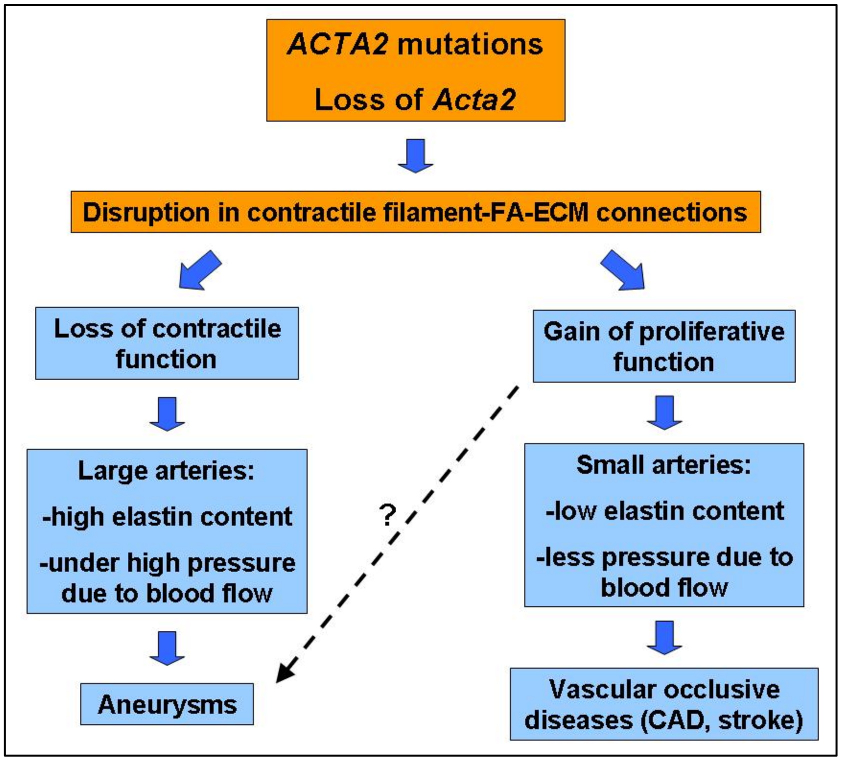
ACTA2 mutations
Loss of *Acta2*
Disruption in contractile filament-FA-ECM connections
Loss of contractile function
Gain of proliferative function
Large arteries:
-high elastin content
-under high pressure due to blood flow
Small arteries:
-low elastin content
-less pressure due to blood flow
?
Aneurysms
Vascular occlusive diseases (CAD, stroke)

Figure VI-1. A model for disease pathogenesis due to loss of SM α-actin filaments.

****

Loss of Contractile Function Resulting From *MYH11* and *ACTA2* Mutations.

Multiple lines of evidence support a loss of contractile function in *ACTA2/MYH11* aortas. All of the currently identified mutations in *MYH11* and *ACTA2* are predicted to disrupt the structure and/or function of the protein. Mutations in *MYH11* located in the

ATPase domain are predicted to impair ATPase activity, and mutations in the coiled-coil domain are predicted to disrupt the structure (36). Mutations in *ACTA2* are predicted to adversely affect actin polymerization and interaction with other proteins (34). Patients with *MYH11* mutations showed a decrease in aortic compliance (86). Mice deficient in either *Acta2* or *Myh11* have decreased contractility of arterial segments, supporting that loss of either of these contractile protein leads to decreased SMC contractility. Our data show that SMCs explanted from both patients with *ACTA2* and *MYH11* mutations failed to form SM α-actin filaments, the thin filaments required for contractile function. Loss of SM α-actin results in decreased aortic contractility in the *Acta2*$^{-/-}$ mouse, demonstrating that SM α-actin is required for maximal force generation by SMCs (117). Therefore, the disruption in contractile filament structure is highly likely to result in decreased contractile function.

In addition to the histologic data in patients' SMCs and myofibroblasts, our study of FAs in *Acta2*$^{-/-}$ mouse SMCs also support the notion that the decreased contractility due to loss of SM α-actin filaments disrupts FAs and actin filament associated proteins in SMCs. Immunofluorescent labeling of vinculin, a marker for FAs, showed a marked reduction in FAs, with the remaining FAs located mainly at the cell periphery in *Acta2*$^{-/-}$ SMCs. The amount of vinculin localized in FAs correlates with the amount of contractile force being generated across FAs by SMCs, and vinculin localization to FAs is necessary in order to transmit this contractile force (207). Therefore, the disruption in vinculin likely indicates a loss of contractile function in the *Acta2*$^{-/-}$ SMCs. Actin thin filaments are anchored to the cell at integrin-containing FAs in SMCs (60). Since integrin signaling at FAs allows for communication with the ECM and transduction of mechanical force between the cell and the

ECM, a disruption in one component of this mechanism is likely to disrupt the development of mechanical force by the SMC (178).

Data from these studies strengthen a growing body of evidence that one of the primary underlying defects in TAAD pathogenesis is the disruption of the structure and/or function of the SMC contractile unit (12). This disruption leads to an impairment of cell-matrix communication, and secondarily may lead to secretion of cytokines and growth factors, as well as release of latent factors from the ECM. Interestingly, a similar pathogenesis has been suggested for mutations in cardiac contractile protein mutations that lead to hypertrophic cardiomyopathy (96). Our data showing the upregulation of IGF-1 transcript levels in patients with *ACTA2* and *MYH11* mutations suggest that the SMCs are compensating for a loss of contractile function by increasing production of this particular growth factor, which is known to drive the expression of contractile proteins in SMCs

Additional studies from our lab and from others support this hypothesis. Other factors that lead to increased pressures on aortic SMC contractile units, such as hypertension or heavy weightlifting, lead to ascending aortic aneurysm formation. This overload of SMCs may induce activation of SMC pathways in a similar manner to pathways induced due to defects in SMC contraction due to mutations in contractile proteins. In addition, other mutant genes identified to predispose to thoracic aortic disease may also lead to decreased contractile function of SMCs. Experimental evidence suggests that SMCs from *TGFBR2* mutant individuals fail to maintain a differentiated, contractile phenotype (Inamoto et al., manuscript submitted). Mutations in *MLCK* disrupt kinase activity of the enzyme, suggesting disruption in SMC contractility (Wang et al., manuscript submitted). Even in cases of *FBN1* mutations, where TGF-β1 has been shown to play a role in disease pathogenesis, the mutations are also likely to disrupt contractile function. As mentioned previously, fibrillin-1 binds to αvβ3, α5β1, and αvβ6 integrins on the surface of SMCs, and fibrillin-1 containing microfibrils form an essential part of the connections between SMCs and elastic fibers (11;13). Missense mutations in *FBN1* disrupt formation of these microfibrils, leading to decreased microfibrils in the vessel wall (12). Therefore, *FBN1* mutations may also perturb the SMC mechanotransduction complex and lead to decreased contractility. In mice that underexpress fibrillin-1, one of the early pathologic abnormalites noted was a smooth appearance of elastic fibers, suggestive of a loss of connectivity between the ECM and SMCs (22). Decreased contractility has also been reported in the aortas of MFS mice harboring a heterozygous missense mutation in fibrillin-1, due to loss of elastic fibers and increased matrix metalloprotease activity (24). This is consistent with the idea that any disruption in the connections between SMC contractile filaments, focal adhesions, and the ECM ultimately result in a decrease in contractility.

Gain of Proliferative Function

Our data also indicate a gain of proliferative function in smaller arteries, which has been a major focus of this work. Histologic and clinical data from patients heterozygous for either *ACTA2* or *MYH11* mutations, as well as data from *Acta2*$^{-/-}$ mice, suggest that SMC hyperproliferation occurs associated with *ACTA2* mutations, both *in vitro* and *in vivo*. Histologic data show focal areas of increased SMCs in the aortic media of *ACTA2* and *MYH11* patients. Additionally, thickening of the medial layer of the arteries in the vasa vasorum due to increased SMCs was noted, leading to stenosis or occlusion of these arteries. Abnormal thickening of epicardial arteries, and luminal narrowing or a coronary artery due to fibrocellular intimal plaque formation was observed. Clinical data also indicate that excessive SMC proliferation may be occurring. Individuals harboring *ACTA2* mutations have increased likelihood of developing CAD, stroke, or Moyamoya disease, in the absence of other cardiovascular risk factors including hypertension, smoking, and hypercholesterolemia. An individual heterozygous for a recently identified *de novo ACTA2* mutation, R179C, was found to have aortic coarctation, a narrowing of the aorta resulting from hyperproliferation of SMCs (Dianna Milewicz, personal communication) (212). Other individuals with the same *de novo* mutation had primary pulmonary hypertension, which was diagnosed based on SMC proliferative lesions in the pulmonary vasculature (Dianna Milewicz, personal communication). Data indicating medial thickening in *Acta2*$^{-/-}$ mouse aortas suggest that SMC proliferation is occurring *in vivo* in these mice due to total loss of SM α-actin. Future study will determine whether this proliferation is occurring before or during expansion of the vessel wall. In addition, more excessive SMC proliferation leading to significant stenoses of arteries was found with arterial injury in the *Acta2*$^{-/-}$ mouse when compared with wildtype mice (Dianna Milewicz, personal communication).

SMCs and myofibroblasts expressing SM α-actin from *ACTA2* mutant individuals displayed a significant increase in proliferation *in vitro* compared with controls. Complete loss of *Acta2* leads to increased SMC proliferation as well as migration *in vitro*, consistent with published data from *Acta2*$^{-/-}$ kidney myofibroblasts (124). Further investigation revealed a role for FAs, and specifically a role for excessive activation of FAK signaling, in mediating proliferation in *Acta2*$^{-/-}$ SMCs. Treatment of *Acta2*$^{-/-}$ SMCs with two different FAK inhibitors completely blocked increased proliferation when the cells were plated on fibronectin-1, suggesting a role for FAK in *Acta2*$^{-/-}$ SMC proliferation.

Focal Adhesion Dependent Regulation of Proliferation in *Acta2*$^{-/-}$ SMCs

We are proposing a novel vascular disease mechanism in which disruption of a SMC-specific contractile protein leads to SMC hyperplasia through altered signaling at focal adhesions, and propose this increased proliferation can lead to occlusive vascular lesions. SM α-actin stabilizes FAs in myofibroblasts (181). In our model of disease progression, loss of SM α-actin filaments would lead to destabilization of FA complexes, resulting in localization of FA complexes mainly at the cell periphery. Consistent with this notion, vinculin was localized mainly at the cell periphery in *Acta2*$^{-/-}$ SMCs. We also observed increased phosphorylated FAK localization at the cell periphery. Since FAK activation in part drives SM α-actin expression in response to external forces on the cell, it is possible that increased phosphorylated FAK at the cell periphery is a compensatory response due to loss of SM α-actin in the *Acta2*$^{-/-}$ mice (183). Activated FAK facilitates FA turnover, and also leads to activation of multiple cellular pathways capable of driving increased proliferation, including ERK, PI3K/Akt, Rho/ROCK, and Rac/JNK (67;68;184;185). Therefore, we propose that loss of *Acta2* leads to a destabilization of FAs and subsequent increase in FAK signaling, and that FAK activates multiple cellular pathways to drive proliferation (**Figure VI-2**).

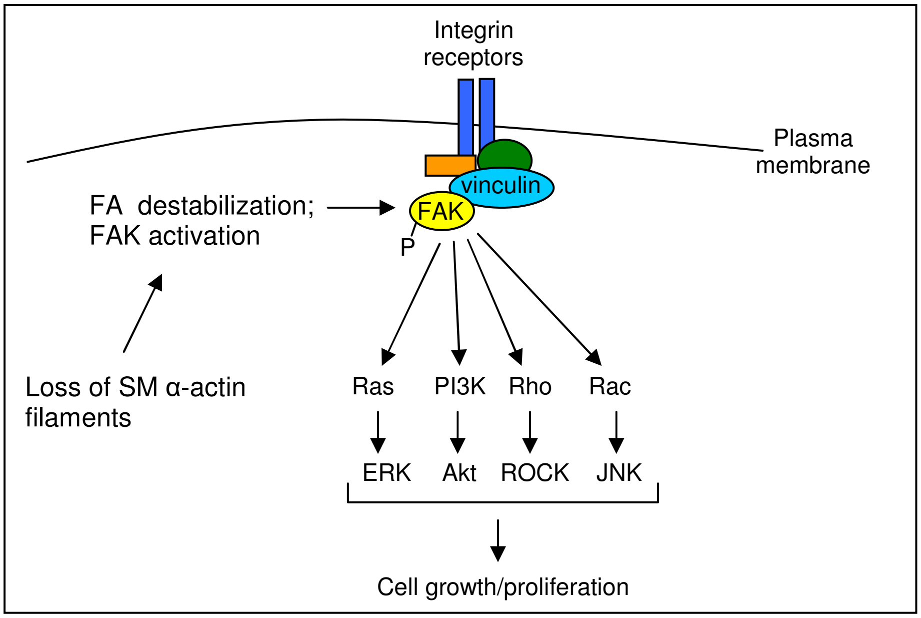
Integrin receptors
Plasma membrane
vinculin
FAK
P
FA destabilization; FAK activation
Loss of SM α-actin filaments
Ras
PI3K
Rho
Rac
ERK
Akt
ROCK
JNK
Cell growth/proliferation

Figure VI-2. Pathways downstream of FAK potentially driving increased proliferation in *Acta2*$^{-/-}$ SMCs compared with wildtype SMCs.

****

Inhibitor assays using two different FAK inhibitors reversed the increased proliferation in *Acta2*$^{-/-}$ SMCs to levels similar to wildtype cells, suggesting that *Acta2-/-* SMCs proliferate in a FAK-dependent manner. Further, this FAK-dependent proliferation may be driving occlusive vascular lesions in response to injury. Data obtained in our lab show that neointimal formation is increased following carotid artery ligation in *Acta2*$^{-/-}$ mice compared with wildtype. Additionally, other models of carotid injury-induced proliferation are connected with FA regulation. Balloon injury of rat carotid arteries leads to decreased expression of integrin-linked kinase and disruption of FA formation (73). These data are consistent with another report that deletion of integrin-linked kinase (ILK), another FA-associated kinase, disrupts FA maturation (201). Together, these data provide support for a novel pathway in which *Acta2* deficiency leads to increased proliferation through disruption of FAs and subsequent increases in FAK-dependent signaling. Future work will determine which specific pathways downstream of FAK are driving the increased proliferation.

Parallels With *NF1* Vasculopathy

The diffuse vasculopathy found in *ACTA2* patients bears similarities to the vasculopathy found in patients with Neurofibromatosis type I (NF1), an autosomal dominant disorder that results in effects on mainly the nervous system, but also the vascular system as well. NF1 has been shown to lead to stenosis or occlusion of arteries, and less commonly, to aneurysm formation. Both *ACTA2* mutations and NF1 can also lead to occlusive disease in multiple vascular beds, and this spectrum of occlusive disease includes aortic coarctation, and also Moyamoya disease (213). The human *NF1* gene, encoding neurofibromin, functions as a negative regulator of Ras signaling in SMCs, suggesting a link between *NF1* mutations and the SMC hyperplasia leading to vessel stenosis and occlusion (214).

Nf1 deficient mice display increased responsiveness to vascular injury compared to their wildtype counterparts. Mice with heterozygous for a deletion in the *Nf1* gene display increased neointimal formation after vascular injury (72). This proliferation can be inhibited both by blocking Ras-mediated signaling and through treatment of the mice with Gleevec, a pharmacological inhibitor of Ras (72;215). The proliferative response to injury in *Acta2*$^{-/-}$ mice parallels the response to carotid injury observed in *Nf1* deficient mice. Interestingly, neurofibromin, the protein encoded by *Nf1*, was recently found to interact directly with FAK (216). *Nf1*$^{-/-}$ MEF cells are more elongated, and FAK is redistributed to the cell periphery, specifically at the leading edge of the cells (216). Together, these data, along with our data from *Acta2*$^{-/-}$ mice, support the notion that disruptions in a single gene can lead to occlusive disease in multiple vascular beds. Further, these studies implicate SMC proliferation in the formation of these occlusive diseases and further support our hypothesis that disruptions in FAs lead to a proliferative vascular response to injury.

Future Research Directions

Future work will focus both on mouse models of *ACTA2* and *MYH11* mutations and confirmation of results in human tissue and cell samples. Plans for the immediate future include further characterization of the *Acta2*$^{-/-}$ mouse model, as well as development of transgenic and knock-in mice that carry the R258C mutation, one of the more severe mutations in *ACTA2*. Mice will be imaged using MRA, as well as echocardiography, to confirm aneurysm formation and determine the earliest age of onset of disease. Pathological study of these mice should provide further insight into the major mechanisms driving aneurysm formation due to SMC contractile mutations. Mouse models will aid in elucidating the specific role of FAs and FAK in increased proliferation leading to the occlusive lesions *in vivo*. *Acta2*$^{-/-}$ mice display increased neointimal formation post carotid artery ligation: future work will determine 1) whether this holds true in transgenic and knock-in mouse models and 2) whether this increase can be blocked through treatment of mice with a FAK inhibitor.

The mouse models will also aid in determining whether increased proliferation plays a role in aneurysm formation, and whether this proliferation is FAK-dependent. Some experimental evidence exists to suggest a role for increased cell proliferation in aneurysm formation. The observation of focal areas of increased SMCs in *ACTA2* and *MYH11* aortic tissues supports this idea. Also, LDLR-related protein (LRP) deficient mice develop aneurysms with medial thickening, atherosclerosis, and SMC hyperplasia (217). Another group reported medial thickening and sustained SMC density in TAA, implying that SMCs proliferated to maintain the same density as the aortic wall expanded (82). It is interesting to note that aneurysm formation is evident in *Acta2*$^{-/-}$ mice with only minimal changes typical of medial degeneration (increased proteoglycans and elastic fiber degradation). The only pathologic abnormality noted is increased SMCs in the aortic medial layer. This observation raises the possibility that excessive SMC proliferation may contribute to aneurysm formation. Furthermore, we are interested in determining if blocking this proliferation will prevent aneurysm formation. Once a role for FAK inhibitors in preventing neointimal proliferation in response to carotid ligation has been established, mice will be treated with FAK inhibitors prior to the onset of TAA formation. MRA and histologic studies will be used to determine whether FAK inhibition prevents aneurysm formation and associated medial degeneration.

Further work is needed to better quantify and characterize the specific alterations in FAs in *Acta2*$^{-/-}$ mice as well as in human samples. Our studies of *Acta2*$^{-/-}$ mice showed alterations in vinculin as well as zyxin. Total internal reflection fluorescence (TIRF) microscopy will be used to quantify the amounts of these and other FA proteins, including FAK and tensin, localized specifically on the cell membrane. Additionally, the results showing alterations in zyxin localization require follow-up to 1) confirm the results are bona fide and 2) determine the specific subcellular structure(s) that zyxin is localized to in the *Acta2*$^{-/-}$ SMCs.

We also plan to determine whether FAs are altered in human myofibroblast and SMC samples from TAAD patients. Initial study will focus on samples harboring *ACTA2* or

MYH11 mutations, and will later be expanded to determine whether alterations in FAs are commonly disrupted in TAAD. There is a possibility that other TAAD mutations lead to a common disruption of FA formation and/or maturation. Data from our lab showing that MYLK mutations disrupt myosin light chain kinase function in SMCs, together with another study showing that myosin light chain kinase inhibitors prevent FA maturation, support this idea (Wang et al., manuscript submitted) (218).

Another issue to pursue using the mouse models is the question of whether TGF-β1 signaling contributes to the pathogenesis of aneurysms caused by contractile mutations. While our initial data from human subjects does not indicate that increased TGF-β1 signaling is present, we currently cannot completely rule out the possibility of TGF-β1 involvement in pathogenesis. We have proposed that the major underlying defect in these patients, and the initial insult that leads to disease progression, is the defective ability of SMCs to contract properly, resulting in alterations in focal adhesion maturation and/or stability. However, TGF-β1 may still play a role in disease pathogenesis. Treatments that have been utilized in preventing aneurysm formation in mouse models of MFS such as TGF-β1 neutralizing antibodies, Doxycycline, or Losartan should provide insight into 1) whether TGF-β1 is contributing to pathogenesis in the *Acta2*$^{-/-}$ and transgenic and knock-in mouse models, and 2) whether similar treatments under development for treating MFS would also be beneficial for treating familial TAAD patients, particularly those with mutations in *MYH11*/*ACTA2*.

Since we observed increases in IGF-1 in *ACTA2* and *MYH11* patients, it is particularly interesting to note that the IGF-1 receptor and FAK interact in SMCs as well as other cell types. The IGF-1 receptor stimulates FAK phosphorylation in SMCs (219).

Conversely, FAK activates the IGF-1 receptor independently of IGF-1R autophosphorylation and also stabilizes the expression of the receptor (220). In human pancreatic adenocarcinoma cells, multiple combinations of FAK and IGF-1R inhibitors synergistically blocked cell proliferation, whereas proliferation was not inhibited with use of either FAK inhibitors or IGF-1R inhibitors alone (221). In our studies, an IGF-1R inhibitor failed to prevent increased proliferation in *ACTA2* mutant myofibroblasts. It is possible that either a FAK inhibitor alone, or dual inhibition using lower doses of both FAK and IGF-1R inhibitors may completely prevent *ACTA2* mutant myofibroblast proliferation.

In conclusion, the data gained from this study provide support for the existence of a hyperplastic vasculomyopathy leading to diffuse and diverse vascular diseases in the absence of other cardiovascular risk factors including hyperlipidemia, smoking, and hypertension. Further, the ideas of 1) FAK dependent mechanism of SMC hyperproliferation and 2) a role for SMC proliferation in aneurysm formation suggest that FAK inhibition may be a viable treatment option in the future for TAAD associated with early-onset vascular occlusive diseases.

REFERENCES

1. Ince, H. and C. A. Nienaber. 2007. Etiology, pathogenesis and management of thoracic aortic aneurysm. *Nat. Clin. Pract. Cardiovasc. Med.* 4:418-427.

2. Gillum, R. F. 1995. Epidemiology of aortic aneurysm in the United States. *J. Clin. Epidemiol.* 48:1289-1298.

3. Pannu, H., V. Tran-Fadulu, and D. M. Milewicz. 2005. Genetic basis of thoracic aortic aneurysms and aortic dissections. *Am. J. Med. Genet. C. Semin. Med. Genet.* 139:10-16.

4. Milewicz, D. M., H. Chen, E. S. Park, E. M. Petty, H. Zaghi, G. Shashidhar, M. Willing, and V. Patel. 1998. Reduced penetrance and variable expressivity of familial thoracic aortic aneurysms/dissections. *Am. J. Cardiol.* 82:474-479.

5. Ramanath, V. S., J. K. Oh, T. M. Sundt, III, and K. A. Eagle. 2009. Acute aortic syndromes and thoracic aortic aneurysm. *Mayo Clin. Proc.* 84:465-481.

6. Hagan, P. G., C. A. Nienaber, E. M. Isselbacher, D. Bruckman, D. J. Karavite, P. L. Russman, A. Evangelista, R. Fattori, T. Suzuki, J. K. Oh, A. G. Moore, J. F. Malouf, L. A. Pape, C. Gaca, U. Sechtem, S. Lenferink, H. J. Deutsch, H. Diedrichs, J. Robles, A. Llovet, D. Gilon, S. K. Das, W. F. Armstrong, G. M. Deeb, and K. A. Eagle. 2000. The International Registry of Acute Aortic Dissection (IRAD): new insights into an old disease. *JAMA* 283:897-903.

7. Hasham, S. N., M. R. Lewin, V. T. Tran, H. Pannu, A. Muilenburg, M. Willing, and D. M. Milewicz. 2004. Nonsyndromic genetic predisposition to aortic dissection: a

newly recognized, diagnosable, and preventable occurrence in families. *Ann. Emerg. Med.* 43:79-82.

8. Shores, J., K. R. Berger, E. A. Murphy, and R. E. Pyeritz. 1994. Progression of aortic dilatation and the benefit of long-term beta- adrenergic blockade in Marfan's syndrome [see comments]. *N. Engl. J. Med.* 330:1335-1341.
9. Kamalakannan, D., H. S. Rosman, and K. A. Eagle. 2007. Acute aortic dissection. *Crit Care Clin.* 23:779-800, vi.
10. Habashi, J. P., D. P. Judge, T. M. Holm, R. D. Cohn, B. L. Loeys, T. K. Cooper, L. Myers, E. C. Klein, G. Liu, C. Calvi, M. Podowski, E. R. Neptune, M. K. Halushka, D. Bedja, K. Gabrielson, D. B. Rifkin, L. Carta, F. Ramirez, D. L. Huso, and H. C. Dietz. 2006. Losartan, an AT1 antagonist, prevents aortic aneurysm in a mouse model of Marfan syndrome. *Science* 312:117-121.
11. Wagenseil, J. E. and R. P. Mecham. 2007. New insights into elastic fiber assembly. *Birth Defects Res. C. Embryo. Today* 81:229-240.
12. Milewicz, D. M., D. Guo, V. Tran-Fadulu, A. Lafont, C. Papke, S. Inamoto, and H. Pannu. 2008. Genetic Basis of Thoracic Aortic Aneurysms and Dissections: Focus on Smooth Muscle Cell Contractile Dysfunction. *Annu. Rev. Genomics Hum. Genet.* 9:283-302.
13. Jovanovic, J., S. Iqbal, S. Jensen, H. Mardon, and P. Handford. 2008. Fibrillin-integrin interactions in health and disease. *Biochem. Soc. Trans.* 36:257-262.

14. Chaudhry, S. S., S. A. Cain, A. Morgan, S. L. Dallas, C. A. Shuttleworth, and C. M. Kielty. 2007. Fibrillin-1 regulates the bioavailability of TGFbeta1. *J. Cell Biol.* 176:355-367.

15. Kaartinen, V. and D. Warburton. 2003. Fibrillin controls TGF-beta activation. *Nat. Genet.* 33:331-332.

16. McLaughlin, P. J., Q. Chen, M. Horiguchi, B. C. Starcher, J. B. Stanton, T. J. Broekelmann, A. D. Marmorstein, B. McKay, R. Mecham, T. Nakamura, and L. Y. Marmorstein. 2006. Targeted disruption of fibulin-4 abolishes elastogenesis and causes perinatal lethality in mice. *Mol. Cell Biol.* 26:1700-1709.

17. Nakamura, T., P. R. Lozano, Y. Ikeda, Y. Iwanaga, A. Hinek, S. Minamisawa, C. F. Cheng, K. Kobuke, N. Dalton, Y. Takada, K. Tashiro, J. J. Ross, T. Honjo, and K. R. Chien. 2002. Fibulin-5/DANCE is essential for elastogenesis in vivo. *Nature* 415:171-175.

18. Li, D. Y., G. Faury, D. G. Taylor, E. C. Davis, W. A. Boyle, R. P. Mecham, P. Stenzel, B. Boak, and M. T. Keating. 1998. Novel arterial pathology in mice and humans hemizygous for elastin. *J. Clin. Invest* 102:1783-1787.

19. Klima, T., H. J. Spjut, A. Coelho, A. G. Gray, D. C. Wukasch, G. J. Reul, Jr., and D. A. Cooley. 1983. The morphology of ascending aortic aneurysms. *Hum. Pathol.* 14:810-817.

20. Guo, D., S. Hasham, S. Q. Kuang, C. J. Vaughan, E. Boerwinkle, H. Chen, D. Abuelo, H. C. Dietz, C. T. Basson, S. S. Shete, and D. M. Milewicz. 2001. Familial

thoracic aortic aneurysms and dissections: genetic heterogeneity with a major locus mapping to 5q13-14. *Circulation* 103:2461-2468.

21. He, R., D. C. Guo, A. L. Estrera, H. J. Safi, T. T. Huynh, Z. Yin, S. N. Cao, J. Lin, T. Kurian, L. M. Buja, Y. J. Geng, and D. M. Milewicz. 2006. Characterization of the inflammatory and apoptotic cells in the aortas of patients with ascending thoracic aortic aneurysms and dissections. *J. Thorac. Cardiovasc. Surg.* 131:671-678.

22. Bunton, T. E., N. J. Biery, L. Myers, B. Gayraud, F. Ramirez, and H. C. Dietz. 2001. Phenotypic alteration of vascular smooth muscle cells precedes elastolysis in a mouse model of marfan syndrome. *Circ. Res.* 88:37-43.

23. LeMaire, S. A., X. Wang, J. A. Wilks, S. A. Carter, S. Wen, T. Won, D. Leonardelli, G. Anand, L. D. Conklin, X. L. Wang, R. W. Thompson, and J. S. Coselli. 2005. Matrix metalloproteinases in ascending aortic aneurysms: bicuspid versus trileaflet aortic valves. *J. Surg. Res.* 123:40-48.

24. Chung, A. W., Y. K. Au, G. G. Sandor, D. P. Judge, H. C. Dietz, and B. C. van. 2007. Loss of elastic fiber integrity and reduction of vascular smooth muscle contraction resulting from the upregulated activities of matrix metalloproteinase-2 and -9 in the thoracic aortic aneurysm in Marfan syndrome. *Circ. Res.* 101:512-522.

25. El-Hamamsy, I. and M. H. Yacoub. 2009. Cellular and molecular mechanisms of thoracic aortic aneurysms. *Nat. Rev. Cardiol.* 6:771-786.

26. Dietz, H. C., G. R. Cutting, R. E. Pyeritz, C. L. Maslen, L. Y. Sakai, G. M. Corson, E. G. Puffenberger, A. Hamosh, E. J. Nanthakumar, and S. M. Curristin. 1991.

Marfan syndrome caused by a recurrent de novo missense mutation in the fibrillin gene. *Nature* 352:337-339.

27. Robinson, P. N. and P. Booms. 2001. The molecular pathogenesis of the Marfan syndrome. *Cell Mol. Life Sci.* 58:1698-1707.

28. Milewicz, D. M., R. E. Pyeritz, E. S. Crawford, and P. H. Byers. 1992. Marfan syndrome: defective synthesis, secretion, and extracellular matrix formation of fibrillin by cultured dermal fibroblasts. *J. Clin. Invest* 89:79-86.

29. Biddinger, A., M. Rocklin, J. Coselli, and D. M. Milewicz. 1997. Familial thoracic aortic dilatations and dissections: a case control study. *J. Vasc. Surg.* 25:506-511.

30. Coady, M. A., R. R. Davies, M. Roberts, L. J. Goldstein, M. J. Rogalski, J. A. Rizzo, G. L. Hammond, G. S. Kopf, and J. A. Elefteriades. 1999. Familial patterns of thoracic aortic aneurysms. *Arch. Surg.* 134:361-367.

31. Vaughan, C. J., M. Casey, J. He, M. Veugelers, K. Henderson, D. Guo, R. Campagna, M. J. Roman, D. M. Milewicz, R. B. Devereux, and C. T. Basson. 2001. Identification of a chromosome 11q23.2-q24 locus for familial aortic aneurysm disease, a genetically heterogeneous disorder. *Circulation* 103:2469-2475.

32. Pannu, H., V. Fadulu, J. Chang, A. Lafont, S. N. Hasham, E. Sparks, P. F. Giampietro, C. Zaleski, A. L. Estrera, H. J. Safi, S. Shete, M. C. Willing, C. S. Raman, and D. M. Milewicz. 2005. Mutations in transforming growth factor-beta receptor type II cause familial thoracic aortic aneurysms and dissections. *Circulation* 112:513-520.

33. Zhu, L., R. Vranckx, K. P. Khau Van, A. Lalande, N. Boisset, F. Mathieu, M. Wegman, L. Glancy, J. M. Gasc, F. Brunotte, P. Bruneval, J. E. Wolf, J. B. Michel, and X. Jeunemaitre. 2006. Mutations in myosin heavy chain 11 cause a syndrome associating thoracic aortic aneurysm/aortic dissection and patent ductus arteriosus. *Nat. Genet.* 38:343-349.

34. Guo, D. C., H. Pannu, C. L. Papke, R. K. Yu, N. Avidan, S. Bourgeois, A. L. Estrera, H. J. Safi, E. Sparks, D. Amor, L. Ades, V. McConnell, C. E. Willoughby, D. Abuelo, M. Willing, R. A. Lewis, D. H. Kim, S. Scherer, P. P. Tung, Ahn C., L. M. Buja, C. S. Raman, S. Shete, and D. M. Milewicz. 2007. Mutations in smooth muscle alpha-actin (*ACTA2*) lead to thoracic aortic aneurysms and dissections. *Nat. Genet* 39:1488-1493.

35. Tran-Fadulu, V. T., H. Pannu, D. H. Kim, G. W. Vick, III, C. M. Lonsford, A. L. Lafont, C. Boccalandro, S. Smart, K. L. Peterson, J. Zenger-Hain, M. C. Willing, J. Coselli, S. A. LeMaire, C. Ahn, P. H. Byers, and D. M. Milewicz. 2009. Analysis of Multigenerational Families with Thoracic Aortic Aneurysms and Dissections Due to TGFBR1 or TGFBR2 Mutations. *J. Med. Genet.*

36. Pannu, H., V. Tran-Fadulu, C. L. Papke, S. Scherer, Y. Liu, C. Presley, D. Guo, A. L. Estrera, H. J. Safi, A. R. Brasier, G. W. Vick, A. J. Marian, C. S. Raman, L. M. Buja, and D. M. Milewicz. 2007. MYH11 mutations result in a distinct vascular pathology driven by insulin-like growth factor 1 and angiotensin II. *Hum. Mol. Genet.* 16:3453-3462.

37. Furlong, J., T. W. Kurczynski, and J. R. Hennessy. 1987. New Marfanoid syndrome with craniosynostosis. *Am J Med. Genet* 26:599-604.

38. Loeys, B. L., J. Chen, E. R. Neptune, D. P. Judge, M. Podowski, T. Holm, J. Meyers, C. C. Leitch, N. Katsanis, N. Sharifi, F. L. Xu, L. A. Myers, P. J. Spevak, D. E. Cameron, B. J. De, J. Hellemans, Y. Chen, E. C. Davis, C. L. Webb, W. Kress, P. Coucke, D. B. Rifkin, A. M. De Paepe, and H. C. Dietz. 2005. A syndrome of altered cardiovascular, craniofacial, neurocognitive and skeletal development caused by mutations in TGFBR1 or TGFBR2. *Nat. Genet.* 37:275-281.

39. Ades, L. C., K. Sullivan, A. Biggin, E. A. Haan, M. Brett, K. J. Holman, J. Dixon, S. Robertson, A. D. Holmes, J. Rogers, and B. Bennetts. 2006. FBN1, TGFBR1, and the Marfan-craniosynostosis/mental retardation disorders revisited. *Am J Med. Genet A* 140A:1047-1058.

40. Mizuguchi, T., G. Collod-Beroud, T. Akiyama, M. Abifadel, N. Harada, T. Morisaki, D. Allard, M. Varret, M. Claustres, H. Morisaki, M. Ihara, A. Kinoshita, K. Yoshiura, C. Junien, T. Kajii, G. Jondeau, T. Ohta, T. Kishino, Y. Furukawa, Y. Nakamura, N. Niikawa, C. Boileau, and N. Matsumoto. 2004. Heterozygous TGFBR2 mutations in Marfan syndrome. *Nat. Genet.* 36:855-860.

41. Ki, C. S., D. K. Jin, S. H. Chang, J. E. Kim, J. W. Kim, B. K. Park, J. H. Choi, I. S. Park, and H. W. Yoo. 2005. Identification of a novel TGFBR2 gene mutation in a Korean patient with Loeys-Dietz aortic aneurysm syndrome; no mutation in TGFBR2 gene in 30 patients with classic Marfan's syndrome. *Clin. Genet* 68:561-563.

42. Stheneur, C., G. Collod-Beroud, L. Faivre, L. Gouya, G. Sultan, J. M. Le Parc, B. Moura, D. Attias, C. Muti, M. Sznajder, M. Claustres, C. Junien, C. Baumann, V. Cormier-Daire, M. Rio, S. Lyonnet, H. Plauchu, D. Lacombe, B. Chevallier, G. Jondeau, and C. Boileau. 2008. Identification of 23 TGFBR2 and 6 TGFBR1 gene mutations and genotype-phenotype investigations in 457 patients with Marfan syndrome type I and II, Loeys-Dietz syndrome and related disorders. *Hum. Mutat.* 29:E284-E295.

43. Superti-Furga, A., E. Gugler, R. Gitzelmann, and B. Steinmann. 1988. Ehlers-Danlos syndrome type IV: a multi-exon deletion in one of the two COL3A1 alleles affecting structure, stability, and processing of type III procollagen. *J. Biol. Chem.* 263:6226-6232.

44. Sheen, V. L., A. Jansen, M. H. Chen, E. Parrini, T. Morgan, R. Ravenscroft, V. Ganesh, T. Underwood, J. Wiley, R. Leventer, R. R. Vaid, D. E. Ruiz, G. M. Hutchins, J. Menasha, J. Willner, Y. Geng, K. W. Gripp, L. Nicholson, E. Berry-Kravis, A. Bodell, K. Apse, R. S. Hill, F. Dubeau, F. Andermann, J. Barkovich, E. Andermann, Y. Y. Shugart, P. Thomas, M. Viri, P. Veggiotti, S. Robertson, R. Guerrini, and C. A. Walsh. 2005. Filamin A mutations cause periventricular heterotopia with Ehlers-Danlos syndrome. *Neurology* 64:254-262.

45. Elsheikh, M., D. B. Dunger, G. S. Conway, and J. A. Wass. 2002. Turner's syndrome in adulthood. *Endocr. Rev.* 23:120-140.

46. Isotalo, P. A., M. M. Guindi, P. Bedard, M. P. Brais, and J. P. Veinot. 1999. Aortic dissection: a rare complication of osteogenesis imperfecta. *Can. J. Cardiol.* 15:1139-1142.

47. Kamath, B. M., N. B. Spinner, K. M. Emerick, A. E. Chudley, C. Booth, D. A. Piccoli, and I. D. Krantz. 2004. Vascular anomalies in Alagille syndrome: a significant cause of morbidity and mortality. *Circulation* 109:1354-1358.

48. Adeola, T., O. Adeleye, J. L. Potts, M. Faulkner, and A. Oso. 2001. Thoracic aortic dissection in a patient with autosomal dominant polycystic kidney disease. *J. Natl Med. Assoc.* 93:282-287.

49. Chen, L., X. Wang, S. A. Carter, Y. H. Shen, H. R. Bartsch, R. W. Thompson, J. S. Coselli, D. L. Wilcken, X. L. Wang, and S. A. LeMaire. 2006. A single nucleotide polymorphism in the matrix metalloproteinase 9 gene (-8202A/G) is associated with thoracic aortic aneurysms and thoracic aortic dissection. *J. Thorac. Cardiovasc. Surg.* 131:1045-1052.

50. Majesky, M. W. 2007. Developmental basis of vascular smooth muscle diversity. *Arterioscler. Thromb. Vasc. Biol.* 27:1248-1258.

51. Gadson, P. F., Jr., M. L. Dalton, E. Patterson, D. D. Svoboda, L. Hutchinson, D. Schram, and T. H. Rosenquist. 1997. Differential response of mesoderm- and neural crest-derived smooth muscle to TGF-beta1: regulation of c-myb and alpha1 (I) procollagen genes. *Exp. Cell Res.* 230:169-180.

52. Ahuja, P., P. Sdek, and W. R. MacLellan. 2007. Cardiac myocyte cell cycle control in development, disease, and regeneration. *Physiol Rev.* 87:521-544.

53. Strohman, R. C., B. Paterson, R. Fluck, and A. Przybyla. 1974. Cell fusion and terminal differentiation of myogenic cells in culture. *J. Anim Sci.* 38:1103-1110.

54. Owens, G. K., M. S. Kumar, and B. R. Wamhoff. 2004. Molecular regulation of vascular smooth muscle cell differentiation in development and disease. *Physiol Rev.* 84:767-801.

55. Sobue, K., K. Hayashi, and W. Nishida. 1999. Expressional regulation of smooth muscle cell-specific genes in association with phenotypic modulation. *Mol. Cell Biochem.* 190:105-118.

56. Rzucidlo, E. M., K. A. Martin, and R. J. Powell. 2007. Regulation of vascular smooth muscle cell differentiation. *J. Vasc. Surg.* 45 Suppl A:A25-A32.

57. Karnik, S. K., B. S. Brooke, A. Bayes-Genis, L. Sorensen, J. D. Wythe, R. S. Schwartz, M. T. Keating, and D. Y. Li. 2003. A critical role for elastin signaling in vascular morphogenesis and disease. *Development* 130:411-423.

58. Mack, C. P. and J. S. Hinson. 2005. Regulation of smooth muscle differentiation by the myocardin family of serum response factor co-factors. *J. Thromb. Haemost.* 3:1976-1984.

59. Huxley, H. E. 1985. The crossbridge mechanism of muscular contraction and its implications. *J. Exp. Biol.* 115:17-30.

60. Ali, F., P. D. Pare, and C. Y. Seow. 2005. Models of contractile units and their assembly in smooth muscle. *Can. J. Physiol Pharmacol.* 83:825-831.

61. Rayment, I., W. R. Rypniewski, K. Schmidt-Base, R. Smith, D. R. Tomchick, M. M. Benning, D. A. Winkelmann, G. Wesenberg, and H. M. Holden. 1993. Three-dimensional structure of myosin subfragment-1: a molecular motor. *Science* 261:50-58.

62. Rayment, I., H. M. Holden, M. Whittaker, C. B. Yohn, M. Lorenz, K. C. Holmes, and R. A. Milligan. 1993. Structure of the actin-myosin complex and its implications for muscle contraction. *Science* 261:58-65.

63. Herrera, A. M., B. E. McParland, A. Bienkowska, R. Tait, P. D. Pare, and C. Y. Seow. 2005. 'Sarcomeres' of smooth muscle: functional characteristics and ultrastructural evidence. *J. Cell Sci.* 118:2381-2392.

64. Tang, D. D. and Y. Anfinogenova. 2008. Physiologic properties and regulation of the actin cytoskeleton in vascular smooth muscle. *J. Cardiovasc. Pharmacol. Ther.* 13:130-140.

65. Gerthoffer, W. T. and S. J. Gunst. 2001. Invited review: focal adhesion and small heat shock proteins in the regulation of actin remodeling and contractility in smooth muscle. *J. Appl. Physiol* 91:963-972.

66. Ingber, D. E. 1997. Tensegrity: the architectural basis of cellular mechanotransduction. *Annu. Rev. Physiol* 59:575-599.

67. Burridge, K. and M. Chrzanowska-Wodnicka. 1996. Focal adhesions, contractility, and signaling. *Annu. Rev. Cell Dev. Biol.* 12:463-518.

68. Ilic, D., C. H. Damsky, and T. Yamamoto. 1997. Focal adhesion kinase: at the crossroads of signal transduction. *J. Cell Sci.* 110 (Pt 4):401-407.

69. Tang, D. D. and S. J. Gunst. 2001. Depletion of focal adhesion kinase by antisense depresses contractile activation of smooth muscle. *Am. J. Physiol Cell Physiol* 280:C874-C883.

70. Wagenseil, J. E. and R. P. Mecham. 2009. Vascular extracellular matrix and arterial mechanics. *Physiol Rev.* 89:957-989.

71. Kumar, A. and V. Lindner. 1997. Remodeling with neointima formation in the mouse carotid artery after cessation of blood flow. *Arterioscler. Thromb. Vasc. Biol.* 17:2238-2244.

72. Lasater, E. A., W. K. Bessler, L. E. Mead, W. E. Horn, D. W. Clapp, S. J. Conway, D. A. Ingram, and F. Li. 2008. Nf1 +/- Mice Have Increased Neointima Formation Via Hyperactivation of a Gleevec Sensitive Molecular Pathway. *Hum. Mol. Genet.*

73. Ho, B., G. Hou, J. G. Pickering, G. Hannigan, B. L. Langille, and M. P. Bendeck. 2008. Integrin-linked kinase in the vascular smooth muscle cell response to injury. *Am. J. Pathol.* 173:278-288.

74. Lacro, R. V., H. C. Dietz, L. M. Wruck, T. J. Bradley, S. D. Colan, R. B. Devereux, G. L. Klein, J. S. Li, L. L. Minich, S. M. Paridon, G. D. Pearson, B. F. Printz, R. E.

Pyeritz, E. Radojewski, M. J. Roman, J. P. Saul, M. P. Stylianou, and L. Mahony. 2007. Rationale and design of a randomized clinical trial of beta-blocker therapy (atenolol) versus angiotensin II receptor blocker therapy (losartan) in individuals with Marfan syndrome. *Am. Heart J.* 154:624-631.

75. Ailawadi, G., C. W. Moehle, H. Pei, S. P. Walton, Z. Yang, I. L. Kron, C. L. Lau, and G. K. Owens. 2009. Smooth muscle phenotypic modulation is an early event in aortic aneurysms. *J. Thorac. Cardiovasc. Surg.* 138:1392-1399.

76. Xiong, W., R. A. Knispel, H. C. Dietz, F. Ramirez, and B. T. Baxter. 2008. Doxycycline delays aneurysm rupture in a mouse model of Marfan syndrome. *J. Vasc. Surg.* 47:166-172.

77. Chung, A. W., H. H. Yang, M. W. Radomski, and B. C. van. 2008. Long-term doxycycline is more effective than atenolol to prevent thoracic aortic aneurysm in marfan syndrome through the inhibition of matrix metalloproteinase-2 and -9. *Circ. Res.* 102:e73-e85.

78. He, R., D. C. Guo, W. Sun, C. L. Papke, S. Duraisamy, A. L. Estrera, H. J. Safi, C. Ahn, L. M. Buja, F. C. Arnett, J. Zhang, Y. J. Geng, and D. M. Milewicz. 2008. Characterization of the inflammatory cells in ascending thoracic aortic aneurysms in patients with Marfan syndrome, familial thoracic aortic aneurysms, and sporadic aneurysms. *J. Thorac. Cardiovasc. Surg.* 136:922-9, 929.

79. Ejiri, J., N. Inoue, T. Tsukube, T. Munezane, Y. Hino, S. Kobayashi, K. Hirata, S. Kawashima, S. Imajoh-Ohmi, Y. Hayashi, H. Yokozaki, Y. Okita, and M.

Yokoyama. 2003. Oxidative stress in the pathogenesis of thoracic aortic aneurysm: protective role of statin and angiotensin II type 1 receptor blocker. *Cardiovasc. Res.* 59:988-996.

80. Lopez-Candales, A., D. R. Holmes, S. Liao, M. J. Scott, S. A. Wickline, and R. W. Thompson. 1997. Decreased vascular smooth muscle cell density in medial degeneration of human abdominal aortic aneurysms. *Am. J. Pathol.* 150:993-1007.

81. Collins, M. J., V. Dev, B. H. Strauss, P. W. Fedak, and J. Butany. 2008. Variation in the histopathological features of patients with ascending aortic aneurysms: a study of 111 surgically excised cases. *J. Clin. Pathol.* 61:519-523.

82. Tang, P. C., M. A. Coady, C. Lovoulos, A. Dardik, M. Aslan, J. A. Elefteriades, and G. Tellides. 2005. Hyperplastic cellular remodeling of the media in ascending thoracic aortic aneurysms. *Circulation* 112:1098-1105.

83. Guo, D. C., C. L. Papke, V. Tran-Fadulu, E. S. Regalado, N. Avidan, R. J. Johnson, D. H. Kim, H. Pannu, M. C. Willing, E. Sparks, R. E. Pyeritz, M. N. Singh, R. L. Dalman, J. C. Grotta, A. J. Marian, E. A. Boerwinkle, L. Q. Frazier, S. A. LeMaire, J. S. Coselli, A. L. Estrera, H. J. Safi, S. Veeraraghavan, D. M. Muzny, D. A. Wheeler, J. T. Willerson, R. K. Yu, S. S. Shete, S. E. Scherer, C. S. Raman, L. M. Buja, and D. M. Milewicz. 2009. Mutations in smooth muscle alpha-actin (ACTA2) cause coronary artery disease, stroke, and moyamoya disease, along with thoracic aortic disease. *Am. J. Hum. Genet.* 84:617-627.

84. Glancy, D. L., M. Wegmann, and R. W. Dhurandhar. 2001. Aortic dissection and patent ductus arteriosus in three generations. *Am. J. Cardiol.* 87:813-5, A9.

85. Khau, V. K., J. E. Wolf, F. Mathieu, L. Zhu, N. Salve, A. Lalande, C. Bonnet, G. Lesca, H. Plauchu, A. Dellinger, A. Nivelon-Chevallier, F. Brunotte, and X. Jeunemaitre. 2004. Familial thoracic aortic aneurysm/dissection with patent ductus arteriosus: genetic arguments for a particular pathophysiological entity. *Eur. J. Hum. Genet.* 12:173-180.

86. Van Kien, P. K., F. Mathieu, L. Zhu, A. Lalande, C. Betard, M. Lathrop, F. Brunotte, J. E. Wolf, and X. Jeunemaitre. 2005. Mapping of familial thoracic aortic aneurysm/dissection with patent ductus arteriosus to 16p12.2-p13.13. *Circulation* 112:200-206.

87. Oldfors, A. 2007. Hereditary myosin myopathies. *Neuromuscul. Disord.* 17:355-367.

88. Morano, I., G. X. Chai, L. G. Baltas, V. Lamounier-Zepter, G. Lutsch, M. Kott, H. Haase, and M. Bader. 2000. Smooth-muscle contraction without smooth-muscle myosin. *Nat. Cell Biol.* 2:371-375.

89. Geisterfer-Lowrance, A. A., S. Kass, G. Tanigawa, H. P. Vosberg, W. McKenna, C. E. Seidman, and J. G. Seidman. 1990. A molecular basis for familial hypertrophic cardiomyopathy: a beta cardiac myosin heavy chain gene missense mutation. *Cell* 62:999-1006.

90. Iwai, S., D. Hanamoto, and S. Chaen. 2006. A point mutation in the SH1 helix alters elasticity and thermal stability of myosin II. *J. Biol. Chem.* 281:30736-30744.

91. Iwai, S. and S. Chaen. 2007. Mutation in the SH1 helix reduces the activation energy of the ATP-induced conformational transition of myosin. *Biochem. Biophys. Res. Commun.* 357:325-329.

92. Marian, A. J. and R. Roberts. 2001. The molecular genetic basis for hypertrophic cardiomyopathy. *J. Mol. Cell Cardiol.* 33:655-670.

93. Li, R. K., G. Li, D. A. Mickle, R. D. Weisel, F. Merante, H. Luss, V. Rao, G. T. Christakis, and W. G. Williams. 1997. Overexpression of transforming growth factor-beta1 and insulin-like growth factor-I in patients with idiopathic hypertrophic cardiomyopathy. *Circulation* 96:874-881.

94. Li, G., M. A. Borger, W. G. Williams, R. D. Weisel, D. A. Mickle, E. D. Wigle, and R. K. Li. 2002. Regional overexpression of insulin-like growth factor-I and transforming growth factor-beta1 in the myocardium of patients with hypertrophic obstructive cardiomyopathy. *J Thorac. Cardiovasc. Surg.* 123:89-95.

95. Suzuki, J., S. Baba, I. Ohno, M. Endoh, J. Nawata, S. Miura, Y. Yamamoto, Y. Sekiguchi, T. Takita, M. Ogata, K. Tamaki, J. Ikeda, and K. Shirato. 1999. Immunohistochemical analysis of platelet-derived growth factor-B expression in myocardial tissues in hypertrophic cardiomyopathy. *Cardiovasc. Pathol.* 8:223-231.

96. Marian, A. J. 2000. Pathogenesis of diverse clinical and pathological phenotypes in hypertrophic cardiomyopathy. *Lancet* 355:58-60.

97. Arad, M., J. G. Seidman, and C. E. Seidman. 2002. Phenotypic diversity in hypertrophic cardiomyopathy. *Hum. Mol. Genet.* 11:2499-2506.

98. Delaughter, M. C., G. E. Taffet, M. L. Fiorotto, M. L. Entman, and R. J. Schwartz. 1999. Local insulin-like growth factor I expression induces physiologic, then pathologic, cardiac hypertrophy in transgenic mice. *FASEB J.* 13:1923-1929.

99. Sugden, P. H. 2002. Signaling pathways activated by vasoactive peptides in the cardiac myocyte and their role in myocardial pathologies. *J. Card Fail.* 8:S359-S369.

100. Marian, A. J. 2002. Modifier genes for hypertrophic cardiomyopathy. *Curr. Opin. Cardiol.* 17:242-252.

101. Lechin, M., M. A. Quinones, A. Omran, R. Hill, Q. T. Yu, H. Rakowski, D. Wigle, C. C. Liew, M. Sole, R. Roberts, and . 1995. Angiotensin-I converting enzyme genotypes and left ventricular hypertrophy in patients with hypertrophic cardiomyopathy. *Circulation* 92:1808-1812.

102. Yamada, Y., S. Ichihara, T. Fujimura, and M. Yokota. 1997. Lack of association of polymorphisms of the angiotensin converting enzyme and angiotensinogen genes with nonfamilial hypertrophic or dilated cardiomyopathy. *Am. J. Hypertens.* 10:921-928.

103. Berk, B. C. 2001. Vascular smooth muscle growth: autocrine growth mechanisms. *Physiol Rev.* 81:999-1030.

104. Recinos, A., III, W. S. Lejeune, H. Sun, C. Y. Lee, B. C. Tieu, M. Lu, T. Hou, I. Boldogh, R. G. Tilton, and A. R. Brasier. 2007. Angiotensin II induces IL-6 expression and the Jak-STAT3 pathway in aortic adventitia of LDL receptor-deficient mice. *Atherosclerosis* 194:125-133.

105. Wang, Y. X., B. Martin-McNulty, A. D. Freay, D. A. Sukovich, M. Halks-Miller, W. W. Li, R. Vergona, M. E. Sullivan, J. Morser, W. P. Dole, and G. G. Deng. 2001. Angiotensin II increases urokinase-type plasminogen activator expression and induces aneurysm in the abdominal aorta of apolipoprotein E-deficient mice. *Am. J. Pathol.* 159:1455-1464.

106. Delafontaine, P., Y. H. Song, and Y. Li. 2004. Expression, regulation, and function of IGF-1, IGF-1R, and IGF-1 binding proteins in blood vessels. *Arterioscler. Thromb. Vasc. Biol.* 24:435-444.

107. Standley, P. R., T. J. Obards, and C. L. Martina. 1999. Cyclic stretch regulates autocrine IGF-I in vascular smooth muscle cells: implications in vascular hyperplasia. *Am. J. Physiol* 276:E697-E705.

108. Zhao, G., R. L. Sutliff, C. S. Weber, J. Wang, J. Lorenz, R. J. Paul, and J. A. Fagin. 2001. Smooth muscle-targeted overexpression of insulin-like growth factor I results in enhanced vascular contractility. *Endocrinology* 142:623-632.

109. Chetty, A., G. J. Cao, and H. C. Nielsen. 2006. Insulin-like Growth Factor-I signaling mechanisms, type I collagen and alpha smooth muscle actin in human fetal lung fibroblasts. *Pediatr. Res.* 60:389-394.

110. Fath, K. A., R. W. Alexander, and P. Delafontaine. 1993. Abdominal coarctation increases insulin-like growth factor I mRNA levels in rat aorta. *Circ. Res.* 72:271-277.

111. Cercek, B., M. C. Fishbein, J. S. Forrester, R. H. Helfant, and J. A. Fagin. 1990. Induction of insulin-like growth factor I messenger RNA in rat aorta after balloon denudation. *Circ. Res.* 66:1755-1760.

112. Grant, M. B., T. J. Wargovich, D. M. Bush, D. W. Player, S. Caballero, M. Foegh, and P. E. Spoerri. 1999. Expression of IGF-1, IGF-1 receptor and TGF-beta following balloon angioplasty in atherosclerotic and normal rabbit iliac arteries: an immunocytochemical study. *Regul. Pept.* 79:47-53.

113. Zhu, B., G. Zhao, D. P. Witte, D. Y. Hui, and J. A. Fagin. 2001. Targeted overexpression of IGF-I in smooth muscle cells of transgenic mice enhances neointimal formation through increased proliferation and cell migration after intraarterial injury. *Endocrinology* 142:3598-3606.

114. Daugherty, A., M. W. Manning, and L. A. Cassis. 2000. Angiotensin II promotes atherosclerotic lesions and aneurysms in apolipoprotein E-deficient mice. *J Clin. Invest* 105:1605-1612.

115. Takagi, Y., K. Kikuta, K. Nozaki, and N. Hashimoto. 2007. Histological features of middle cerebral arteries from patients treated for Moyamoya disease. *Neurol. Med. Chir (Tokyo)* 47:1-4.

116. Marco-Ferreres, R., J. J. Arredondo, B. Fraile, and M. Cervera. 2005. Overexpression of troponin T in Drosophila muscles causes a decrease in the levels of thin-filament proteins. *Biochem. J.* 386:145-152.

117. Schildmeyer, L. A., R. Braun, G. Taffet, M. Debiasi, A. E. Burns, A. Bradley, and R. J. Schwartz. 2000. Impaired vascular contractility and blood pressure homeostasis in the smooth muscle alpha-actin null mouse. *FASEB J.* 14:2213-2220.

118. Vandekerckhove, J. and K. Weber. 1978. At least six different actins are expressed in a higher mammal: an analysis based on the amino acid sequence of the amino-terminal tryptic peptide. *J. Mol. Biol.* 126:783-802.

119. McHugh, K. M., K. Crawford, and J. L. Lessard. 1991. A comprehensive analysis of the developmental and tissue-specific expression of the isoactin multigene family in the rat. *Dev. Biol.* 148:442-458.

120. Kim, H. R., C. Gallant, P. C. Leavis, S. J. Gunst, and K. G. Morgan. 2008. Cytoskeletal remodeling in differentiated vascular smooth muscle is actin isoform dependent and stimulus dependent. *Am. J. Physiol Cell Physiol* 295:C768-C778.

121. Fatigati, V. and R. A. Murphy. 1984. Actin and tropomyosin variants in smooth muscles. Dependence on tissue type. *J. Biol. Chem.* 259:14383-14388.

122. Nowak, K. J., G. Ravenscroft, C. Jackaman, A. Filipovska, S. M. Davies, E. M. Lim, S. E. Squire, A. C. Potter, E. Baker, S. Clement, C. A. Sewry, V. Fabian, K. Crawford, J. L. Lessard, L. M. Griffiths, J. M. Papadimitriou, Y. Shen, G. Morahan, A. J. Bakker, K. E. Davies, and N. G. Laing. 2009. Rescue of skeletal muscle alpha-actin-null mice by cardiac (fetal) alpha-actin. *J. Cell Biol.* 185:903-915.

123. Jaeger, M. A., K. J. Sonnemann, D. P. Fitzsimons, K. W. Prins, and J. M. Ervasti. 2009. Context-dependent functional substitution of alpha-skeletal actin by gamma-cytoplasmic actin. *FASEB J.* 23:2205-2214.

124. Takeji, M., T. Moriyama, S. Oseto, N. Kawada, M. Hori, E. Imai, and T. Miwa. 2006. Smooth muscle alpha-actin deficiency in myofibroblasts leads to enhanced renal tissue fibrosis. *J. Biol. Chem.* 281:40193-40200.

125. North, A. J., M. Gimona, Z. Lando, and J. V. Small. 1994. Actin isoform compartments in chicken gizzard smooth muscle cells. *J. Cell Sci.* 107 (Pt 3):445-455.

126. Stromer, M. H., M. S. Mayes, and R. M. Bellin. 2002. Use of actin isoform-specific antibodies to probe the domain structure in three smooth muscles. *Histochem. Cell Biol.* 118:291-299.

127. Hashida, N., N. Ohguro, Y. Morimoto, E. Oiki, H. Morisaki, T. Morisaki, and Y. Tano. 2009. Ultrastructural appearance of iris flocculi associated with a thoracic aortic aneurysm and dissections. *Br. J. Ophthalmol.* 93:1409-1410.

128. Morisaki, H., K. Akutsu, H. Ogino, N. Kondo, I. Yamanaka, Y. Tsutsumi, T. Yoshimuta, T. Okajima, H. Matsuda, K. Minatoya, H. Sasaki, H. Tanaka, H. Ishibashi-Ueda, and T. Morisaki. 2009. Mutation of ACTA2 gene as an important cause of familial and nonfamilial nonsyndromatic thoracic aortic aneurysm and/or dissection (TAAD). *Hum. Mutat.* 30:1406-1411.

129. Olson, T. M., V. V. Michels, S. N. Thibodeau, Y. S. Tai, and M. T. Keating. 1998. Actin mutations in dilated cardiomyopathy, a heritable form of heart failure. *Science* 280:750-752.

130. Mogensen, J., I. C. Klausen, A. K. Pedersen, H. Egeblad, P. Bross, T. A. Kruse, N. Gregersen, P. S. Hansen, U. Baandrup, and A. D. Borglum. 1999. Alpha-cardiac actin is a novel disease gene in familial hypertrophic cardiomyopathy. *J. Clin. Invest* 103:R39-R43.

131. Zhu, M., T. Yang, S. Wei, A. T. DeWan, R. J. Morell, J. L. Elfenbein, R. A. Fisher, S. M. Leal, R. J. Smith, and K. H. Friderici. 2003. Mutations in the gamma-actin gene (ACTG1) are associated with dominant progressive deafness (DFNA20/26). *Am. J. Hum. Genet* 73:1082-1091.

132. Procaccio, V., G. Salazar, S. Ono, M. L. Styers, M. Gearing, A. Davila, R. Jimenez, J. Juncos, C. A. Gutekunst, G. Meroni, B. Fontanella, E. Sontag, J. M. Sontag, V. Faundez, and B. H. Wainer. 2006. A mutation of beta -actin that alters depolymerization dynamics is associated with autosomal dominant developmental malformations, deafness, and dystonia. *Am. J. Hum. Genet* 78:947-960.

133. Nunoi, H., T. Yamazaki, H. Tsuchiya, S. Kato, H. L. Malech, I. Matsuda, and S. Kanegasaki. 1999. A heterozygous mutation of beta-actin associated with neutrophil dysfunction and recurrent infection. *Proc. Natl. Acad. Sci. U. S. A* 96:8693-8698.

134. Nowak, K. J., D. Wattanasirichaigoon, H. H. Goebel, M. Wilce, K. Pelin, K. Donner, R. L. Jacob, C. Hubner, K. Oexle, J. R. Anderson, C. M. Verity, K. N. North, S. T.

Iannaccone, C. R. Muller, P. Nurnberg, F. Muntoni, C. Sewry, I. Hughes, R. Sutphen, A. G. Lacson, K. J. Swoboda, J. Vigneron, C. Wallgren-Pettersson, A. H. Beggs, and N. G. Laing. 1999. Mutations in the skeletal muscle alpha-actin gene in patients with actin myopathy and nemaline myopathy. *Nat. Genet.* 23:208-212.

135. Sparrow, J. C., K. J. Nowak, H. J. Durling, A. H. Beggs, C. Wallgren-Pettersson, N. Romero, I. Nonaka, and N. G. Laing. 2003. Muscle disease caused by mutations in the skeletal muscle alpha-actin gene (ACTA1). *Neuromuscul. Disord.* 13:519-531.

136. Ilkovski, B., K. J. Nowak, A. Domazetovska, A. L. Maxwell, S. Clement, K. E. Davies, N. G. Laing, K. N. North, and S. T. Cooper. 2004. Evidence for a dominant-negative effect in ACTA1 nemaline myopathy caused by abnormal folding, aggregation and altered polymerization of mutant actin isoforms. *Hum. Mol. Genet* 13:1727-1743.

137. Tanaka, M., H. Fujiwara, T. Onodera, D. J. Wu, M. Matsuda, Y. Hamashima, and C. Kawai. 1987. Quantitative analysis of narrowings of intramyocardial small arteries in normal hearts, hypertensive hearts, and hearts with hypertrophic cardiomyopathy. *Circulation* 75:1130-1139.

138. Mundhenke, M., B. Schwartzkopff, and B. E. Strauer. 1997. Structural analysis of arteriolar and myocardial remodelling in the subendocardial region of patients with hypertensive heart disease and hypertrophic cardiomyopathy. *Virchows Arch.* 431:265-273.

139. Ochala, J. 2008. Thin filament proteins mutations associated with skeletal myopathies: defective regulation of muscle contraction. *J. Mol. Med.* 86:1197-1204.

140. Bookwalter, C. S. and K. M. Trybus. 2006. Functional consequences of a mutation in an expressed human alpha-cardiac actin at a site implicated in familial hypertrophic cardiomyopathy. *J. Biol. Chem.* 281:16777-16784.

141. Desmouliere, A., A. Geinoz, F. Gabbiani, and G. Gabbiani. 1993. Transforming growth factor-beta 1 induces alpha-smooth muscle actin expression in granulation tissue myofibroblasts and in quiescent and growing cultured fibroblasts. *J. Cell Biol.* 122:103-111.

142. Chambers, R. C., P. Leoni, N. Kaminski, G. J. Laurent, and R. A. Heller. 2003. Global expression profiling of fibroblast responses to transforming growth factor-beta1 reveals the induction of inhibitor of differentiation-1 and provides evidence of smooth muscle cell phenotypic switching. *Am. J. Pathol.* 162:533-546.

143. Arora, P. D., N. Narani, and C. A. McCulloch. 1999. The compliance of collagen gels regulates transforming growth factor-beta induction of alpha-smooth muscle actin in fibroblasts. *Am. J. Pathol.* 154:871-882.

144. Desmouliere, A., C. Chaponnier, and G. Gabbiani. 2005. Tissue repair, contraction, and the myofibroblast. *Wound. Repair Regen.* 13:7-12.

145. Ehrlich, H. P., G. M. Allison, and M. Leggett. 2006. The myofibroblast, cadherin, alpha smooth muscle actin and the collagen effect. *Cell Biochem. Funct.* 24:63-70.

146. Desmouliere, A., L. Rubbia-Brandt, G. Grau, and G. Gabbiani. 1992. Heparin induces alpha-smooth muscle actin expression in cultured fibroblasts and in granulation tissue myofibroblasts. *Lab Invest* 67:716-726.

147. Comer, K. A., P. A. Dennis, L. Armstrong, J. J. Catino, M. B. Kastan, and C. C. Kumar. 1998. Human smooth muscle alpha-actin gene is a transcriptional target of the p53 tumor suppressor protein. *Oncogene* 16:1299-1308.

148. Masur, S. K., H. S. Dewal, T. T. Dinh, I. Erenburg, and S. Petridou. 1996. Myofibroblasts differentiate from fibroblasts when plated at low density. *Proc. Natl. Acad. Sci. U. S. A* 93:4219-4223.

149. Arora, P. D. and C. A. McCulloch. 1999. The deletion of transforming growth factor-beta-induced myofibroblasts depends on growth conditions and actin organization. *Am. J. Pathol.* 155:2087-2099.

150. Schmierer, B. and C. S. Hill. 2007. TGFbeta-SMAD signal transduction: molecular specificity and functional flexibility. *Nat. Rev. Mol. Cell Biol.* 8:970-982.

151. Roy, S. G., Y. Nozaki, and S. H. Phan. 2001. Regulation of alpha-smooth muscle actin gene expression in myofibroblast differentiation from rat lung fibroblasts. *Int. J. Biochem. Cell Biol.* 33:723-734.

152. Thannickal, V. J., D. Y. Lee, E. S. White, Z. Cui, J. M. Larios, R. Chacon, J. C. Horowitz, R. M. Day, and P. E. Thomas. 2003. Myofibroblast differentiation by transforming growth factor-beta1 is dependent on cell adhesion and integrin signaling via focal adhesion kinase. *J. Biol. Chem.* 278:12384-12389.

153. Serini, G., M. L. Bochaton-Piallat, P. Ropraz, A. Geinoz, L. Borsi, L. Zardi, and G. Gabbiani. 1998. The fibronectin domain ED-A is crucial for myofibroblastic phenotype induction by transforming growth factor-beta1. *J. Cell Biol.* 142:873-881.

154. Greenberg, R. S., A. M. Bernstein, M. Benezra, I. H. Gelman, L. Taliana, and S. K. Masur. 2006. FAK-dependent regulation of myofibroblast differentiation. *FASEB J.* 20:1006-1008.

155. Lien, S. C., S. Usami, S. Chien, and J. J. Chiu. 2006. Phosphatidylinositol 3-kinase/Akt pathway is involved in transforming growth factor-beta1-induced phenotypic modulation of 10T1/2 cells to smooth muscle cells. *Cell Signal.* 18:1270-1278.

156. Ji, Q. S., M. J. Mulvihill, M. Rosenfeld-Franklin, A. Cooke, L. Feng, G. Mak, M. O'Connor, Y. Yao, C. Pirritt, E. Buck, A. Eyzaguirre, L. D. Arnold, N. W. Gibson, and J. A. Pachter. 2007. A novel, potent, and selective insulin-like growth factor-I receptor kinase inhibitor blocks insulin-like growth factor-I receptor signaling in vitro and inhibits insulin-like growth factor-I receptor dependent tumor growth in vivo. *Mol. Cancer Ther.* 6:2158-2167.

157. Rohlik, Q. T., D. Adams, F. C. Kull, Jr., and S. Jacobs. 1987. An antibody to the receptor for insulin-like growth factor I inhibits the growth of MCF-7 cells in tissue culture. *Biochem. Biophys. Res. Commun.* 149:276-281.

158. Hwang, C. C., K. Fang, L. Li, and S. H. Shih. 1995. Insulin-like growth factor-I is an autocrine regulator for the brain metastatic variant of a human non-small cell lung cell line. *Cancer Lett.* 94:157-163.

159. King-Briggs, K. E. and C. M. Shanahan. 2000. TGF-beta superfamily members do not promote smooth muscle-specific alternative splicing, a late marker of vascular smooth muscle cell differentiation. *Differentiation* 66:43-48.

160. Hilgers, R. H. and R. C. Webb. 2005. Molecular aspects of arterial smooth muscle contraction: focus on Rho. *Exp. Biol. Med. (Maywood.)* 230:829-835.

161. Tomasek, J. J., C. J. Haaksma, R. J. Schwartz, D. T. Vuong, S. X. Zhang, J. D. Ash, J. X. Ma, and M. R. Al-Ubaidi. 2006. Deletion of smooth muscle alpha-actin alters blood-retina barrier permeability and retinal function. *Invest Ophthalmol. Vis. Sci.* 47:2693-2700.

162. Okamoto-Inoue, M., S. Taniguchi, H. Sadano, T. Kawano, G. Kimura, G. Gabbiani, and T. Baba. 1990. Alteration in expression of smooth muscle alpha-actin associated with transformation of rat 3Y1 cells. *J. Cell Sci.* 96 (Pt 4):631-637.

163. Okamoto-Inoue, M., S. Kamada, G. Kimura, and S. Taniguchi. 1999. The induction of smooth muscle alpha actin in a transformed rat cell line suppresses malignant properties in vitro and in vivo. *Cancer Lett.* 142:173-178.

164. Loirand, G., P. Guerin, and P. Pacaud. 2006. Rho kinases in cardiovascular physiology and pathophysiology. *Circ. Res.* 98:322-334.

165. Mack, C. P., A. V. Somlyo, M. Hautmann, A. P. Somlyo, and G. K. Owens. 2001. Smooth muscle differentiation marker gene expression is regulated by RhoA-mediated actin polymerization. *J. Biol. Chem.* 276:341-347.

166. Mammoto, A., S. Huang, K. Moore, P. Oh, and D. E. Ingber. 2004. Role of RhoA, mDia, and ROCK in cell shape-dependent control of the Skp2-p27kip1 pathway and the G1/S transition. *J. Biol. Chem.* 279:26323-26330.

167. Croft, D. R. and M. F. Olson. 2006. The Rho GTPase effector ROCK regulates cyclin A, cyclin D1, and p27Kip1 levels by distinct mechanisms. *Mol. Cell Biol.* 26:4612-4627.

168. Olson, M. F., A. Ashworth, and A. Hall. 1995. An essential role for Rho, Rac, and Cdc42 GTPases in cell cycle progression through G1. *Science* 269:1270-1272.

169. Laufs, U., D. Marra, K. Node, and J. K. Liao. 1999. 3-Hydroxy-3-methylglutaryl-CoA reductase inhibitors attenuate vascular smooth muscle proliferation by preventing rho GTPase-induced down-regulation of p27(Kip1). *J. Biol. Chem.* 274:21926-21931.

170. Liu, B., H. Itoh, O. Louie, K. Kubota, and K. C. Kent. 2002. The signaling protein Rho is necessary for vascular smooth muscle migration and survival but not for proliferation. *Surgery* 132:317-325.

171. Szasz, T., K. Thakali, G. D. Fink, and S. W. Watts. 2007. A comparison of arteries and veins in oxidative stress: producers, destroyers, function, and disease. *Exp. Biol. Med. (Maywood.)* 232:27-37.

172. Miano, J. M. 2003. Serum response factor: toggling between disparate programs of gene expression. *J. Mol. Cell Cardiol.* 35:577-593.

173. Posern, G. and R. Treisman. 2006. Actin' together: serum response factor, its cofactors and the link to signal transduction. *Trends Cell Biol.* 16:588-596.

174. Iyer, D., D. Chang, J. Marx, L. Wei, E. N. Olson, M. S. Parmacek, A. Balasubramanyam, and R. J. Schwartz. 2006. Serum response factor MADS box serine-162 phosphorylation switches proliferation and myogenic gene programs. *Proc. Natl. Acad. Sci. U. S. A* 103:4516-4521.

175. Parmacek, M. S. 2007. Myocardin-related transcription factors: critical coactivators regulating cardiovascular development and adaptation. *Circ. Res.* 100:633-644.

176. Miralles, F., G. Posern, A. I. Zaromytidou, and R. Treisman. 2003. Actin dynamics control SRF activity by regulation of its coactivator MAL. *Cell* 113:329-342.

177. Zaromytidou, A. I., F. Miralles, and R. Treisman. 2006. MAL and ternary complex factor use different mechanisms to contact a common surface on the serum response factor DNA-binding domain. *Mol. Cell Biol.* 26:4134-4148.

178. Romer, L. H., K. G. Birukov, and J. G. Garcia. 2006. Focal adhesions: paradigm for a signaling nexus. *Circ. Res.* 98:606-616.

179. Zaidel-Bar, R., M. Cohen, L. Addadi, and B. Geiger. 2004. Hierarchical assembly of cell-matrix adhesion complexes. *Biochem. Soc. Trans.* 32:416-420.

180. Goffin, J. M., P. Pittet, G. Csucs, J. W. Lussi, J. J. Meister, and B. Hinz. 2006. Focal adhesion size controls tension-dependent recruitment of alpha-smooth muscle actin to stress fibers. *J. Cell Biol.* 172:259-268.

181. Hinz, B., V. Dugina, C. Ballestrem, B. Wehrle-Haller, and C. Chaponnier. 2003. Alpha-smooth muscle actin is crucial for focal adhesion maturation in myofibroblasts. *Mol. Biol. Cell* 14:2508-2519.

182. Dugina, V., L. Fontao, C. Chaponnier, J. Vasiliev, and G. Gabbiani. 2001. Focal adhesion features during myofibroblastic differentiation are controlled by intracellular and extracellular factors. *J. Cell Sci.* 114:3285-3296.

183. Chan, M. W., P. D. Arora, P. Bozavikov, and C. A. McCulloch. 2009. FAK, PIP5KIgamma and gelsolin cooperatively mediate force-induced expression of alpha-smooth muscle actin. *J. Cell Sci.* 122:2769-2781.

184. Parsons, J. T. 2003. Focal adhesion kinase: the first ten years. *J. Cell Sci.* 116:1409-1416.

185. Gilmore, A. P. and L. H. Romer. 1996. Inhibition of focal adhesion kinase (FAK) signaling in focal adhesions decreases cell motility and proliferation. *Mol. Biol. Cell* 7:1209-1224.

186. Golubovskaya, V. M., F. A. Kweh, and W. G. Cance. 2009. Focal adhesion kinase and cancer. *Histol. Histopathol.* 24:503-510.

187. Walker, H. A., J. M. Whitelock, P. J. Garl, R. A. Nemenoff, K. R. Stenmark, and M. C. Weiser-Evans. 2003. Perlecan up-regulation of FRNK suppresses smooth muscle cell proliferation via inhibition of FAK signaling. *Mol. Biol. Cell* 14:1941-1952.

188. Sundberg, L. J., L. M. Galante, H. M. Bill, C. P. Mack, and J. M. Taylor. 2003. An endogenous inhibitor of focal adhesion kinase blocks Rac1/JNK but not Ras/ERK-dependent signaling in vascular smooth muscle cells. *J. Biol. Chem.* 278:29783-29791.

189. Taylor, J. M., C. P. Mack, K. Nolan, C. P. Regan, G. K. Owens, and J. T. Parsons. 2001. Selective expression of an endogenous inhibitor of FAK regulates proliferation and migration of vascular smooth muscle cells. *Mol. Cell Biol.* 21:1565-1572.

190. Owens, L. V., L. Xu, W. A. Marston, X. Yang, M. A. Farber, M. V. Iacocca, W. G. Cance, and B. A. Keagy. 2001. Overexpression of the focal adhesion kinase (p125FAK) in the vascular smooth muscle cells of intimal hyperplasia. *J. Vasc. Surg.* 34:344-349.

191. Bond, M., G. B. Sala-Newby, and A. C. Newby. 2004. Focal adhesion kinase (FAK)-dependent regulation of S-phase kinase-associated protein-2 (Skp-2) stability. A novel mechanism regulating smooth muscle cell proliferation. *J. Biol. Chem.* 279:37304-37310.

192. Roy, J., P. K. Tran, P. Religa, M. Kazi, B. Henderson, K. Lundmark, and U. Hedin. 2002. Fibronectin promotes cell cycle entry in smooth muscle cells in primary culture. *Exp. Cell Res.* 273:169-177.

193. 2009. Ingenuity Pathways Analysis. *Ingenuity Systems®, www. ingenuity. com.*

194. Finlay, G. A., A. J. Malhowski, Y. Liu, B. L. Fanburg, D. J. Kwiatkowski, and D. Toksoz. 2007. Selective inhibition of growth of tuberous sclerosis complex 2 null cells by atorvastatin is associated with impaired Rheb and Rho GTPase function and reduced mTOR/S6 kinase activity. *Cancer Res.* 67:9878-9886.

195. Reif, S., A. Lang, J. N. Lindquist, Y. Yata, E. Gabele, A. Scanga, D. A. Brenner, and R. A. Rippe. 2003. The role of focal adhesion kinase-phosphatidylinositol 3-kinase-akt signaling in hepatic stellate cell proliferation and type I collagen expression. *J. Biol. Chem.* 278:8083-8090.

196. Geiger, B., J. P. Spatz, and A. D. Bershadsky. 2009. Environmental sensing through focal adhesions. *Nat. Rev. Mol. Cell Biol.* 10:21-33.

197. Brisset, A. C., H. Hao, E. Camenzind, M. Bacchetta, A. Geinoz, J. C. Sanchez, C. Chaponnier, G. Gabbiani, and M. L. Bochaton-Piallat. 2007. Intimal smooth muscle cells of porcine and human coronary artery express S100A4, a marker of the rhomboid phenotype in vitro. *Circ. Res.* 100:1055-1062.

198. Doughman, R. L., A. J. Firestone, and R. A. Anderson. 2003. Phosphatidylinositol phosphate kinases put PI4,5P(2) in its place. *J. Membr. Biol.* 194:77-89.

199. Ivanov, D., M. Philippova, V. Tkachuk, P. Erne, and T. Resink. 2004. Cell adhesion molecule T-cadherin regulates vascular cell adhesion, phenotype and motility. *Exp. Cell Res.* 293:207-218.

200. Tanaka, K., T. Arao, M. Maegawa, K. Matsumoto, H. Kaneda, K. Kudo, Y. Fujita, H. Yokote, K. Yanagihara, Y. Yamada, I. Okamoto, K. Nakagawa, and K. Nishio. 2009. SRPX2 is overexpressed in gastric cancer and promotes cellular migration and adhesion. *Int. J. Cancer* 124:1072-1080.

201. Stanchi, F., C. Grashoff, C. F. Nguemeni Yonga, D. Grall, R. Fassler, and E. Van Obberghen-Schilling. 2009. Molecular dissection of the ILK-PINCH-parvin triad reveals a fundamental role for the ILK kinase domain in the late stages of focal-adhesion maturation. *J. Cell Sci.* 122:1800-1811.

202. Cattaruzza, M., C. Lattrich, and M. Hecker. 2004. Focal adhesion protein zyxin is a mechanosensitive modulator of gene expression in vascular smooth muscle cells. *Hypertension* 43:726-730.

203. Yoshigi, M., L. M. Hoffman, C. C. Jensen, H. J. Yost, and M. C. Beckerle. 2005. Mechanical force mobilizes zyxin from focal adhesions to actin filaments and regulates cytoskeletal reinforcement. *J. Cell Biol.* 171:209-215.

204. Nakamura, K., H. Yano, E. Schaefer, and H. Sabe. 2001. Different modes and qualities of tyrosine phosphorylation of Fak and Pyk2 during epithelial-mesenchymal transdifferentiation and cell migration: analysis of specific phosphorylation events using site-directed antibodies. *Oncogene* 20:2626-2635.

205. Slack-Davis, J. K., K. H. Martin, R. W. Tilghman, M. Iwanicki, E. J. Ung, C. Autry, M. J. Luzzio, B. Cooper, J. C. Kath, W. G. Roberts, and J. T. Parsons. 2007. Cellular

characterization of a novel focal adhesion kinase inhibitor. *J. Biol. Chem.* 282:14845-14852.

206. Roberts, W. G., E. Ung, P. Whalen, B. Cooper, C. Hulford, C. Autry, D. Richter, E. Emerson, J. Lin, J. Kath, K. Coleman, L. Yao, L. Martinez-Alsina, M. Lorenzen, M. Berliner, M. Luzzio, N. Patel, E. Schmitt, S. LaGreca, J. Jani, M. Wessel, E. Marr, M. Griffor, and F. Vajdos. 2008. Antitumor activity and pharmacology of a selective focal adhesion kinase inhibitor, PF-562,271. *Cancer Res.* 68:1935-1944.

207. Opazo, S. A., W. Zhang, Y. Wu, C. E. Turner, D. D. Tang, and S. J. Gunst. 2004. Tension development during contractile stimulation of smooth muscle requires recruitment of paxillin and vinculin to the membrane. *Am. J. Physiol Cell Physiol* 286:C433-C447.

208. Sun, C. K., K. Man, K. T. Ng, J. W. Ho, Z. X. Lim, Q. Cheng, C. M. Lo, R. T. Poon, and S. T. Fan. 2008. Proline-rich tyrosine kinase 2 (Pyk2) promotes proliferation and invasiveness of hepatocellular carcinoma cells through c-Src/ERK activation. *Carcinogenesis* 29:2096-2105.

209. Ivanov, D., M. Philippova, R. Allenspach, P. Erne, and T. Resink. 2004. T-cadherin upregulation correlates with cell-cycle progression and promotes proliferation of vascular cells. *Cardiovasc. Res.* 64:132-143.

210. Goetz, J. G., B. Joshi, P. Lajoie, S. S. Strugnell, T. Scudamore, L. D. Kojic, and I. R. Nabi. 2008. Concerted regulation of focal adhesion dynamics by galectin-3 and tyrosine-phosphorylated caveolin-1. *J. Cell Biol.* 180:1261-1275.

211. Gerthoffer, W. T. 2007. Mechanisms of vascular smooth muscle cell migration. *Circ. Res.* 100:607-621.

212. Schurch, W., F. H. Messerli, J. Genest, R. Lefebvre, P. Roy, P. Carter, and J. M. Rojo-Ortega. 1975. Arterial hypertension and neurofibromatosis: renal artery stenosis and coarctation of abdominal aorta. *Can. Med. Assoc. J.* 113:879-885.

213. Friedman, J. M., J. Arbiser, J. A. Epstein, D. H. Gutmann, S. J. Huot, A. E. Lin, B. McManus, and B. R. Korf. 2002. Cardiovascular disease in neurofibromatosis 1: report of the NF1 Cardiovascular Task Force. *Genet Med.* 4:105-111.

214. Li, F., A. M. Munchhof, H. A. White, L. E. Mead, T. R. Krier, A. Fenoglio, S. Chen, X. Wu, S. Cai, F. C. Yang, and D. A. Ingram. 2006. Neurofibromin is a novel regulator of RAS-induced signals in primary vascular smooth muscle cells. *Hum. Mol. Genet.* 15:1921-1930.

215. Xu, J., F. A. Ismat, T. Wang, J. Yang, and J. A. Epstein. 2007. NF1 regulates a Ras-dependent vascular smooth muscle proliferative injury response. *Circulation* 116:2148-2156.

216. Kweh, F., M. Zheng, E. Kurenova, M. Wallace, V. Golubovskaya, and W. G. Cance. 2009. Neurofibromin physically interacts with the N-terminal domain of focal adhesion kinase. *Mol. Carcinog.* 48:1005-1017.

217. Boucher, P., M. Gotthardt, W. P. Li, R. G. Anderson, and J. Herz. 2003. LRP: role in vascular wall integrity and protection from atherosclerosis. *Science* 300:329-332.

218. Levinson, H., K. E. Moyer, G. C. Saggers, and H. P. Ehrlich. 2004. Calmodulin-myosin light chain kinase inhibition changes fibroblast-populated collagen lattice contraction, cell migration, focal adhesion formation, and wound contraction. *Wound. Repair Regen.* 12:505-511.

219. Baron, V., V. Calleja, P. Ferrari, F. Alengrin, and O. E. Van. 1998. p125Fak focal adhesion kinase is a substrate for the insulin and insulin-like growth factor-I tyrosine kinase receptors. *J. Biol. Chem.* 273:7162-7168.

220. Andersson, S., P. D'Arcy, O. Larsson, and B. Sehat. 2009. Focal adhesion kinase (FAK) activates and stabilizes IGF-1 receptor. *Biochem. Biophys. Res. Commun.* 387:36-41.

221. Liu, W., D. A. Bloom, W. G. Cance, E. V. Kurenova, V. M. Golubovskaya, and S. N. Hochwald. 2008. FAK and IGF-IR interact to provide survival signals in human pancreatic adenocarcinoma cells. *Carcinogenesis* 29:1096-1107.

VITA

Christina Leann Papke was born in Poughkeepsie, New York on September 6, 1983, the daughter of Mary Ann Papke and Brian Lee Papke. After completing her work at Fort Bend Baptist Academy, Houston, Texas in 2001, she entered Cedarville University in Cedarville, Ohio. She received the degree of Bachelor of Science with a major in Biology from Cedarville in May, 2005. In May of 2005 she entered The University of Texas Health Science Center at Houston Graduate School of Biomedical Sciences. She joined the Cell and Regulatory Biology program and will graduate with her Doctorate of Philosophy in May of 2010.

Permanent address:
1885 El Paseo St. Apt. 328
Houston, Texas 77054